

Effects of Solute Interactions on Mechanical Properties of
Vanadium Alloys Developed for Fusion Reactors

Jiming Chen

DOCTOR OF PHILOSOPHY

Department of Fusion Science
School of Physical Sciences
The Graduate University for Advanced Studies

2005 (School Year)

Content

1. Introduction	1
1.1 World energy supply and consumption--present and future	
1.2 Fusion energy--attractiveness and issues	
1.3 Candidate structural materials and issues	
1.4 Progress towards the solution of critical issues of vanadium alloys for fusion reactor	
1.5 Objectives and characteristics of the present study	
2. The preparation of the alloys	33
2.1 Alloy design according to phase diagram	
2.2 Low activation analysis	
2.3 Alloy preparation	
3. Experimental procedures	37
3.1 Hydrogen charging and mechanical property test	
3.2 Hardness recovery test	
3.3 High temperature tensile test	
3.4 Aging and tensile test of the aged alloy	
3.5 Tests to evaluate hydrogen release and plastic flow at constant stress at room temperature	
4. Solid solution hardening	43
4.1 Results and discussions	
4.2 Summary	
5. Precipitation, cold-rolling and their hardening	47

5.1 During isochronally annealing	
5.2 During aging	
5.3 Effect of aging hardening on tensile properties	
5.4 Hardening by cold rolling and its recovery	
5.5 Discussions and summary	
6. Motion of interstitial solutes and DSA	66
6.1 Effect of C, N and O on recovery behavior and the role of alloying elements	
6.2 High temperature tensile tests	
6.3 Hydrogen release during tensile loading at room temperature	
6.4 Discussions and summary	
7. Degradation of mechanical properties by hydrogen	89
7.1 Hydrogen induced ductility loss and the embrittlement	
7.2 Effect of specimen thickness on hydrogen induced ductility loss	
7.3 Fracture toughness, impact property and the possible mechanisms	
7.4 Effect of alloying elements	
7.5 Effect of tensile strain rate and specimen dimension on the hydrogen induced hardening	
7.6 Oxygen increasing the sensitivity of the alloy to hydrogen embrittlement	
7.7 Summary	
8. Plastic flow at constant stress at RT	108
8.1 Behavior of plastic flow at room temperature	
8.2 Effect of hold stress and hydrogen on plastic flow rate	
8.3 Discussions and summary	
9. Summary and conclusions	116

Acknowledgement	123
References	125
List of the published papers	137

Abstract

Fossil fuels will be depleted if people continue to burn them for energy, and an energy shortfall would appear in less than fifty years. People are looking for innovative energies to meet the demand. The most attractive but challenging one is to make nuclear fusion work on earth. If this is successful, we will have a clean energy source that is inexhaustible owing to the abundant fuel in seawater. One of the promising approaches to fusion is the magnetic confinement concept. A dozen of Tokamak devices have been built around the world. DT plasmas are confined in the torus vessels by magnetic field. When the plasmas are heated up to over 100 million degree with high density and long holding time, fusion reaction will take place. A breakeven condition for energy in and out has been achieved by Tokamak devices and the experiments are approaching an ignition. ITER will be constructed with an expectation of 10 times more energy produced than used for heating the plasma.

It is a great challenge to make fusion a commercial reality. The size, the cost and the complexity of the reactor must be reduced. A safe and efficient tritium handling technique must be developed. Development of fusion materials is also a great concern. The materials must be able to survive high heat flux, retain strength and ductility despite neutron irradiation and have a low activation property. In terms of the applications in a fusion reactor, major fusion materials are classified into plasma facing materials (PFM) and structural materials for vacuum vessel and blanket. Many candidate structural materials have been studied with the high potentiality of ferritic/martensitic (F/M) steel, vanadium alloy and SiC/SiC composite for near, middle and long-term applications. In spite of less experience in large-scale application, vanadium alloy has many advantages over F/M steel, such as better lower activation property, higher thermal load capability and stronger resistance to neutron irradiation. V-4Cr-4Ti is referred as the leading one for fusion application because of its quite low DBTT and acceptable high temperature strength.

There remain a number of critical issues to be resolved for vanadium alloys despite their good properties. One of the issues is the effect of O, C and N interstitials and their precipitates on mechanical properties. Although there were studies showing their effects

on recovery, recrystallization, precipitation hardening, high temperature tensile and creep strength, the influence of substitutional solutes were scarcely studied. DSA (dynamic strain aging) caused by the impurities is known to be strongly affected by Ti. But the studies on the effect of Cr were rarely reported. Precipitation is generally not welcome in high temperature service for the purpose of keeping a good thermal stability. But small effort has been made on the feasibility to utilize the precipitation for enhancing the strength of vanadium alloy structures. Effect of alloying elements on precipitation needs to be studied further. Hydrogen in the alloy causes hydrogen embrittlement. Although the embrittlement has been evaluated with tensile tests, the data on the effect of hydrogen on fracture toughness was quite limited and might be more serious. Hydrogen release during annealing or deformation was reported but its effect on mechanical properties was not well understood. Room temperature plastic flow at constant stress is a phenomenon that has never been investigated.

The objective of the present study is to clarify the effects of interstitial and substitutional solutes on mechanical properties of vanadium alloys for fusion reactors. Emphases were placed on the mechanisms of hardening by C, N, O and H, effects of Ti on the role of these interstitial solutes, role of Cr on the interaction of Ti with C, N and O. The role of substitutional solute of W, which is a potential alternative to Cr, was also investigated. The effects of the solutes on hydrogen embrittlement and hydrogen-induced change of mechanical properties were also studied, including the effect of hydrogen release behavior. The study was oriented to supporting to optimize chemical compositions and processing steps of vanadium alloys and the impurity control during the use in the blanket structure.

In the present study, many sorts of V-based alloys, designed according to phase diagram and neutron induced activity, were developed in laboratory including some new alloys with addition of W. The alloys were V-4Ti, V-4Cr-4Ti, V-4Ti-3Al, V-3Ti-1Al-Si, V-8W, V-7W-0.3Al, V-6W-(1-4)Ti and so forth. Alloys were melted in a magnetic floating furnace, forged at ~950-1150°C and hot rolled at 400-850°C in air with surface protection, and cold rolled to 0.5-1 mm thick plate finally. 50%CW (defined as thickness reduction by cold rolling) plates were used to study their recovery and recrystallization behavior by isochronal annealing at 200-1100°C for 1h. The solid

solution hardening by the alloying elements was investigated from the hardness data of the 1100°C-annealed samples. Some complete recrystallized alloys were tensile tested at 400-800°C in vacuum to study DSA and the role of alloying elements. To clarify precipitation hardening, alloy plates in solid solution state were again isochronally annealed at 200-1100°C for 1h. An aging was then conducted at 600°C for 1-393 hrs to learn the time dependence of the hardening. Following the aging, samples were further annealed at 200-1100°C for 1h to study the thermal stability of the hardening. For all cases, hardness test was performed at room temperature (RT). Hydrogen embrittlement was evaluated by tensile, J_{1c} and impact tests at RT. The specimens were charged with hydrogen at 500-800°C in a H₂ atmosphere. During tensile test, plastic flow at constant stress and hydrogen release were observed and more tests to show their behaviors were performed at various stress levels. TEM and SEM were used to analyze microstructures and fracture features.

Results showed that all alloying elements and interstitial solutes of C, N, O and H are strong solid solution strengtheners. The hardening coefficient of the interstitial solutes is much higher than that by the substitutional solutes of Cr, Ti and W being about 9.55, 8.92 and 7.13Hv/%mass, respectively. Cr contributed more to the solid solution hardening than Ti. Considering the much bigger atomic weight of W, W should be the strongest species per atom to strengthen the alloy at room temperature among the substitutional atoms.

The alloys with many previously formed large precipitates showed weak or no further precipitation in the annealing at 200-1100°C. Precipitation occurred at 600~800°C for Ti-bearing alloys in solid solution annealing state. The annealing at 600~700°C produced high number density of fine precipitates of Ti-CON, which hardened the alloy significantly. Peak hardening occurred at 700°C for V-4Cr-4Ti but 600°C for V-6W-4Ti in the isochronally annealing for 1 hr. The hardening of V-4Cr-4Ti is more prominent than V-6W-4Ti alloy by aging at 600°C, indicating Cr contributes also to precipitation hardening. The growth of the precipitates is controlled by Ti diffusion, thus Cr is presumed to slow down Ti diffusion due to Cr-Ti interaction. The precipitation hardening is stable at <500°C, since Ti is relatively immobile below the temperature. The aging hardening has a slight effect on ductility of the alloy and at

certain aging condition even increases its static fracture toughness, defined as the absorbed energy during tensile test. So the precipitation hardening may be used to attain a high strength vanadium alloy.

Alloying elements studied in the present study showed little effect on the annealing temperature for complete recrystallization. However, the starting temperature for notable hardness recovery of the 50%CW cold-rolled alloys was increased by $\sim 100^{\circ}\text{C}$ by alloying V with Ti. Besides, unlike V-8W and unalloyed V, the Ti-bearing alloys showed no additional hardening at $\sim 300^{\circ}\text{C}$. Interstitial C, N and O impurities in matrix also showed a certain effect on the recovery behavior. More C, N and O in matrix led to less hardness recovery and even additional hardening around 600°C for the alloys with 4%Ti in mass. All these behaviors seem to be resulted from both the resistance of the interstitials to dislocation motion and the role of Ti reducing the mobility of the interstitials.

During the tensile tests at $400\text{-}700^{\circ}\text{C}$ in certain strain rate range, interstitial impurities moved to dislocations and caused DSA for V-Ti alloys. As a result, load-displacement serrations occurred and the strength of the alloy increased. The strongest serrations appeared at $\sim 300^{\circ}\text{C}$ for unalloyed V. Due to the role of Ti decreasing the mobility of interstitial impurities, the temperature for the serrations shifted to $\sim 600^{\circ}\text{C}$ for both V-6W-4Ti and V-4Cr-4Ti. Tensile strength started to increase at $\sim 400^{\circ}\text{C}$ with increasing temperature for both alloys, but the V-4Cr-4Ti alloy shows better mechanical performance than V-6W-4Ti at higher than 600°C . The tensile strength of V-6W-4Ti began to decrease above 600°C while that of the V-4Cr-4Ti continued to increase till 700°C . Their different precipitation-hardening behaviors give evidence that Ti and interstitial impurities in V-4Cr-4Ti are less mobile than those in V-6W-4Ti, probably caused by the Cr-Ti interaction. This should account for the difference in high temperature mechanical performance of V-4Cr-4Ti and V-6W-4Ti.

Though H is mobile at room temperature (RT), DSA didn't appear in tensile tests of V-4Cr-4Ti containing 119-341 wppm H at RT. Both yield strength and ultimate tensile strength decreased with decreasing tensile strain rate. On the other hand, it was found that the slope of the tensile curve in elastic regime, the young's modulus, increased with decreasing strain rate. This suggests that hydrogen release took place; since hydrogen in

solid solution could reduce the atomic binding force to which young's modulus is proportional. Further studies by tensile test at fixed load in the elastic regime showed the shrinkage of the tensile specimen with hold time in a decreasing rate. After the fixed-stress loading, tensile tests indicated the decrease of the ultimate tensile strength and Hydrogen concentration measurements showed the decrease of the concentration. So it is suggested that tensile stress could enhance hydrogen release even at RT.

Hydrogen in vanadium alloys causes hardening and embrittlement. In the present study, the embrittlement occurred for all alloys at critical hydrogen concentrations (CHC), below which the uniform elongation hardly changed with hydrogen while the hardening showed an approximately linear increase with the hydrogen concentration. Alloying elements had a strong effect on the behavior. The Ti-bearing alloys showed weaker hardening and had higher CHC in contrast to V-8W. An atomic model was used to explain the behavior and it suggested that alloying elements with bigger difference in atomic size to V could increase the resistance to hydrogen embrittlement. Other results showed that the specimen size had certain effects on the behavior as well. Thicker specimen behaved more sensitive to the embrittlement. The absorbed energy of the Charpy specimen decreased drastically with increasing hydrogen concentration though the fracture seemed to be more ductile as compared to the tensile specimen. It was presumed that in thicker specimens less hydrogen was released and impact loading caused hydrogen embrittlement more pronounced. By comparison, CT (compact tension) specimen in J_{1c} test was much more sensitive to the embrittlement. Estimated from the results, CHC evaluated by tensile test for V-4Cr-4Ti was 215-310wppm but less than 130wppm by J_{1c} test. Additionally, oxygen in vanadium alloys enhanced the embrittlement significantly.

Constant plastic flow was observed at room temperature for V-4Cr-4Ti and V-6W-2.5Ti when they were loaded at a fixed stress above their yield points. The deformation seemed to obey the three-stage behavior with time. The first stage and the second stage were very short, about 2-2.5hrs in total. The 3rd stage, apparently a steady-state plastic flow, took longer time and had a much bigger deformation rate than the 2nd stage. For V-6W-2.5Ti, the rate at 300 MPa was about $1.11 \times 10^{-3}/h$ in the 3rd stage. The rate increased at higher stress. It was found that hydrogen in the alloy enhanced the

plastic flow due to hydrogen release, namely detrapping of hydrogen from dislocations enhanced dislocation glide. Since the applied stress was higher than yield strength, the plastic flow was considered to be dislocation-glide assisted.

The conclusions of the present study are as follows.

- (1) The effect of solutes and solute interactions on mechanical properties of vanadium alloys was significant. All of the solutes concerned were solid solution strengtheners. The hardening coefficient of the interstitial solutes was much higher than that of the substitutional solutes.
- (2) Ti and the interstitial C, N and O were necessary and were responsible for higher high-temperature strength and keeping the cold-rolling hardening at elevated temperature. Additionally they were the cause of precipitation, and the resulting hardening could be utilized for enhancing strength of the vanadium alloy for relatively low temperature application. For these properties, Cr also provided large positive contribution by its effect to reduce the mobility of Ti due to Cr-Ti interaction.
- (3) A critical new issue of plastic flow at room temperature at constant stress higher than yield strength was found for which more studies should be addressed.
- (4) As for the hydrogen effect, the hydrogen embrittlement could be a great concern for the fusion application due to the strong sensitivity of the fracture toughness. In addition, the hydrogen release could cause dimensional instability. Oxygen in vanadium alloys enhanced the embrittlement significantly. Alloying V with species that had relatively large difference in atomic size to V could improve the property against hydrogen embrittlement.
- (5) All these results showed interactive role of interstitial and substitutional solutes on mechanical properties of vanadium alloys through solid solution hardening, mutual binding or trapping, interaction with dislocations, precipitation and precipitate resolution.

1 Introduction

1.1 World energy supply and consumption--present and future

Humanity owes its existence to the fusion engine on the sun. In addition to fission energy, all the energy we used today is from the sun, such as petroleum, natural gas, coal, hydroelectric, wind and others. Petroleum, natural gas and coal are known as fossil fuels or mineral fuels, which are non-renewable energy sources that formed more than 300 million years ago during the Carboniferous Period long before the dinosaurs roamed the Earth. About from 1900 with the use of the 1st steam engine, human began to consume the resources on a large scale. So far about half of the reserves have been depleted. It was predicted that the reserves would be totally depleted in 2 to 3 centuries at our present rate of use, including the non-breeder fission fuels.

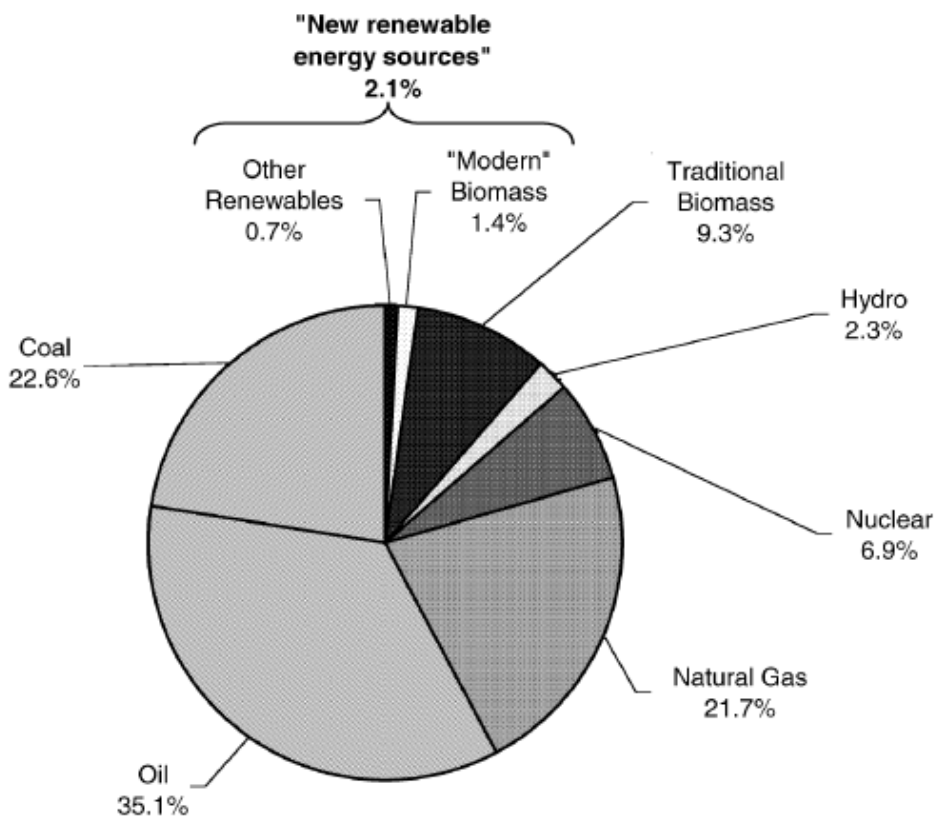


Fig. 1.1 World primary energy production by source in 2001.

Figure 1.1 shows the world primary energy sources in use in 2001 [1]. Clearly non-renewable sources are dominant today. Fossil fuels accounted for about 80% of

the primary energy consumption, while the renewable sources of hydro and new renewable ones merely represented 4.4% of the energy consumption. A statistic in 2000 showed that fossil fuels supplied 90% of global energy with crude oil accounting for 40% of the total, coal 25% and natural gas 25% [2,3]. The new renewable ones include modern biomass, wind, solar, marine and geothermal energy. Although these renewable energy sources are almost environmental friend but are commonly geographically limited. On the contrary, fossil fuels are the source with many problems difficult to resolve such as environmental degradation at the local, regional and global level. Burning fossil fuels to get energy causes air pollution, acid rain and produces CO₂. The release of CO₂ causes a critical environmental issue of “green house effect”, which increases global warming and may cause more critical issues of abominable global climate.

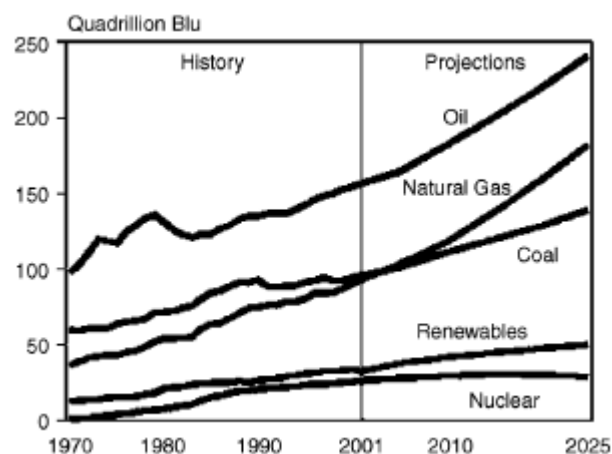


Fig. 1.2 Energy consumption by fuel type.

With the growth of population and enhanced industrialization/living standards for an increasing number of inhabitants on the globe — all available outlooks forecast a further dramatic rise of the primary energy requirements. Fig. 1.2 shows the increase of the energy consumption by various fuel types, with the projections into near future [4]. There seems to have a faster increase of demand to oil and natural gas beyond ~2005 and the consumption for natural gas will exceed the coal consumption hereafter. Fossil energy carriers have limited resources. Data on known and commercially exploitable reserves show that coals are widely distributed around the globe and cover

roughly 70% of the proven fossil fuel reserves whilst gas and oil share the remaining 30% with about 20 and 13%, respectively [4]. This distribution is obviously in contrast to the above-mentioned consumption of primary energy sources with the unavoidable consequence of oil and gas reserves to become exhausted within a much shorter time period than solid fossil fuels.

It was predicted by Donald L. Klass [5] that oil reserves will be used up within 20-70 years at an annual growth rate in consumption of 2.3% and 30-70 years for the natural gas at an annual growth rate of 3.2%. R. Toschi [6] reported in 1997 that the proven recoverable reserves of energy were 800, 200, 200 and 80TWY for coal, oil, natural gas and nuclear fuel, and could be used for about 300, 50, 80, 100 years at the consumption rate of the year. Figure 1.3 illustrated the change of the energy consumption in unit of billion barrels of oil equivalent per year (bb/y) [7]. According to this figure, energy shortfall will occur in less than 50 years at our present rate of use. Thus, it was said that the fossil fuel era is almost over and alternative sources must be used in the future.

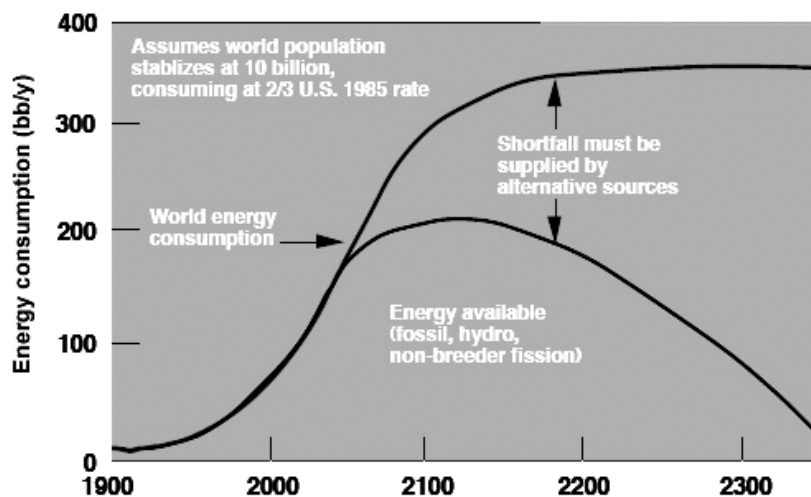


Fig. 1.3 The world energy consumption demand and the energy available [7].

There are possible solutions to these problems, such as extending the life of fossil fuel reserves or expanding the share of renewable in the world energy system [1]. Improvement in the end-use efficiency in fossil fuels can be a very powerful instrument to extend the life of reserves. This has to be firstly accomplished by improvements of the present energy conversion technologies in efficiency, availability,

maintainability, advanced control and automation in order to increase their productivity and, thus, reduce the specific resource consumption [4]. Secondly, it is necessary to develop new technologies to utilize the large untapped deposits in lower quality [1]. To solve the problem of environment pollution due to combustion of fossil fuels and to get a sustainable energy supply, renewable energy should be more used in the future. It requires expanding the share of the technology for the renewable around the world for developed and developing countries.

After a brief analysis of the fossil, fission and renewable energy sources, R. Toschi [6] concluded that present non-fossil energy sources might not be able to meet in the long term the increasing energy demand. This is because most of the renewable energy sources are geographically limited and expensive, such as the solar source for which huge numbers of solar cells are required for an adequate power generation. Therefore, we must look for innovative energy capable to meet the following criteria.

- (1) Fuel: supply abundant and largely available to all countries, i.e. not constrained by political instabilities;
- (2) Safety: all 'internal' accidents cause either by plant failures or by operator mistakes and conceivable 'external' accidents should not disrupt the life of the population;
- (3) Pollution: human health and eco-system not affected by emission into atmosphere;
- (4) Waste: isolation from environment. If necessary, only for no longer than a few generations;
- (5) Other environmental impacts: minimum use of land and of fresh water;
- (6) Proliferation: no direct linkage to nuclear weaponry;
- (7) Cost accessibility: energy cost competitive and predictable;
- (8) Technical accessibility: source technology manageable by countries most in need of energy;
- (9) Service suitability: no severe constraints on size and location.

People have sought for such kind of energy for many years. The typical one is fusion energy that powers the sun and the stars. Scientists have sought to make fusion

work on earth for over 40 years. If successful, mankind will have an energy source that is inexhaustible. Argentina's dictator Juan Peron funds fusion research on a remote island in 1951, resulting news stories galvanize US establishment of fusion energy research. Two years later, project Sherwood established for fusion energy research. In 1958, project Sherwood declassified at a conference and the fusion energy research became open worldwide. Late in 1960's, Russian announced 200eV electron temperature in a tokamak device in which plasma of hydrogen or its isotopes were held for fusion reaction, then US scientists visited Moscow to confirm the result. Thereafter, tokamak devices were constructed in major laboratory in US and also worldwide. Today, there are more than a dozen of tokamak devices around the world. The plasma in these devices is getting closer and closer to ignition. If all go well, commercial application will be possible around the middle of this century, providing humankind a safe, clean and inexhaustible energy source for the future.

1.2 Fusion energy--attractiveness and issues

1.2.1 Basic process of fusion [8,9]

In contrary to fission, fusion reaction leads two light nuclei into one heavier nucleus with the release of substantial amounts of energy. The practical fusion reactions for energy on earth are listed in Table 1.1. Obviously fusion reactions occur at very high temperatures. The most suitable reaction occurs between the nuclei of two isotopes of hydrogen, deuterium (D) and tritium (T), at relatively the lowest ignition temperature. The DT reaction has the largest fusion cross-section among the reactions [8]. It is the focus of the current fusion program, although other fusion reactions might play a role in longer term. A small amount of matter is "lost" and converted into energy during the reaction. The mass loss is only 0.38% of the initial reactants for the DT reaction [9]; however, as Einstein's famous equation $E = mc^2$ indicates, even a small amount of matter can produce enormous amounts of energy. From Table 1.1, the total energy output for the DT reaction is 17.6MeV with 14.1MeV carried by the neutron and 3.5MeV by ^4He [8]. The high-energy of neutron is in some

way a convenient form to extract energy from the reaction due to its penetrating power. The 3.5 MeV alpha particle is confined within the plasma and yields its energy to the background plasma. When the alpha particle energy matches the energy loss from the plasma, the reaction is self-sustaining and is often said to be ignited.

Table 1.1 Different fusion fuel mixtures ignite at different temperatures with different output energies on earth. [9]

Reactions	Output energy	Typical fusion temperature
Fuel \rightarrow Products	(keV)	(Million of $^{\circ}$ K)
$D + T \rightarrow {}^4\text{He} + n$	17600	~ 50
$D + {}^3\text{He} \rightarrow {}^4\text{He} + p$	18300	350
$D + D \rightarrow \begin{cases} {}^3\text{He} + n \\ T + H \end{cases}$	3250	400
	4000	400

At the temperatures required for the D-T fusion reaction the fuel has changed its state from gas to plasma. Within plasma, electrons have been separated from the atomic nuclei and move freely. Usually DT gas will change into plasma state at more than 10,000K. For the fusion reaction, the two nuclei of D^+ and T^+ must be very close. However, there is electrostatic repulsion between the two nuclei. The nuclei must have very high kinetic energy enough to overcome the repulsion for fusion reaction. Therefore, fusion process requires even higher temperature. In addition, the density of the plasma is another key factor to affect the reaction. For instance, the sun's plasma is at temperatures in excess of 10 million Kelvin. Without the extremely high density of the sun, the temperatures almost 10 times higher or 50 to 200 million Kelvin are needed to sustain the fusion reaction on earth.

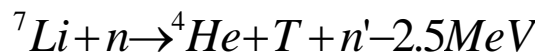
Besides DT, the other reactions also receive attentions for possible energy application. The DD reaction eliminates the need for tritium breeding but has much higher ignition temperature and requirement for plasma energy confinement.

Therefore it will require either a larger system or a more powerful method of plasma confinement. D-³He has a somewhat larger reaction cross-section, lower ignition temperature than DD but is more difficult to use than DT. The major concern is for the actual source of ³He fuel. This isotope is found on earth in very small quantities but there are adequate supplies in the near-surface crust of the moon due to deposits from solar wind over the ages. The feasibility and cost of recovery of such resources are serious issues. Other fusion reactions involving Lithium have marginal or even negative net energy yields and are highly questionable as practical fusion power reactions.

1.2.2 The advantages of fusion energy

Fusion energy is very attractive to humankind due to (1) fuel availability and accessibility, (2) energy density of the fuel and (3) safety.

The fuels of fusion reaction, D and T, are essentially inexhaustible. D could be easily extracted from seawater. The D content in seawater is about 30ppm, that is, one liter of seawater contains about 0.03 g deuterium. The total volume of the seawater on the earth is about 13.7 billion cubic km, thus the D in the seawater is in the level of several billion billion kg. Tritium is a low-energy beta emitter with a half-life of 12.4y and thus there are few resources on the earth. However, it can be bred by causing the n released by the DT reaction to interaction with isotopes of lithium as follows [8]:



The 2nd reaction is endothermic and has a threshold of ~2.7MeV. The 1st reaction can result from slow or thermalized neutrons. Natural lithium is about 93%Li⁷ and 7%Li⁶, and there is abundant Li in the earth's crust. Unlike other natural sources, these fuels are available worldwide and no country can control their supply.

The energy density of the fuels for fusion is very high. As listed in Table 1.1, one atom of D reacting with T by fusion produces 17600keV energy. But the complete combustion of one carbon atom merely produces 4eV energy. One kilogram of

deuterium contains approximately the same amount of energy as 4kg uranium fuel for fission energy or 10000 tons of coal. It is estimated that the fusion energy released by the deuterium in 1 liter of seawater is equivalent to the energy produced by the combustion of 300 liters of oil. D is the most compact fuel known to man.

Fusion energy is clean and safe. Unlike fission reaction, fusion reaction in a device will stop immediately if something goes wrong or in case of an accident because in such case the fuel (plasma) will cool down rapidly. The waste gas of the fusion reaction is helium, an inert gas without any impact on the environment, unlike the combustion of fossil fuels to emit CO₂ and cause greenhouse effect. And yet, no products of radioactive waste like that produced by the fission fuels. Another product of fusion reaction is the 14MeV energetic neutron, which is the source of the fusion energy and is stopped in the blanket of a fusion reactor. It has little impact on the environment. The reactor wall will be activated by the neutron and the material becomes radioactive, but the half-life is many orders-of-magnitude lower than fission products. The radioactivity can be minimized by careful selection of low-activation structural materials.

After assessment of fusion against social acceptability criteria, R. Toschi [6] concluded that fusion has the potential to meet the highest standards in social acceptability and therefore to be competitive with other sources if assessment criteria includes social and environmental costs.

1.2.3 Issues in achieving fusion on earth

For about a half a century, scientists have studied the methods to control fusion reactions. At the early time for the studies, it was optimistically expected that controlling fusion reactions would be as easy as controlling fission reactions and fusion energy would be soon utilized commercially. This early optimism soon gave way to the sobering reality that controlling fusion would be accomplished only after many years of painstaking research, technological advancements and engineering breakthroughs.

As stated above, one principal requirement for fusion is that the fuels have

sufficient high temperature to overcome the electrostatic repulsion of the positive-charged nuclei. For DT reaction, this temperature is about 10 keV at which the fuels have changed into the state of plasma. Another principle requirement is that the fusion reaction rate must be high enough such that the alpha power exceeds the energy losses from the plasma. As a result, the fuel density (usually given in terms of the electron density n_e) and the confinement time (τ_E) of the high-temperature plasma should meet the Lawson criterion [10] as

$$n_e \tau_E \geq 10^{20} \text{ m}^{-3}\text{s}.$$

Such plasma must be created and confined under very good vacuum conditions so as to ensure low purity and high temperatures of the plasma. Another important parameter to show the performance of fusion performance is the so-called fusion triple product of $n_{D0} \tau_E T_{i0}$, where n_{D0} is the peak ion density, τ_E is the overall plasma energy confinement time and T_{i0} is the peak ion temperature. For a self-sustaining burning the product is required in a value of $7 \times 10^{21} \text{ keV}\cdot\text{s}\cdot\text{m}^{-3}$ [8].

As the fuel is ionized at the temperature, the plasma could be confined by magnetic field. One of the promising confinements that mostly studied is the Tokamak concept. In a Tokamak device the magnetic field confines the plasma within a torus vessel and keeps the high-temperature plasma away from the vessel wall. Today, there are many Tokamak devices with the largest ones of TFTR in the U.S, JET in Europe and JT-60U in Japan.

Scientists worldwide have made many efforts for these goals. Much progress has been made and much remains to be done. Fig. 1.4 shows the fusion performance and the fusion power achieved. Obviously we are getting closer to our goals. Major achievements could be summarized as (1) ion temperature as high as 45 KeV and density of $\sim 10^{20} \text{ m}^{-3}$ in TFTR [11]; (2) values of fusion triple product of $1.5 \times 10^{21} \text{ keV}\cdot\text{s}\cdot\text{m}^{-3}$ in JT-60U in pulsed operation [12]; (3) the actual peak DT fusion power of 10.7 MW for TFTR [11] and 16.1 MW for JET [13], corresponding to Q values of ~ 0.27 and 0.62, respectively. Here Q is defined as the total fusion power divided by total injected beam power; (4) clear demonstration of alpha heating in JET and TFTR

during the D-T experiments [11,13].

It is evident that these confinement requirements have almost met by the present results with an exception of the fusion triple product of about 1/5 of the required for an ignited fusion reactor. However, ITER (International Thermonuclear Experimental Reactor) will be constructed and is expected to have its first plasma at 2014. The device is marginal for ignition, since the minimum triple-product for sustained ignition with 1% Be in plasma is approximately 2×10^{21} keV.s.m⁻³ [14]. The objectives of ITER are to demonstrate ignition and extended burns of DT plasmas with steady-state as an ultimate goal, demonstrate the integration of technologies for reactors and serve as a test facility for advanced components such as blankets. According to the early design, the ITER had a goal to produce 1.5GW fusion power for a nominal burn time of 1000 s [14]. In 1998 a reduced cost design started in response to the requests from the participant parties [15]. The size of ITER decreased, such as the major radius reduced from 8.1m to 6.2m. Thereafter the fusion power is designed to be reduced to 500-700 MW while the burn time is more than 400s [16,17]. It is expected that the plasma in ITER will burn at $Q \geq 10$ using inductive driven, whilst not precluding the possibility of controlled plasma ignition ($Q = \infty$). In less than 50 years another reactor of DEMO, the 1st one demonstrating electricity generation, will be constructed after ITER.

The achievements of the present large tokamak devices and those expected on ITER indicate that it is scientifically feasible to make fusion on earth. From now on, emphases should put on making fusion energy competitive to other energy sources. W.D. D'haeseleer pointed out that two major issues must be concentrated on for a future economic viability of fusion power plants [18]. The capital cost should be as low as possible, and the down time of the reactor should be reduced to the minimum. To reduce the capital cost, it must be strived for small, simple and thus cheap reactor. For example, ITER is too complicated for routine electricity generation. In addition, it should be considered to use fusion energy as a heat for various industrial applications to enhance the energy efficiency of the entire fusion plant [19]. On the issue of limited

down time of a nuclear fusion plant, it is of uttermost importance that the fusion plant has a high availability. Availability percentage of 80% over the entire lifetime should be aimed for. To keep the high availability, the following technical issues should be resolved. First, a safe and efficient tritium handling technique must be developed. Second, the fusion reactor materials must be able to survive high heat flux, retain strength at high temperature and keep ductility despite neutron irradiation and be low activity. In terms of the applications in a fusion reactor, major fusion materials are classified into plasma facing materials (PFMs) and structural materials (SM) for vacuum vessel and blanket. Furthermore, any component, especially the in-vessel ones, should have high performance and be sufficient long lifetime.

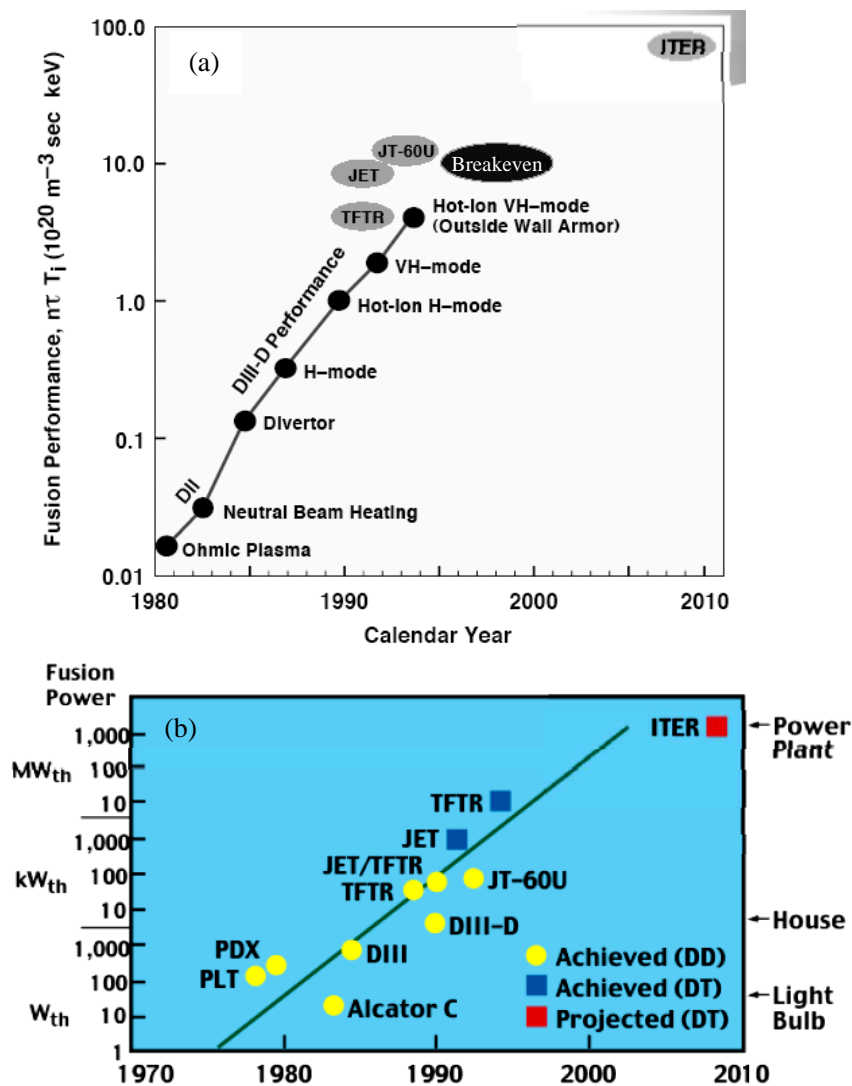


Fig. 1.4 The progress of fusion triple product (a) and fusion power (b) [7].

Plasma-facing materials have to withstand particles and heat loads from the plasma and neutron loads during reactor operation. The critical plasma-wall interaction issues for plasma-facing materials (PFMs) were summarized in [20]. The surface of the plasma-facing material (PFM) is subjected to erosion by energetic ions and neutral atoms escaping from the plasma. In addition, high transient heat loads during strong edge localized mode (ELM) activity of the plasma or off-normal events like disruptions can cause ablation from the heated surface. Tritium is absorbed by the PFMs or it can be chemically bonded to redeposited material. Neutron damage can lead to the degradation of the mechanical properties and in some cases to a decrease of the thermal conductivity and dimensional changes of the PFMs [21]. Major candidates are W [22] (high-Z PFM), Graphite or Carbon based materials such as CFC [23,24], Be (PFM to be used in ITER) [25, 26] and so on.

It is expected that the experiences gained by the ITER operation will allow the operation of a fusion reactor under stationary and non-disruptive plasma conditions. The sputtering erosion process of the PFMs during normal operation will determine the component lifetime and leads to plasma contamination. Among the candidate PFMs is the W having the lowest sputtering rate with the present good control of the edge plasma temperature to several eV. W has been used as PFMs in the ASDEX Upgrade tokamak device [22]. Big progress has been achieved and the operation results indicated that W would be a viable candidate for the future device, and the authors even suggested using W as first wall armour in ITER in the late phase of its operation.

1.3 Candidate structural materials and issues

1.3.1 General

The long-term goal of fusion materials researches is to develop structural materials that will permit fusion to be developed as a safe, environmentally acceptable, and economically competitive energy source. Three material systems have been judged to have the potential for being developed as fusion power system structural

materials. They are reduced activation ferritic/martensitic steels (RAFM), V-based alloys, and SiC composites for near-, mediate- and long-term applications. The common requirements for fusion structural materials are that

- (1) the material could withstand high neutron wall loads under temperatures and coolant pressure conditions necessary to drive efficient thermodynamic cycles in a blanket;
- (2) the lifetime of structural material must be long enough to minimize the necessary replacements of near-plasma components; and
- (3) the material should be of low activation in order to achieve the ultimate environmental attractiveness of fusion power.

Table 1.2 shows the general parameters of the future fusion devices [27], based on present knowledge in plasma and fusion technology. ITER is just an experimental reactor while the other two are reactors for power plants. In comparison, ITER has much lower fusion power and neutron wall load. 316L(N), essentially not a low activation material, will be used as the major structural material for ITER. For future fusion power reactors, the neutron wall load would be high up to 3 MW/m^2 , and hence advanced structural materials should be used. The integrated neutron wall load in MWy/m^2 and the derived displacement damage will limit the lifetime of reactor components.

Table 1.2 General performance parameter for fusion devices^a

	ITER	DEMO	REACTOR
Fusion Power, GW	0.5	2-4	3-4
Neutron wall loading (first wall), MW/m^2	0.57-0.78	2-3	2-3
Integrated wall load (first wall)			
In MWy/m^2	~0.3-1	3-8	10-15
In displacements per atom (dpa)	1.7-5.5	30-80	100-150
Operation mode	Pulsed	Quasi-continuous	

^a Some data for ITER are modified according to ITER documents [28].

Several fusion reactor blanket concepts were proposed based on the properties of the candidate structural materials, the available tritium breeders and neutron multipliers. They are listed in Table 1.3 and could be classified with regard to the breeding materials into two categories: solid ceramic and liquid metal breeders with

the options of self-cooled or separately cooled versions. Primary expected temperature ranges of operation for structural materials and thermal efficiency for various blanket concept design [29-31] are indicated. The temperature ranges are based on estimations of achievable maximum temperatures, limited by high temperature creep-rupture strength and/or corrosion resistance by breeding materials or coolant, and on coolant inlet temperature or possible low temperature limits set by irradiation hardening and embrittlement. The thermal efficiency increases with the increase of the upper operation temperature, and could be further increased by use of more advanced material/technology and blanket concept. A Li/W blanket could have an efficiency of ~60%. Similarly, the use of oxide dispersion strengthened steels or vanadium alloys makes certain increase in the efficiency.

Table 1.3 Major breeding blanket concepts [27,29-31]

	Coolant	Breeding material	Structural material	Neutron multiplier	Operation Temperature (°C)	Thermal efficiency (%)
He/LiCe/FS/Be*	He	LiCe	F/M steel	Be	250-550	~40
He/LiCe/SiC/SiC/Be	He	LiCe	SiC/SiC	Be	450-950	50
Li/V	Li	Li	V-alloy	Li	350-750	46
He/Pb-Li/FS	He	Pb-Li	F/M steel	Pb-Li	250-550	~40

*LiCe – Lithium ceramic breeder materials such as Li_2O , Li_4SiO_4 , Li_2ZrO_3 and Li_2TiO_3 .

From the Table is Li/V blanket obviously the simplest and 2nd most promising one due to its 2nd high thermal efficiency and because it is a self-cooled blanket with Li as both tritium breeding and neutron multiplier materials, providing high economical performance of a fusion reactor. Vanadium alloys have good compatibility with liquid Li [32], and are considered to be the only viable structural material for self-cooled lithium blanket concepts. On the other hand, due to high tritium permeability [33] and incompatibility with even low partial pressure of oxygen [34], self-cooled lithium blanket systems are the only breeder/coolant that is considered to be applicable for vanadium alloys.

Structural materials in a fusion reactor will operate in a very demanding environment that includes various combinations of high temperatures, chemical interactions, time-dependent thermal and mechanical loads, and intense neutron fluxes.

One of the major material issues to be faced in developing attractive fusion power is the effect of the intense neutron fluxes. The 14MeV neutrons by DT reaction not only results in high displacement rates but also causes high transmutation product of He. The neutron irradiation and its products have strong effects on the physical and mechanical properties of structural materials. Thus it could be concluded that the lifetime of a component would depend on the thermal creep and/or fatigue properties of the material with the synergetic effects of other environmental factors unless an accident such as brittle fracture, unstable plastic flow, etc.

Neutron irradiation not only leads to degradation of mechanical properties but also to the production of radioactive materials. To maintain the friendly good environmental characteristics of fusion energy, low activation materials must be used. The proposal criteria for low activation materials could be found in [35], in respect of maintenance, safety, recycling, and waste disposal. As an example, the author mentioned that dose rate inside plasma chamber should be below $1 \times 10^4 \text{Gyh}^{-1}$ after 1day cooling, based on tolerable doses to electronic components for remote maintenance. Only a few of elements have acceptable radiological safety performance and low long-term radiation levels following exposure to the high energetic neutron fluxes. The most promising elements are V, Cr, Ti, C, Si, Fe, Mn, etc. [36, 37]. So V-Cr-Ti alloys and SiC/SiC composites are typical low activation materials for fusion applications. However, cares must be taken to control the common impurities of high long-term radioactivity, such as Ag, Bi, Nb and Mo, to several wppm for Mo and lower than 1 wppm for others for vanadium alloys to keep the low activation nature. For steels, the principle approach adopted to reduce the neutron induced activation involves the substitution of elements of W, V, Mn Ta, etc., which have an equivalent influence on the constitution and structure but a lower radiological impact, for some of the principle alloying elements such as Mo, Nb and Ni in the existing commercial steels. Similar stringent control of the impurities is required as that for vanadium alloy.

Another sequent of induced radioactivity is the decay heat after shutdown of a power reactor. If a non-low-activation material were used, the heat would be very high

enough to melt the material, and to solve this problem forced cooling is required even after the shutdown. In summary, the safety, environmental and economical performances of fusion power system could be highly enhanced by making use of low activation structural materials.

1.3.2 The advantage and disadvantage of the candidate structural materials—a comparison

Each candidate has its advantage and disadvantage as fusion reactor structural material, which are discussed as follows.

(1) The low activation performances of the candidates

There are numbers of studies addressed the issues concerning radioactivity, after-heat decay, contact dose and biological hazard potential of the candidates after neutron irradiation [35,36,38,39]. Vanadium alloys exhibit lower radioactivity, lower after heat, lower contact dose and less biological hazard than the steels at any time and than SiC composite at more than ~60 years after reactor shutdown. Neutron-activated vanadium alloys have high feasibility of recycling utilization after hundreds of years. However, the short-term radioactivity of vanadium alloys is much higher than SiC. W-Re alloys are taken as the potential blanket structural material in the long-term future, this alloy was included in Karl Ehrlich's study [38]. Figure 1.5 presents a clear comparison of the decay heat and contact dose rate for SiC/SiC composite, V-4Cr-4Ti alloy, EUROFER F/M steel and W-5Re alloy as a function of the decay time. The W-5Re alloy shows the worst case, and it is still doubtful whether much better thermo-physical and strength properties of the alloy can outbalance this weakness. At this point of view, SiC/SiC has by far the greatest potential, not only because of the lowest values in the very short term, but also because of a faster decay for short and intermediate decay times. This fast decay is of importance for the case of an immediate shutdown of a reactor since a dispersion of radioactivity by material volatilization could occur and could pose safety problems. But the relatively high long-term dose rate due to the induced ^{26}Al is disadvantageous. It is finally concluded in [35] that it may not be possible to develop materials that simultaneously satisfy the

short-term maintenance and safety and the long-term recycling and waste disposal criteria. However, vanadium alloys appear to represent the best compromise in these aspects.

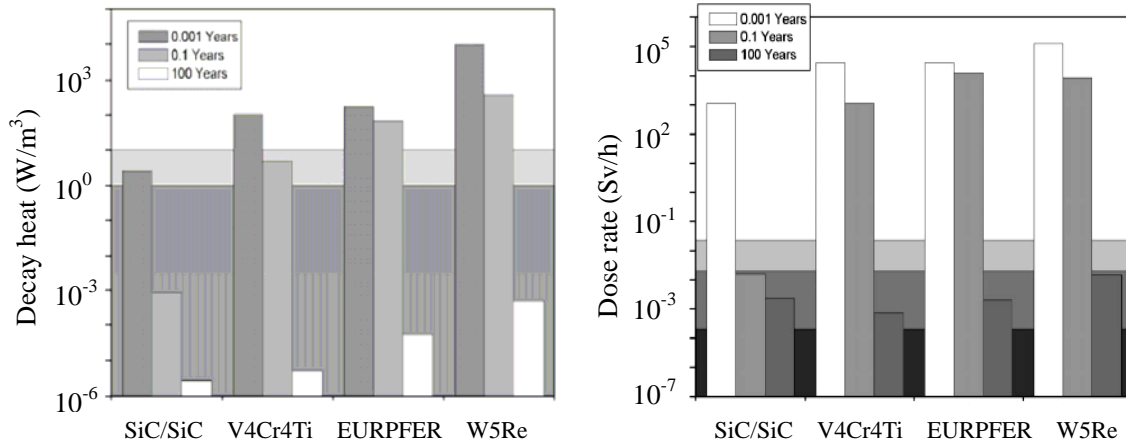


Fig. 1.5 The decay heat (left) and surface- γ -dose rate (right) of structural materials in a DEMO-FW position after an exposure to 10 MW/m^2 as function of the decay time.

(2) High-temperature creep strength

Figure 1.6 shows the creep strength as a dependence on the Larsen-Miller parameter for unirradiated V-base alloys, ferritic steel (HT-9) and austenitic 316 SS either in annealing or 20% CW (cold-working) states. It clearly indicates that vanadium alloy has superior high-temperature creep resistance to the steels, particularly in the high temperature range. The creep strength increases with increasing Cr concentration.

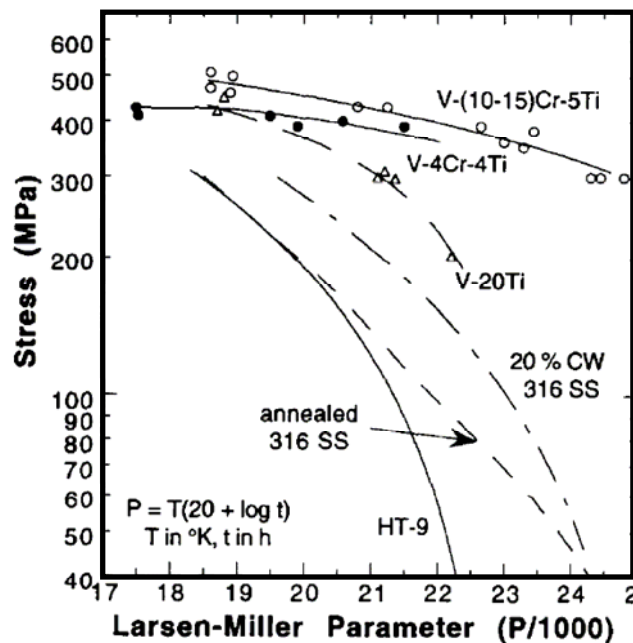


Fig. 1.6 Larsen-Miller plots of creep strength of unirradiated V-4Cr-4Ti and ferritic and austenitic steels [40].

316 SS is better than HT-9 at

high Larsen-Miller parameter. Cold working (CW) could improve its creep property

significantly.

Figure 1.7 shows the creep strength of V-4Cr-4Ti [41], F82H (F/M steel) [42] and ODS-EUROFER (oxide dispersion strengthened EUROFER F/M steel) [43], all are low activation materials. Comparing with that shown in Fig. 1.6, it could be found that the creep property of the low-activation steel exhibited certain improvement at high Larsen-Miller parameter. Though remarkable improvement by the ODS is achieved for F/M steel, ODS-EUROFER is still inferior to vanadium alloys at this creep strength property. The good high temperature creep resistance of V-base alloys should arise from the high melting temperature of V and the combination contribution of Cr, Ti and other interstitial solutes in the alloys as well, which will be further discussed in other sections.

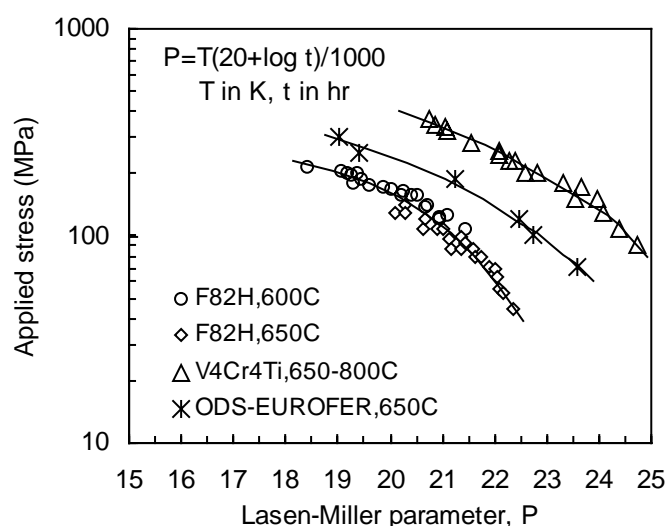


Fig. 1.7 Larsen-Miller plots of creep strength of unirradiated V-4Cr-4Ti and other low-activation-ferritic-martensitic steels.

(3) High-temperature strength

Figure 1.8 shows the ultimate tensile strength as a function of temperature for unirradiated structural materials [44], including potential ones and those to be used for ITER in-vessel components. However, Nb-1Zr alloy, a candidate structural material for space power systems [46], should be impossible for fusion application on earth for its high radioactivity. In the figure is not included the candidate SiC/SiC composite, whose ultimate tensile strength is, strongly dependent on the fiber-matrix interfacial

layer and weekly dependent on test temperature, about 220-240 MPa at 20-1000°C for two products fabricated with cg-Nicalon fibers [45]. The figure shows that the F/M steel has much higher strength at low temperature than the vanadium alloy. But the F/M steel heavily loses its strength at $> \sim 400^\circ\text{C}$, which becomes lower than that of V-4Cr-4Ti at above 600°C. For the EUROFER 97, the temperature may be down to $\sim 550^\circ\text{C}$ since this steel has lower high temperature strength [43] than the F/M steels shown in Fig. 1.8. Ta-8W-2Hf looks very promising for fusion application for its possibly low activation property estimated from Ref. [37] and its excellent high temperature strength [47].

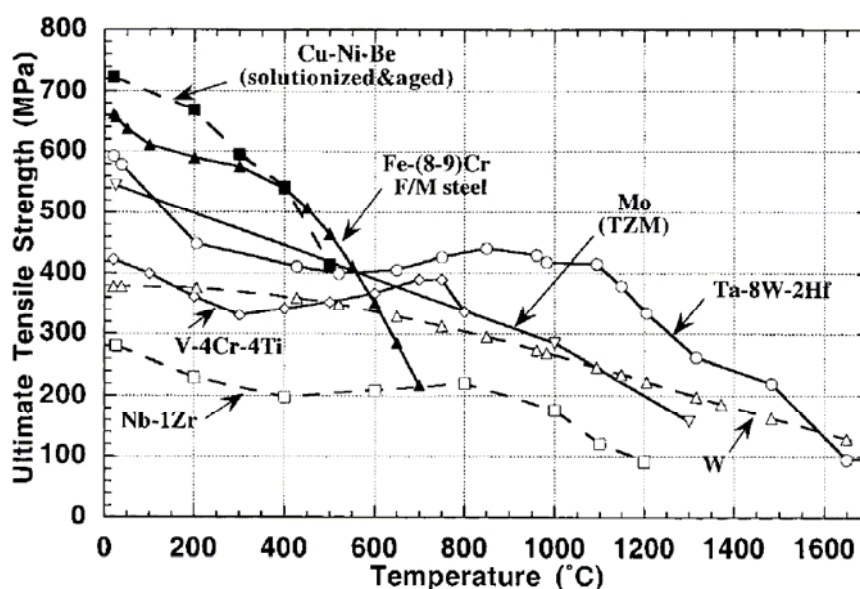


Fig.1.8 Comparison of the ultimate tensile strength of recrystallized refractory alloys, solutionized and aged Cu-2%Ni-0.3%Be and Fe-(8-9%)Cr ferritic-martensitic steel.

(4) Ductile-Brittle transition temperature (DBTT)

DBTT, a very important property for the structural materials, is desired to be low to ensure any component serves above it for safety. Fig. 1.9 shows the Charpy impact test results for two kinds of candidate structural materials of V-4Cr-4Ti and RAFM steels. It indicates the temperature is well below room temperature, particularly for V-4Cr-4Ti, whose DBTT is much lower than that of the RAFM. For heat 832665 in 1000°C/1h annealing state, the DBTT is lower than liquid nitrogen temperature. Therefore, the DBTT for these materials is desirable for the application as blanket

structural materials. But neutron irradiation will generally cause significant increase in DBTT, should be taken into account in their application in fusion reactors.

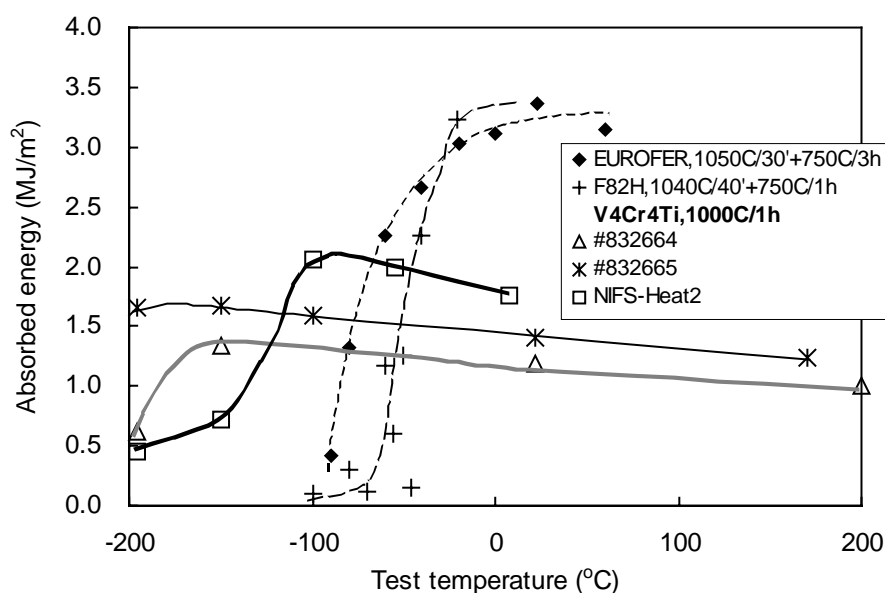


Fig.1.9 Absorbed energy vs. test temperature for RAFM of EUROFER 97 [48] and F82H [42], V-4Cr-4Ti alloy of 832664, 832665 heats [49] and the NIFS-Heat 2 [50].

(5) Low cycle fatigue lifetime of the materials

So far little information is available on fatigue properties of SiC/SiC composites. For vanadium alloys, there are only limited data generated for V-5Cr-5Ti and V-15Cr-5Ti [51]. The fatigue data for V-5Cr-5Ti suggests that it has stronger resistance to fatigue failure than the conventional 316SS in the temperature from 25 to 400°C. There are relatively more fatigue data for ferritic/martensitic steels [52-57]. Data on V-5Cr-5Ti, EUROFER and F82H (mod.) are plotted in Fig. 1.10. It shows that the fatigue life for V-5Cr-5Ti is much longer than the RAFM steels. EUROFER 97 is a little better than F82H mod. due to the crack initiation at precipitates of mixed composition Ta, Al(O,C) near specimen surface for the F82H mod.[43]. The fatigue behavior of the F/M steels is different from that of the vanadium alloys. In contrast to the negative temperature dependence of the fatigue life of the steels, the vanadium alloy showed an increasing fatigue life with increasing temperature. However, fatigue resistance of vanadium alloys can be severely degraded with oxygen contamination even at room temperature [51].

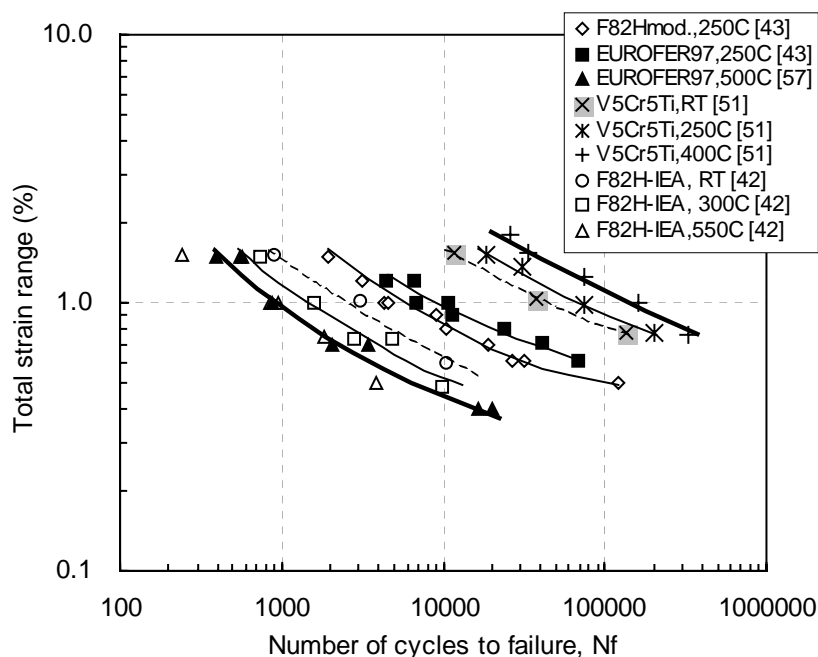


Fig. 1.10 Relation of the total strain range with the number of cycles to failure for EUROFER 97, F82H and V-5Cr-5Ti. The steel specimens were tested at strain rate of 3×10^{-3} /s in vacuum of $\sim 10^{-5}$ Pa, while the vanadium alloy was tested at strain rate of 4×10^{-3} /s in vacuum of 7.3×10^{-6} Pa.

(6) Critical issues

Great progress has been made for the development and understanding the behaviors of structural materials for fusion reactors over the past 25 years [58]. Nowadays, based on the present knowledge on the materials performances, the operating temperature windows have been roughly determined for various tritium breeding/coolant concepts [44,59]. Looking into future, candidate RAFM steels and probably vanadium alloy will soon be used in ITER as structural materials for test blanket modules [60-62]. With the solution of feasibility issues, such as tritium breeding rate and inventory, etc., one will be chosen and improved for future application in DEMO reactor. Though the road map sounds exciting, there are still certain key issues to be investigated, some of which even requires the aid of an intense neutron source of fusion-relevant energy, to be supplied by a planned large accelerator nominated as IFMIF (International Fusion Material Irradiation Facility).

There are many papers described and analyzed the critical issues for the candidate structural materials [27, 56, 58, 63-68]. One of the major issues is the effect of intense

neutron fluxes. The 14 MeV neutron released by the DT reaction not only results in high-displacement rates ($\sim 20\text{dpa/yr}$ at a neutron wall loading of 2 MW/m^2) but also causes high transmutation products of He, H and other impurity nuclei. The neutron irradiation is a particularly important issue, due to both its effects on physical and mechanical properties, as well as the production of radioactive materials, which have strong impacts on the maintenance and on the safety and environmental features of the reactor. Related to this important issue, another important concern is the lack of a fusion-relevant neutron source, the means using to verify the validity of the present results obtained by simulation irradiation with fission neutron and modeling.

For metal materials, atomic displacement by neutron irradiation will generally cause, at high temperature, swelling and at low temperature, hardening and embrittlement which is the determining factor for the low temperature operation limit. These effects could be mitigated by control the chemical composition and microstructure of the material. As an example, for vanadium alloys, the neutron irradiation hardening is resulted from the formation of ultra-fine precipitates, most likely being Ti (CON) type [69-71], and dot dislocation loops in high number density, hence could be mitigated by lowering the C, N and O interstitials in the matrix [72]. In M. Satou's study [72], the low concentration of C, N and O concentration is attained by adding a small amount of Al, Y and Y to V-4Cr-4Ti [73]. The alloy showed weaker irradiation hardening and higher strain hardening capability as compared to V-4Cr-4Ti after irradiation in ATR at $\sim 400^\circ\text{C}$. In addition, a very important finding is the strong effect of pre-irradiation annealing on the irradiation results [71]. The one annealed at 900°C remained an uniform elongation of $>3\%$ while others pre-annealed at higher or lower temperature nearly lost their strain hardening capability completely after irradiation at $\sim 300^\circ\text{C}$ for $\sim 4.6\text{ dpa}$. Virtually, V-4Cr-4Ti in 900°C annealing state contains more large precipitates (thus fewer C, N and O interstitial solutes) [74], having lower strength and higher ductility [50] than those annealed at other temperatures. Therefore, the good resistance to neutron irradiation of the 900°C -annealed one should be related to the low C, N and O concentration in matrix due to the existence of large number of large precipitates.

To suppress irradiation swelling in vanadium alloys, essentially Ti in 3-10%wt is required. Results showed that irradiation swelling is well below 1% at irradiation dose of 73-84 dpa for the alloys with Ti concentration in this level [75]. It was found, in the early study [76], the formation of Ti_5Si_3 precipitates, which act as strong sink sites for radiation-induced point defects, eventually mitigate the swelling when V-Cr-Ti alloys were irradiated at $>400^\circ C$. It well illustrated that swelling by neutron irradiation could be reduced by controlling chemical composition.

For SiC composites, a type of ceramic material, the main issues related to the neutron irradiation is the degradation of thermal conductivity at $<600^\circ C$ even at <1 dpa, and the neutron irradiation induced swelling and creep at $> \sim 1000^\circ C$ [44,65]. These performances determined the operation temperature window of the material.

A major focus related to the radiation effects for the future will certainly be the effect of helium on the microstructural stability of irradiated materials and its impact on properties. The physical phenomenon dominantly depends on irradiation temperature. At low temperatures, enhanced hardening due to He bubbles and the possible change of mechanisms for fracture toughness embrittlement are leading concerns. At intermediate temperatures, void swelling and phase stability will be major topics, particularly the possible maximized swelling near fusion-relevant He/dpa rates. At high temperatures, major concern is helium embrittlement of grain boundaries for steels and refractory alloys.

Table 1.4 illustrated the approximate amount of displacement damage, and H and He transmutation products in candidate structural materials as first wall after an integrated neutron wall load of 15 MWy/m^2 [64]. Values given are only approximate since precise values are dependent on the specific design configuration and the combination of materials. Primary observations from this table include (1) the very high He and H transmutation rates but slightly low displacement damage rate for the SiC/SiC composite, (2) the relatively low He and H transmutation for the vanadium alloys. Based on these data alone, the lifetime of the SiC/SiC composite with the high helium generation rate is a major concern regarding the feasibility of this material. This issue will in all likelihood be exacerbated by the high hydrogen transmutation

rate and the fact that hydrogen diffusion/permeation in SiC is very low. The relatively high He generation rates for all materials compared to those in a fission reactor spectrum represent one of the major lifetime issues for a fusion first wall system [77], and this gives rise to another issue of the difficulty to investigate the combination effects of the fusion-relevant displace damage rate and helium generation rate with the present available fission reactors, as well as the urgency to construct an appropriate fusion materials irradiation facility such as IFMIF. In the designed IFMIF, 35-40 MeV D^+ beams will be focused onto a common flowing liquid lithium target and produces neutrons at high intensity via a stripping reaction with a suitable energy spectrum peaking at around 14 MeV. Details could be found in Ref. [78].

Table 1.4 Neutronic parameters of candidate first-wall/blanket structural materials [64]

Alloy	dpa (15 MWy/m ²)	He transmutation (15 MWy/m ²) appm	H transmutation (15 MWy/m ²) appm
Austenitic steel (316)	170	2400	8550
Ferritic steel (9Cr-1Mo)	170	1800	7350
Vanadium alloy (V-4Cr-4Ti)	170	855	4050
SiC/SiC composite	135	19500	13350

Beside the neutron irradiation effects, other critical issues for the candidate RAFMs, vanadium alloys and SiC/SiC are summarized as follows:

- RAFMs [58]: There seems to be two critical issues to be address in the future. One is the possible adverse effect on plasma control and performance due to the ferromagnetic properties. Another is the relatively low strength at high temperature, which is hard to be improved by alloying such as adding V and N. But fortunately, oxide dispersion strengthened steels may enable significant improvements in the upper temperature capability based on improved thermal creep strength.
- Vanadium alloys [58,79]: There are several critical issues for the alloys used in a self-cooled blanket. The main one is the development of insulator coating to mitigate MHD pressure drop effects in liquid lithium coolant channels. Additional topics where further work is needed include investigation of possible engineering

solutions to the high tritium permeability in vanadium alloys, determination of irradiation creep behaviors at 400-700°C and the fundamental deformation mechanisms that control high temperature thermal creep, and the incomplete understanding of the influence of interstitial impurities such as C, N and O on tensile, creep and fracture properties. The lack of a widespread commercial infrastructure for production of vanadium alloys is also of concern.

- SiC/SiC composite [58,80]: The remaining issues include the low thermal conductivity of most commercially available products, high-strength joining techniques leading to a high difficult for hermeticseals, chemical compatibility with potential liquid coolants, the need to develop engineering structural design criteria for ceramics, and so on. There are also concerns regarding high present-day fabrication costs [44] and the limited industrial technology base for production of large-scale SiC composites.

1.4 Progress towards the solution of critical issues of vanadium alloys for fusion reactor

1.4.1 Technologies for large-scale vanadium alloy products

One of the key issues associated with vanadium alloy development is the absence of a large industrial production infrastructure. Within the past 10 years, big progress has been achieved worldwide in obtaining experiences and technologies for high-quality large vanadium alloy heats.

Two large heats of V-4Cr-4Ti were procured in the US from Oremet-Wah Chang before 1998. Heat 832665 is a 500 kg heat procured by the US Department of Energy for basic fusion structural materials research [81]. Heat 832864 is a 1200 kg heat procured by General Atomics for the DIII-D radiative divertor upgrade project [82]. Around 2000, a middle heat (NIFS-Heat-1, 30 kg) and a larger one (NIFS-Heat-2, 166 kg) were fabricated by National Institute for Fusion Science in Japan [83,84]. IN Russia, two 50 kg heats of V-4Cr-4Ti and V-5Cr-10Ti were fabricated around 1996 [85]. The heats were usually hot extruded, hot and cold rolled, and products in forms of plate, sheet, rod, and tube were successfully obtained in quality. As cares were

taken in the high temperature fabrication process and high purity or purified vanadium metal was used, the alloy products have desirable impurity concentrations of C, N and O. In particular for the NIFS heats, the total concentration of C, N and O are below 340 wppm [84]. These achievements proved the feasibility to fabricate vanadium alloys in large scale with the present industrial bases. However, microstructural inhomogeneity including grains and precipitates was found for these large heats [66, 86] and methods for improvement should be developed in the future.

1.4.2 Improving properties by controlling impurity and microstructure

The microstructure will change with various thermo-mechanical treatments, not only the change in grain size but also the morphology, size and distribution of precipitates in the alloys. For V-4Cr-4Ti, N.J. Heo studied its precipitation behavior [74]. The alloy in SA (Solid-solution Annealing: 1100°C/1h) state has most of its interstitial C, N and O in solid solution [84], making precipitation possible in the following isochronally annealing. Precipitation occurs at ~600-900°C, was also confirmed in NIFS-Heat-2 [50]. Fine precipitates formed at 700°C or lower, and became coarser with increasing temperature. As the precipitates are verified to be T-CON, the interstitial impurities of C, N and O in matrix also changed with the temperature. Both have effects on the mechanical properties of the alloy. Estimated from the numbers and big size of the precipitates, the alloy in ~900°C-annealing state should have the least solution of the interstitials in matrix, resulting in the most softening state.

Both results reported for the US 832665 [49] and the NIFS-Heat-2 V-4Cr-4Ti [50] indicated that the alloys in the state of ~900°C/1 h annealing have almost the lowest DBTT values. And more important as mentioned in last section, the V-4Cr-4Ti-Al-Si-Y alloy in this state has less extent of neutron irradiation hardening and remains more in uniform elongation after neutron irradiation at ~300°C for a dose of about 4.6 dpa [71]. So it seemed to be able to make a conclusion that the alloy should take this temperature annealing process for better properties, or in another word, the interstitial solutes in the alloy should be kept as low as possible for the

purpose. This was partly further verified in a V-(1.6-2.6)Y alloy, which have strong resistance to neutron irradiation hardening, probably due to the depletion of the interstitials by Y during the historical thermo-mechanical treatments [87]. However, investigation on the effects of the impurities on high-temperature creep rate shows that the creep resistance of the NIFS-Heat-2 will become weaker with the reduction of the oxygen concentration or with the pre-annealing temperature getting closer to 900°C [88]. Thus it is necessary to make a compromise between the neutron hardening, DBTT and creep properties, which determines the operation temperature of the alloy for fusion, by controlling the interstitials to an appropriate level.

1.4.3 Welding vanadium alloys

Many different approaches have been investigated, including gas tungsten arc welding (GTA), laser welding, diffusion bonding, resistance welding, explosive bonding, inertia welding, and brazing. Recent efforts devoted to welding technology are focused on GTA and laser welding techniques. GTA is a suitable technique for joining large structural components. The goal is to develop robust joining techniques that produce joints with adequate strength, ductility and fracture toughness.

One of the major effects of the joining is increasing DBTT, ductile-brittle transition temperature. Significant progress has been made in lowering the DBTT of GTA welds created in a glove box environment since 1995 [65, 89-91]. By installing gettering systems to remove oxygen, hydrogen and water vapor from the glove box evacuated to 10^{-4} Pa level followed by filling in with 99.999% argon and using low impurity base vanadium alloy (such as NIFS-Heat-1) and the filler one (36 wppmO), the DBTT was reduced from 228°C to -145°C. High temperature (950°C/2 h) post-weld heat treatments to remove interstitial oxygen from solution by formation of Ti-CON precipitates reduced the DBTT for low-to medium purity GTA welds [89], but was of no benefit on high-purity GTA welds [91].

Development of laser welding techniques has also advanced in the past few years. Laser weld penetration studies utilizing a high-purity argon cover gas have successfully achieved 4 mm penetration depths. Nagasaka et al. [92] recently

completed an exploratory study of the effects of low-dose neutron-irradiation on the impact properties of NIFS Heat-2 welding metal by YAG laser in a high purity Ar. Essentially no change in the oxygen, carbon and nitrogen levels was found, and almost no difference of the DBTT of the weld metal to the base one. Miniature Charpy impact specimens of V-4Cr-4Ti base and weld metal were irradiated at 290 °C to a dose of 0.08 dpa in the JMTR. Weld metal specimens hardened more than base metal specimens, but the effects of neutron irradiation were reduced if a post-weld heat treatment in the range 600–950°C was applied prior to irradiation. However, in the earlier investigation of welding V-4Cr-4Ti (832665) by CO₂ laser in air showed a much higher DBTT of 80°C, and it was pointed out that a post-weld heat treatment of 1000°C/1 h in vacuum is sufficient to restore its impact properties [93].

In summary, the goal to produce joints with adequate strength, ductility and fracture toughness could be reached by using high purity vanadium or filling metal and welding alloy in protection atmospheres containing small amount of impurity gases. Further topics for investigations should be place on the effects of neutron irradiation on the joint property and thermal aging effects at around 700°C due to interstitial impurities releasing into solution by dissolution of Ti-(CON) precipitates during welding.

1.4.4 Insulation coating

One of the major issues for V-Li blanket is the megneto-hydro-dynamic (MHD) pressure drop caused by the Lorenz force due to the interaction of strong magnetic field and the flowing lithium as tritium breeder, neutron multiplier and coolant. To mitigate the MHD pressure drop and hence to maintain high flow velocity of the coolant to reduce the peak temperature of vanadium structures within the operation temperature limit, one of the potential ways is to coat an insulation layer on structural wall to separate the liquid from direct contact with the alloy and decreasing the inductive currents. Theoretical calculations indicated the required resistivity of 1µm coating is about 10⁴ Ω m for a negligible MHD pressure drop [94] or in the range of ~10²-10⁴ Ω m [95].

Over the past 40 years, considerable progress has been made though even today the issue is still a great concern for investigation, far away from solved. Primarily, oxides and nitrides of CaO, Y₂O₃, BeO, MgO, MgAl₂O₄, Y₃Al₂O₁₂, AlN, BN and Si₃N₂ were considered as potential candidates based on thermo-dynamic considerations and electrical resistivities of monolithic materials. With the characterization of their compatibility in lithium, better ones were chosen for further investigation, such as CaO, Y₂O₃, BeO, AlN and Si₃N₂. Over the past decade, CaO and AlN have been extensively investigated [94-98]. There are several methods for the coating, among which self-healing was the most concerned. Both CaO and AlN seemed to be compatible with Li under the reported experimental conditions. The CaO coatings exhibited much higher electrical resistivity than as required, while the electrical properties of AlN are marginal. Most importantly, self-healing of the two coatings seemed to be possible due to that Ca, Al, O and N are soluble in Li, and the healing process was partly confirmed in experiments. However, A compatibility study by Pink, et al., showed that both are not stable in Li particularly at high temperature under certain conditions relevant to the V/Li blanket [97]. Thus both coatings were proved to be not feasible for application in the blanket [98].

Recently, investigations are focused on Y₂O₃ and Er₂O₃, both are stable and have high electrical resistivity. Z. Yao et al. [99] put oxygen pre-charged V-4Cr-4Ti alloys in Li containing 0.15%wt Er at 600°C for times up to 300 h. A 1.5 μm thick surface layer of Er-rich oxide was observed with which the sample showed an electrical resistivity of ~10¹¹ Ω m at room temperature. In US, a 12.5 mm thick Y₂O₃ was prepared by EB-PVD on V-4Cr-4Ti substrates. The coated samples were exposed to Li at 700 and 800°C for 100-1000 h [98]. Again compatibility problem arose due to the formation of a LiYO₂ layer at the Y₂O₃-Li interface.

Considering the unavoidable defects such as cracks in the coating, which will cause the loss of its role to mitigate MHD pressure drop, a dual-layer MHD coating system was proposed, with the first metallic layer such as vanadium alloy as corrosion resistant layer and the second ceramic coating layer as insulating layer [98,100]. In this instance, there will be no compatibility problems for the insulation coating. Big

concern will be firstly the feasibility of fabrication of such a complex structure and secondly the integrity and compatibility issues of the thin top layer.

In summary, insulating coating on vanadium alloy is far more from success. In situ coating has the advantage for complex shape structures and could have the potential of self-healing. This kind of coating should be further investigated, especially on the feasibility to simultaneously form the coating in a flowing Li at 350-750°C, the approximate operation temperature for the V-Li blanket.

1.5 Objectives and characteristics of the present study

As stated above, the researches for vanadium alloys have achieved a lot but a number of issues still remain for further investigation to completely understand the essential philosophies and look for a final solution. As for the effects of interstitial impurities and substitutional solutes on mechanical properties of vanadium alloys, much has been done in the previous decades for optimizing alloy compositions and processing for better performances [101-103]. Many kinds of V-Cr-Ti, V-Cr and V-Ti alloys were developed for the purpose, with Cr in the range of ~3-15%, Ti in 3-20% in mass. By comparing the tensile properties, DBTT values, creep strength and other properties, V-4Cr-4Ti was determined as the best one for its very low DBTT and good thermal creep properties (not as good as the high Cr and high Ti alloys [40]). In recent years, the behaviors are still under investigation as has summarized in the above sections and reported in other papers [104-106]. For each solute, interstitial or substitutional, its role on mechanical properties is almost known well. But the combination effects of the common solutes are not completely understood. Ti is well known to have strong effect on mobility of interstitial C, N and O, and is the cause of major precipitation in V-Cr-Ti alloys, both resulting in strong effects on the recovery, strength at room and high temperature, etc. However, interactions among other alloying elements were scarcely investigated, such as the one between Cr and Ti, which may have certain effects on the mechanical behaviors.

Precipitation is generally not welcome in high temperature service for the purpose

of keeping a good thermal stability of an alloy. But small effort has been made on the feasibility to utilize the precipitation for enhancing the strength of vanadium alloy structures. Effect of alloying elements on precipitation needs to be studied further. In particular, the resistance to low-temperature radiation hardening might be improved due to the precipitation if the precipitation is properly controlled to have most of the interstitial solutes in matrix absorbed.

Hydrogen effects may be an issue for vanadium alloy. Hydrogen may come from the blanket environments and be produced due to transmutation. Previous studies have shown hydrogen embrittlement of V-4Cr-4Ti, evaluated by tensile tests at room temperature [107,108]. The critical hydrogen concentration to embrittle the alloy (#832665) is about 550 wppm. This critical value seemed to be acceptable but the fracture toughness might be severely affected and should be evaluated. But so far data on the effect of hydrogen on fracture toughness was quite limited. Hydrogen release during annealing [109] or deformation [110] was reported but its effect on mechanical properties and its correlation with the applied stress were not well investigated.

The deformation behavior of vanadium alloy is not fully understood, especially the one under constant stress and when a vanadium alloy contains high hydrogen concentration, like the thermal creep.

Eventually, concerning the above issues related to vanadium alloys, the objectives of the present study are:

- (1) To clarify the effects of interstitial and substitutional solutes on mechanical properties of vanadium alloys for fusion application. Emphases were placed on the mechanisms of hardening by C, N and O, effects of Ti on the role of C, N and O, role of Cr on the interaction of Ti with C, N and O. The role of substitutional solute of W, which is a potential alternative to Cr, was also investigated.
- (2) To understand the hydrogen behavior in V-base alloys.
- (3) To identify the factors having great effects on hydrogen embrittlement and hydrogen-induced change of mechanical properties.
- (4) To support the optimization of chemical compositions and processing steps

of vanadium alloys and the impurity control during the use in the blanket structure.

- (5) To accumulate data of significance for the V-4Cr-4Ti alloy for fusion applications.

According to these objective, various alternatives of V-Cr-Ti-W-Al alloys for fusion blanket application were prepared. The recovery and recrystallization, the hardness and the hardening by both precipitation and cold rolling, thermal stability of the hardening, tensile properties at room and elevated temperature, fracture toughness, impact energy absorption, hydrogen release and deformation behavior at constant stress at room temperature were investigated for alloys without hydrogen and with hydrogen charged to study hydrogen embrittlement behavior. Based on these measured results and certain microstructure analysis by SEM, TEM and optical microscope, the effect of interstitial C, N, O and H on these properties or behaviors were studied. Emphasis was placed on the possible interaction between the solutes, particularly between Cr and Ti, that seems to have not been studied before, and the interaction between the interstitials with dislocations, and the mutual effects among the interactions.

2. The preparation of the alloys

2.1 Alloy design according to phase diagram

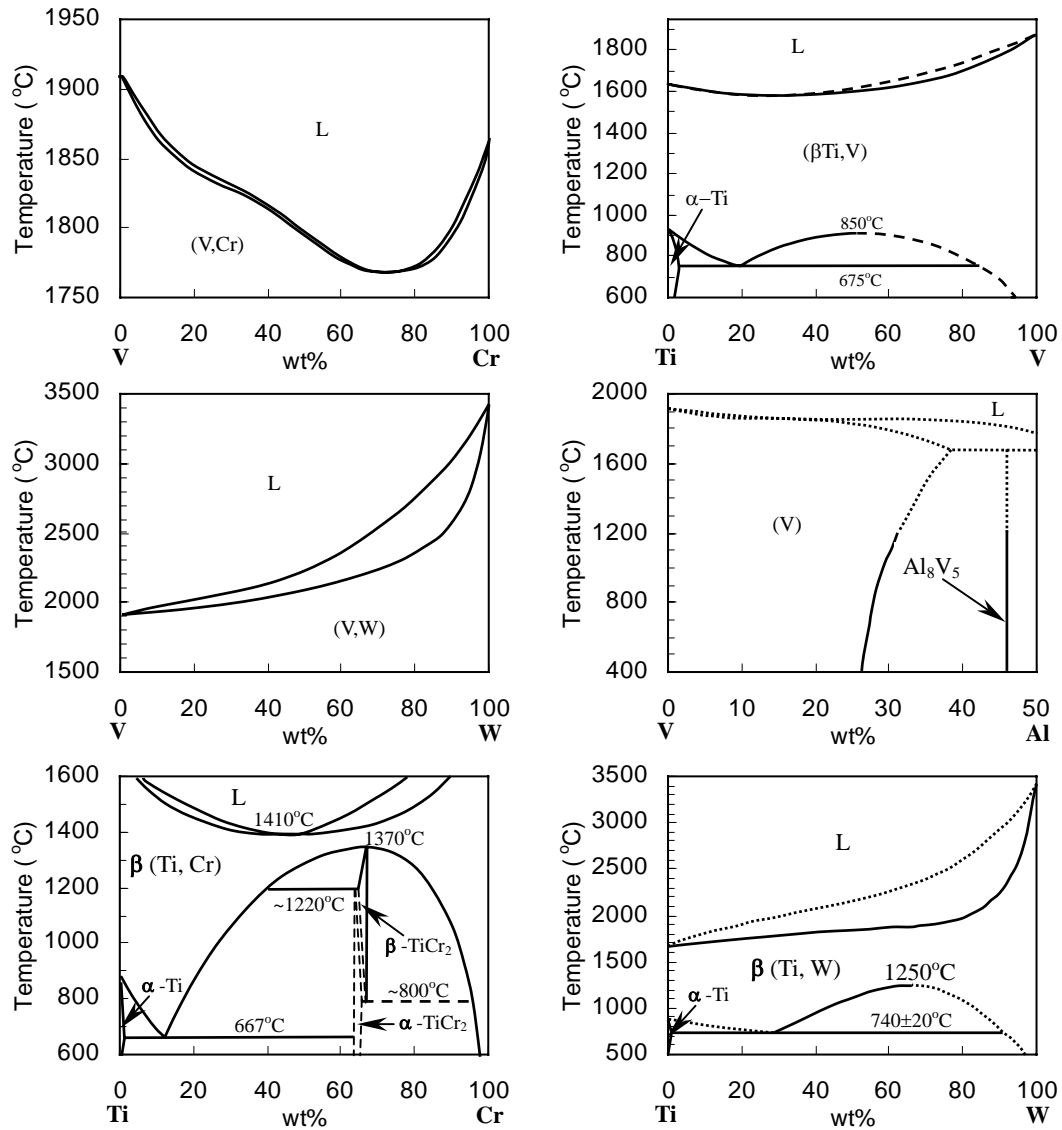


Fig. 2.1 Binary phase diagrams of V-Cr (top left), Ti-V (top right), V-W (middle left), V-Al (middle right), Ti-Cr (bottom left) and Ti-W (bottom right) [111].

Fig. 2.1 shows the binary phase diagram between the main constitutions of vanadium alloys. It could be seen from the figure that V-Cr and V-W could form continuous solid solution alloy due to their similar atomic size. V-Ti could also form continuous solid solution alloy at high temperatures in excess of 850°C but the solid solution phase β-(Ti,V) decomposes into α-Ti and V-rich β-(Ti,V) at 675~850°C depending on the composition. When Ti concentration is less than ~7% in mass such

decomposition may not happen. V-Al is quite different to them. When Al exceeds 25% in mass, intermetallic of Al_xV_y will form. Ti and Cr could form an intermetallic phase of $TiCr_2$ in the Ti-Cr binary system. It is possible that there is a strong interaction between Cr and Ti in V-Cr-Ti system, which may inhibit the diffusion of Ti to form α -Ti. Thus the alloying elements in V-Cr-Ti alloys could distribute homogeneously. The phase diagram of Ti-W is quite similar to Ti-V, a eutectic decomposition occurs at $\sim 740^\circ C$. Based on these phase diagrams, alloying V with single and multi-elements of W, Ti, Cr, Al was designed. The alloys were V-4Ti, V-4Cr-4Ti, V-4Ti-3Al, V-3Ti-1Al-Si, V-8W, V-7W-0.3Al, and V-6W- (1-4) Ti. W is added for an expectation to increase vanadium alloy's high temperature properties since the addition could increase the melting point of vanadium alloys. Al is added to improve oxidation resistance.

2.2 Low activation analysis

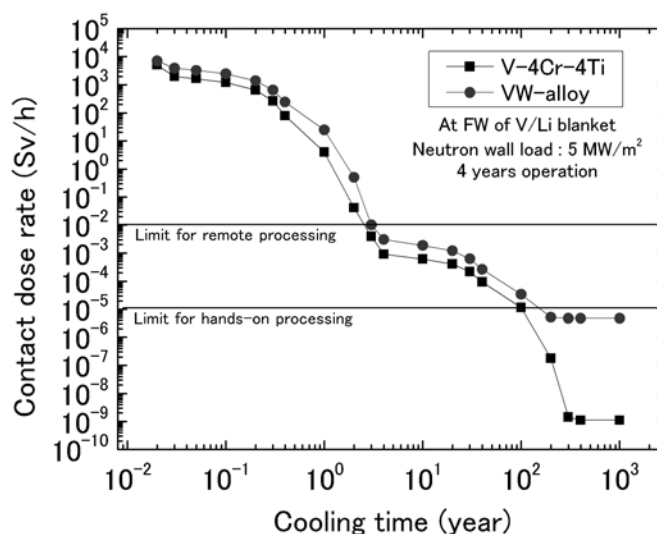


Fig. 2.2 The decay of contact dose rate of V-6W-4Ti (VW-alloy) and V-4Cr-4Ti as a function of cooling time after shut down. The alloys are supposed to have been used in a V/Li blanket for 4 years operation with neutron load of $5 MW/m^2$. Other impurities in the alloys were not considered in the calculation using EASY-99 code.

One of the major merits of vanadium alloy as fusion structural material is its low activation characteristics. The addition of alloying elements should not blemish it much. The decay of contact dose rate of V-6W-4Ti was calculated with an EASY-99 code supposing the alloy had been used in a V/Li blanket for 4 years with a neutron

wall load of 5 MW/m^2 . Results are shown in Figure 2.2, along with that for V-4Cr-4Ti. The activation of VW alloy (V-6.64W-4.12Ti) is a little bit higher than V-4Cr-4Ti, while the shapes of the decay curves are almost same. VW-alloy can achieve the hands-on limit after 200-300 years but its long-term dose-rate is relatively higher than V-4Cr-4Ti, due to the transmutation of W to Re186 by multi-step reactions. Beside, W has high cross section for neutron absorption; hence the use of W may reduce the TBR (tritium breeding rate) [29] of a V/Li blanket. Therefore, the addition of W should be below a critical value to keep the low activation feature of vanadium alloy.

2.3 Alloy preparation

Alloys were melted in a magnetic floating furnace using inductive heating method. Alloying V with W showed some difficulties during melting. The melting temperature of the alloy increases with increasing tungsten concentration. The increase is not so significant in the lower tungsten concentration regime. However, pure W has extremely high melting point and thus could hardly be melted by ordinary heating method such as the inductive heating. In this case, V will be melted first and then W gradually dissolves into the molten vanadium. Figure 2.3 shows the process to prepare the alloys. The original raw materials of V, W, Al and Ti have purity of more than 99.5%. V was in a small powder state and was pressed into large cylindrical rods of about 40 mm in diameter prior to the melting. Higher inductive electrical current could be formed along the outer surface of the cylinder during the heating, leading to a high heating efficiency. Very thin W foils were used in thickness of about 0.1 mm to shorten the dissolution durations. The alloy ingot weight was about 340 grams. The melting was usually conducted for three times, 20 minutes for each, for the homogenization.

The alloy ingots were forged into ~15mm thick plates at $950\sim 1150^\circ\text{C}$ in air. The thickness was further reduced to ~2 mm by the following hot rolling at $\sim 850^\circ\text{C}$, conducted also in air. To reduce air contamination, some plates were rolled at $\sim 500^\circ\text{C}$. Followed certain surface cleaning process the hot-rolling plates were annealed at $980\sim 1020^\circ\text{C}$ or 850°C for 1h in vacuum of $\sim 2 \times 10^{-3} \text{ Pa}$ for recrystallization or stress

relieving, respectively. Finally, the plates were cold rolled to a thickness of ~1mm. Without further annealing, the final plates kept a cold work (CW) of ~50% measured as reduction in thickness. To protect the alloy from air contamination to pick up oxygen and nitrogen, ingots were coated with glass films at ~200°C before forging. A sandblasting treatment was employed to remove the surface coating layer after the forging. Plates were sheathed with copper sheets before hot rolling. However, some primary fabricated plates were not protected, contained much higher gaseous impurity level. Figure 2.4 is a photo of the cold rolling plates.

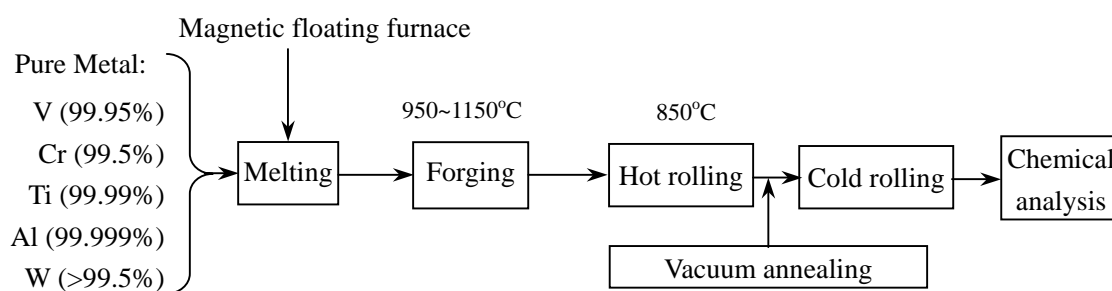


Fig. 2.3 The flow chart showing the process of the alloy preparation.

The chemical composition of the alloy plates was listed in Table 1. It shows that hot rolling at low temperature (500°C) without protection could greatly reduce the oxygen concentration by a factor of ~50%, or a reduction in amount of 310-390 wppm as compared to those rolled at 850°C. Considering the original oxygen concentration in raw V is about 200 wppm, oxygen pick-up during melting, forging and the 500°C-rolling in air is about 190-260 wppm, but 500-900 wppm for those rolled at 850°C. It means that the forging in air causes less oxygen increment in the alloy than the hot rolling. Reasons might come from the fact that the post-forged plate is thick and the thick surface scale containing high oxygen was removed by machining.

Table 2.1 Chemical compositions of the vanadium alloys, the vacuum annealing temperature (VAT) and hot-rolling temperature (HRT)

Alloy	Chemical composition (wt.%, C, N and O in wppm)								VAT (°C)	HRT (°C)	Pro- tection
	Si	Cr	Ti	W	Al	C	N	O			
V4Cr4Ti-O	0.023	3.61	4.11	/	0.21	240	460	900	1020	850	No

V3TiAlSi-O	0.95	0.02	3.20	/	1.07	120	60	800	1020	850	No
V4TiL	0.005	/	4.32	/	0.19	200	20	460	1020	500	No
V4Ti-O	0.012	0.22	4.23	/	0.23	140	20	850	1020	850	No
V4Ti3Al	0.016	/	4.24	/	2.82	190	10	390	1020	500	No
V4Ti3Al-O	0.008	0.02	4.23	/	2.89	190	50	700	1020	850	No
V4TiSi-O	0.24	0.02	3.96	/	0.26	160	520	1100	1020	850	No
V4Ti	0.014	/	3.99	/	/	120	30	280	980	850	Yes
V8W	0.014	/	/	8.28	/	100	40	230	980	850	Yes
V7W0.3Al	0.014	/	/	7.35	0.34	110	30	290	980	850	Yes
V6W1Ti-N	0.014	/	1.10	6.48	0.12	90	30	250	980	850	Yes
V6W1Ti	<0.01	/	1.07	6.04	/	70	5	350	850	850	Yes
V6W2.5Ti	<0.01	/	2.53	5.56	/	80	5	370	850	850	Yes
V6W4Ti	<0.01	/	4.12	5.64	/	50	4	350	850	850	Yes
V6W1TiAl	<0.01	/	1.10	5.85	0.69	60	4	220	850	850	Yes
V4Cr4Ti	0.01	4.18	4.19	/	/	60	3	350	850	850	Yes

Comparing the oxygen concentration of the alloys, it could be found that the Al-bearing alloys have relatively lower oxygen concentration. It indicates that Al in the alloy played a role to increase the resistance of the alloy to oxygen contamination. Fujiwara and Natesan studied the oxidation behavior of V-4Cr-4Ti containing 0.5%wt Al in air [112]. The results indicated



Fig. 2.4 Cold-rolled vanadium alloy plates.

improvement of the oxidation resistance of the alloy by the Al. The oxidation behavior of the present V-4Ti-3Al was also investigated in a previous study, showing a similar improvement [113].

3. Experimental procedures

3.1. Hydrogen charging and mechanical property test

To evaluate the effects of hydrogen on mechanical properties, tensile specimen

V3TiAlSi-O	0.95	0.02	3.20	/	1.07	120	60	800	1020	850	No
V4TiL	0.005	/	4.32	/	0.19	200	20	460	1020	500	No
V4Ti-O	0.012	0.22	4.23	/	0.23	140	20	850	1020	850	No
V4Ti3Al	0.016	/	4.24	/	2.82	190	10	390	1020	500	No
V4Ti3Al-O	0.008	0.02	4.23	/	2.89	190	50	700	1020	850	No
V4TiSi-O	0.24	0.02	3.96	/	0.26	160	520	1100	1020	850	No
V4Ti	0.014	/	3.99	/	/	120	30	280	980	850	Yes
V8W	0.014	/	/	8.28	/	100	40	230	980	850	Yes
V7W0.3Al	0.014	/	/	7.35	0.34	110	30	290	980	850	Yes
V6W1Ti-N	0.014	/	1.10	6.48	0.12	90	30	250	980	850	Yes
V6W1Ti	<0.01	/	1.07	6.04	/	70	5	350	850	850	Yes
V6W2.5Ti	<0.01	/	2.53	5.56	/	80	5	370	850	850	Yes
V6W4Ti	<0.01	/	4.12	5.64	/	50	4	350	850	850	Yes
V6W1TiAl	<0.01	/	1.10	5.85	0.69	60	4	220	850	850	Yes
V4Cr4Ti	0.01	4.18	4.19	/	/	60	3	350	850	850	Yes

Comparing the oxygen concentration of the alloys, it could be found that the Al-bearing alloys have relatively lower oxygen concentration. It indicates that Al in the alloy played a role to increase the resistance of the alloy to oxygen contamination. Fujiwara and Natesan studied the oxidation behavior of V-4Cr-4Ti containing 0.5%wt Al in air [112]. The results indicated



Fig. 2.4 Cold-rolled vanadium alloy plates.

improvement of the oxidation resistance of the alloy by the Al. The oxidation behavior of the present V-4Ti-3Al was also investigated in a previous study, showing a similar improvement [113].

3. Experimental procedures

3.1. Hydrogen charging and mechanical property test

To evaluate the effects of hydrogen on mechanical properties, tensile specimen

(TS) was mainly used, together with compact tension (CT) specimens and half-size Charpy specimens ($\frac{1}{2}$ CS) of the NIFS-Heat 2 alloy for J_{1c} fracture toughness and impact toughness assessment, respectively. Charging hydrogen was carried out at 500~800°C with a pure H_2 atmosphere by two ways. In the early time, hydrogen charging was performed in a hydrogenization device. As the vacuum of the vessel containing the specimen was not high ($\sim 2 \times 10^{-3}$ Pa), oxygen pick-up occurred during the charging. As an example, the as-received NIFS-Heat 2 alloy has an oxygen concentration of 148 wppm, which increased to ~ 360 wppm after the charging

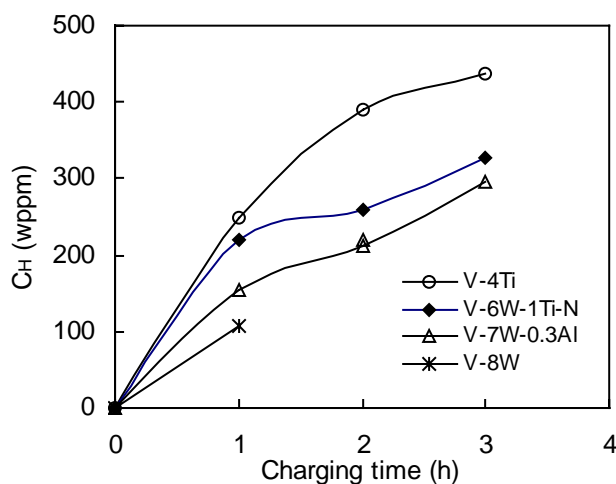


Fig. 3.1 The hydrogen absorption behavior of V-base alloys in quartz tube at 800°C.

at 700°C. Due to this shortcoming, later specimens were hydrogen charged in quartz tubes. Specimens, together with $ZrH_{1.8}$ hydride in a weight ratio of ~ 0.1 over the specimen weight, were enclosed in evacuated quartz tubes. Each tube had a diameter of ~ 20 mm and a length of ~ 200 mm, and a vacuum in the level of 10^{-5} Torr. With this method, hardly any oxygen pick-up was detected at elevated temperature. Detailed hydrogen-charging parameters for several V-base alloys, size of the tensile specimens and the followed tensile test parameters are listed in Table 3.1.

Hydrogen concentration in the specimens was measured with a RH404 type hydrogen determination device that was made by the Leco Co. in US. The measured results are shown in Fig. 3.1. The figure suggests that the hydrogen concentration (C_H) approached saturation with increasing exposure time, and clearly shows that the addition of Ti or Al to V promoted the hydrogen absorption, while the effect of W was much weaker. The enhancement was thought to be due to the strong affinity and solubility of Ti for H. It has been reported that the hydrogen solubility in V - Ti binary alloys increases with titanium concentration [114].

Table 3.1 Experimental parameters for the hydrogen charging and the tensile test.

No.	Annealing state	TS Gauge dimension (mm ³)	H charging temp. (°C)	H charged in	Alloys evaluated	Tensile strain rate (S ⁻¹)
1	1020°C/1h	20x8x1	700	HD	Alloys with high O	4×10^{-3}
2	1000°C/2h	19x4x1.9	700	HD	NIFS-Heat 2 with 360wppmO*	4×10^{-4}
3	980°C/1h	25x8x0.5	800	QT	V8W, V7W0.3Al, V6W1Ti-N, V4Ti	1.1×10^{-3}
4	1000°C/1h	8x3x0.5	500	QT	V-4Cr-4Ti	$0.35 \sim 87.5 \times 10^{-4}$

*Chemical composition could be found in [115]. The high O is caused by hydrogen charging.

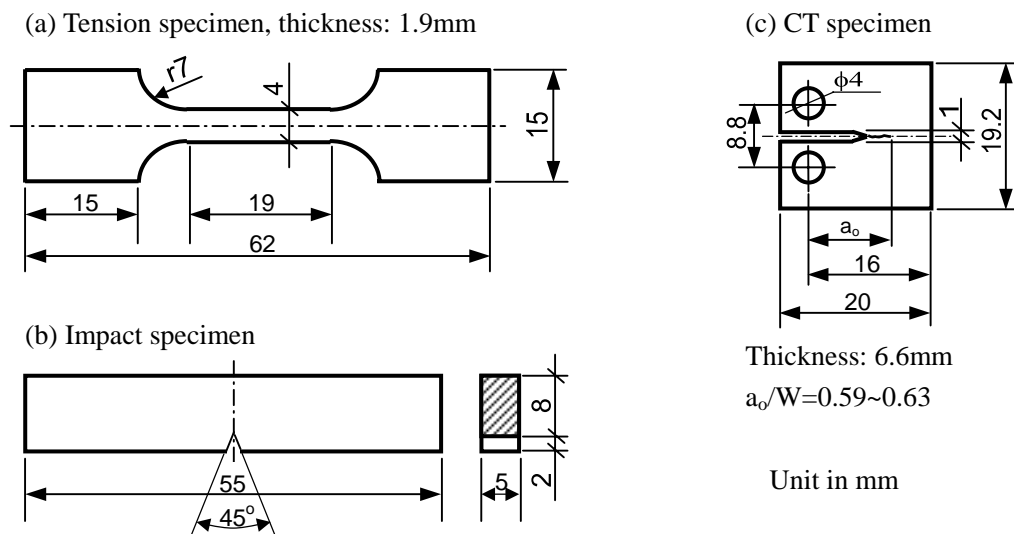


Fig. 3.2 The configuration and size of the test specimens for the hydrogen charged NIFS-Heat 2 alloy.

Figure 3.2 shows the configurations and dimensions of the specimens used for the mechanical property test of the hydrogen charged V-4Cr-4Ti alloy (NIFS-Heat 2). All specimens have their longitude parallel to the rolling direction. V-shape notch in 45° angle was placed on the thin plane of the impact specimen with a depth of 2 mm and a root radius of 0.25mm. Mechanical property tests were performed at room temperature. The Charpy impact test had a velocity of 5m/s. Both tensile test and J_{1c} test were performed on a MTS810 test machine with a strain rate of $\sim 4 \times 10^{-4}$ /s and a crosshead displacement rate of 0.1mm/min, respectively. The CT specimens were pre-cracked on the same machine using a fatigue test method before the hydrogen charging. The pre-fatigue crack length (a_0) was from 9.44 to 10.08mm, keeping the ratio of a_0/W around 0.6. A single-specimen method was used to measure the J

integral. Specimens were unloaded after certain crack extension. Subsequently they were placed in liquid nitrogen and forced to thorough fracture immediately after they were taken out. The initial crack length and the crack propagation distance at the unload point were then measured under an optical microscope.

J integral was calculated according to Eqn. (3.1).

$$J = \frac{A}{Bb} f(a/W), \quad (3.1)$$

where A is the area under the load-displacement curve, a the crack length, b the width of the uncracked ligament, B and W are the thickness and the width of the CT specimen, respectively;

$$f(a/W) = 2(1 + \alpha)/(1 + \alpha^2), \quad (3.2)$$

where

$$\alpha = [(2a/b)^2 + 2(2a/b) + 2]^{1/2} - [(2a/b) + 1]. \quad (3.3)$$

Substituting a and b in Eqn. (3.1) with a_0 and b_0 (the initial crack length and the initial ligament width), we got a J integral called J_Q . If it meets the following validity condition then it is the fracture toughness of the alloy (J_{1c}).

$$a_0, b_0, B \geq 25J_Q / \sigma_y, \quad (3.4)$$

where σ_y is the yield strength of the alloy.

3.2. Hardness recovery test

Samples for the recovery and recrystallization experiments were cut from the ~50% cold-rolled plates in a size of 10x5 mm². Vacuum annealing was conducted at 850°C or 980°C for 1 h prior to the cold rolling. The temperature was shown as VAT in Table 2.1. After mechanically grinding and electro-polishing, the samples were annealed at temperature of 100-1100°C for 1 hour in vacuum less than 1x10⁻⁶ Torr. The microstructures of the samples were analyzed using a scanning electron microscope (SEM) and a transmission electron microscope (TEM). Vickers hardness tests with a load of 500g and duration of 30 s were conducted at room temperature.

For the experiment to study the feasibility of utilizing cold-rolling as a way to get

high strength alloy plate, the thermal stability of the 20%CW NIFS-Heat 2 was evaluated in the same way. Details could be found in Table 3.2.

3.3 High temperature tensile test

Tensile test specimens with a gauge section of $5 \times 1.2 \times 0.25 \text{ mm}^3$ were punched out from 0.25mm thick cold rolling plates. Followed an annealing at 900°C for 1h in vacuum, high temperature tensile tests were performed on a tensile machine in IMR (Institute of Material Research, Japan) at a strain rate of $6.67 \times 10^{-4}/\text{s}$ in a vacuum of $<1 \times 10^{-4} \text{ Pa}$. Test temperatures were from 400 to 800°C . After the tests, fracture surfaces were observed with a scanning electron microscope (SEM).

3.4 Aging and tensile test of the aged alloy

The alloys used were V-4Cr-4Ti, V-6W-4Ti, V-6W-1Ti and the NIFS-Heat-2 V-4Cr-4Ti (NH-2). The chemical composition of NIFS-Heat 2 is: 3.98%Ti, 4.02%Cr, 0.069%C, 0.0122%N and 0.0148%O in mass. The as-received plates of these alloys were machined into rectangular sample in thickness of 1 mm for hardness tests and 0.5 mm thick tensile specimen for tensile property measurement. Hardness samples were ground and polished before any heat treatments. With the accomplishment of certain heat treatments, Vicker's hardness (Hv) test was performed at room temperature with a load of 0.5 kg and duration of 30 s and tensile tests were performed on a MTS810 machine at room temperature at strain rate of $3.5 \times 10^{-4}/\text{s}$. The gauge dimension of the tensile specimens is $8 \times 3 \times 0.5 \text{ mm}^3$. Load and displacement curve was recorded by a computer system. All tensile properties were evaluated in light of the recorded curves, such as the tensile strengths, elongations, strain hardening exponent and the energy absorbed by the specimen.

Two kinds of heat treatments of the specimens were conducted before the hardness test and the tensile test. One is aging and another is isochronally annealing. For the aging, samples or specimens, wrapped in Zr foil, were first solid solution annealed (SA) at 1100°C for 1h in evacuated quartz tube in vacuum level of 10^{-5} torr . In the same way they were then aged at 600°C for different time up to 393h. For the

annealing, NIFS-heat-2 was used. In addition to the SA heat treatment, some of the samples were annealed at 950°C for 1h for recrystallization, leading to a large amount of large precipitates formed in the alloy either in this annealing or in historical thermo-mechanical process [74,86,115]. This treatment is named as CP in the following text due to the Coarse Precipitates. Besides, some SA samples were annealed at 600°C for 10h to produce fine precipitates in the alloy. This treatment is referred as FP. Following these primary heat treatments, all of the samples were isochronally annealed at 200-1100°C for 1 h. For all of these heat treatments, vacuum was less than 1×10^{-6} torr. Samples were cooled down to room temperature in the heat treatment furnace without forcing cooling measure. Details of the thermo-mechanical process are reported in Table 3.2.

Table 3.2 Thermo-mechanical process parameters of the alloys for the aging, cold-rolling induced hardening and thermal stability studies.

ID	Alloy	Thermo-mechanical treatment	For study of
SA*	V-6W-1Ti V-6W-4Ti SWIP-Heat	1100°C/1 hr	Aging (600°C/1-393 hr)
SA	NIFS-Heat 2	1100°C/1 hr	Thermal stability and
SA+20%CW		1100°C/1 hr + 20%CW	TEM observation
FP*		1100°C/1 hr + 600°C/10 hr	(200-1100°C/1 hr)
FP+20%CW		1100°C/1 hr + 600°C/10 hr+20%CW	
CP*		950°C/1 hr	
CP+20%CW		950°C/1 hr + 20%CW	

*SA: Solid solution Annealing; FP: alloy in aging-hardening state containing Fine Precipitates; CP: alloy in recrystallizing state containing Coarse Precipitates.

3.5 Tests to evaluate hydrogen release and plastic flow at constant stress at room temperature

Tensile specimens of V-6W-2.5Ti with or without H, along with the V-4Cr-4Ti with H, were hold at a fixed load for several hours at room temperature. The displacements of the test machine's crosshead were in situ recorded at various hold time. Load was set at any value lower than the ultimate tensile point, higher or lower than the yield points. Two typical size specimens were used, one for post-test hydrogen measurement with relative bigger gauge section of $6 \times 10 \times 1 \text{mm}^3$, another one

with smaller gauge section of $3 \times 1 \times 1 \text{ mm}^3$ for post-test tensile properties measurement. After the hold tests, the specimens for hydrogen measurement were cut into pieces and the center parts were sent for hydrogen concentration measurement immediately. Other specimens were tensile tested to measure its tensile properties. The loading rate for the hold test was 1 N/s , and the followed tensile tests had a strain rate of $8.3 \times 10^{-4} \text{ /s}$.

4. Solid solution hardening

4.1 Results and discussions

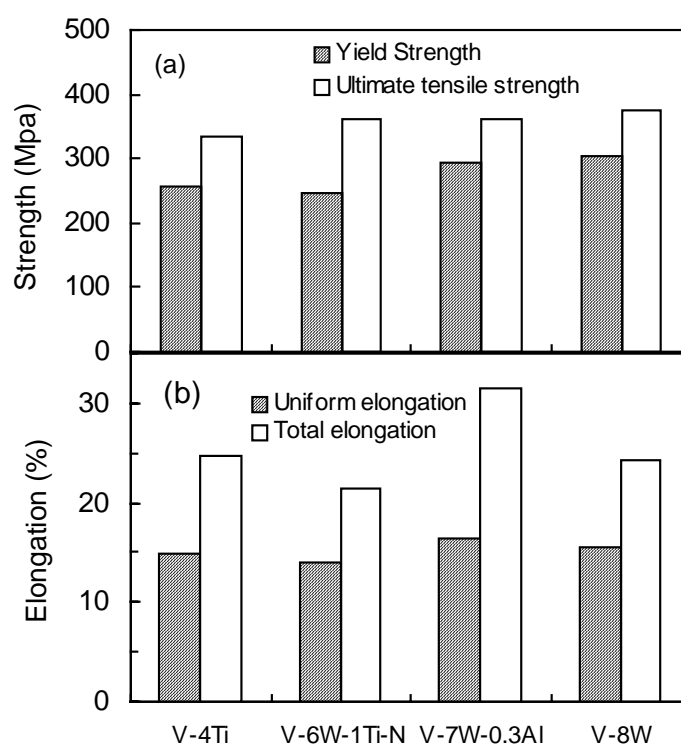


Fig. 4.1 The tensile properties of some alloys at room temperature, strain rate: $1.1 \times 10^{-3} \text{ /s}$.

Figure 4.1 shows the tensile properties for V-4Ti and some other alloys containing W. The alloys were annealed at 980°C for 1 h in vacuum. The mean grain sizes of the alloys were about 32, 30, 36 and 35 μm for V-4Ti, V-6W-1Ti-N, V-7W-0.3Al, and V-8W, respectively. In the figure the strengthening by W could be identified. Both yield and ultimate tensile strength increased with increasing W concentration, while the tensile elongations didn't change much with an exception of V-7W-0.3Al. This alloy has relatively higher uniform elongation and much higher

with smaller gauge section of $3 \times 1 \times 1 \text{ mm}^3$ for post-test tensile properties measurement. After the hold tests, the specimens for hydrogen measurement were cut into pieces and the center parts were sent for hydrogen concentration measurement immediately. Other specimens were tensile tested to measure its tensile properties. The loading rate for the hold test was 1 N/s , and the followed tensile tests had a strain rate of $8.3 \times 10^{-4} \text{ /s}$.

4. Solid solution hardening

4.1 Results and discussions

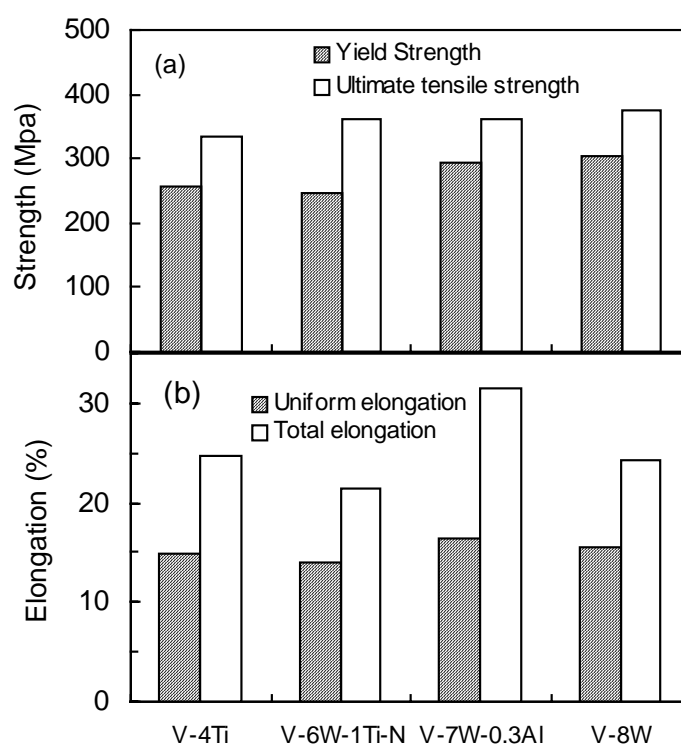


Fig. 4.1 The tensile properties of some alloys at room temperature, strain rate: $1.1 \times 10^{-3} \text{ /s}$.

Figure 4.1 shows the tensile properties for V-4Ti and some other alloys containing W. The alloys were annealed at 980°C for 1 h in vacuum. The mean grain sizes of the alloys were about 32, 30, 36 and 35 μm for V-4Ti, V-6W-1Ti-N, V-7W-0.3Al, and V-8W, respectively. In the figure the strengthening by W could be identified. Both yield and ultimate tensile strength increased with increasing W concentration, while the tensile elongations didn't change much with an exception of V-7W-0.3Al. This alloy has relatively higher uniform elongation and much higher

total elongation than the others, which was thought to be benefited from the Al addition. Al could improve ductility due to its role to reduce oxygen concentration in the V-base alloys [116]. This role was confirmed in another study by C. Nishimura et al. [117]. In his report the oxygen concentration of V-Al alloys decreased from 231 to 41 wppm as Al increased from 10 to 40% in mass.

The hardness was measured for some of the alloys at room temperature to assess the solid solution hardening of the alloying elements. The samples were annealed at 1100°C for 1 h to obtain a nearly full solid solution state. Figure 4.2 (a) shows the dependence of the Vicker's hardness on the Ti concentration in the V-6W-Ti alloys. The hardness increases with Ti amount. The increasing rate was about 8.87 Hv/%Ti based on a linear correlation. In order to get the hardening coefficient more precisely, the contribution of other impurities in the alloys must be removed. Eqn. (4.1) gives a relation among the hardness (Hv) and the concentrations of the species (C_m) in an alloy based on solid solution hardening assumption.

$$Hv = H_0 + \sum_m H_m C_m , \quad (4.1)$$

here H_m is the hardening coefficient of the solid solution species (m) and H_0 is a constant. From the previous studies by T. Nagasaka, et al. [106], the hardening coefficient of N and O, and H_0 in unalloyed V was about 0.12 Hv/wppm, 0.057 Hv/wppm and 48 Hv, respectively. Assuming that the coefficients are not changed in the present alloys, the contribution of the impurities to the hardness could be subtracted. The solid square symbols in Fig. 4.2 (a) show the results. The hardening coefficient of Ti, thus, is about 8.92 Hv/%mass. The remaining contribution of ~6 %W and H_0 is about 88.99 Hv in total. Therefore, the hardening coefficient of W in the alloys is about 7.13 Hv/%mass, which is a little lower than that of Ti. The hardness of the V-4Cr-4Ti alloy was measured to be 145.6 Hv. In the same way, the hardening coefficient of Cr in V-4Cr-4Ti alloy was calculated to be about 9.55 Hv/%mass. So Cr contributed more strongly to the solid solution hardening than Ti. Considering the much bigger atomic weight of W, W should be the strongest species per atom to strengthen the alloy at room temperature.

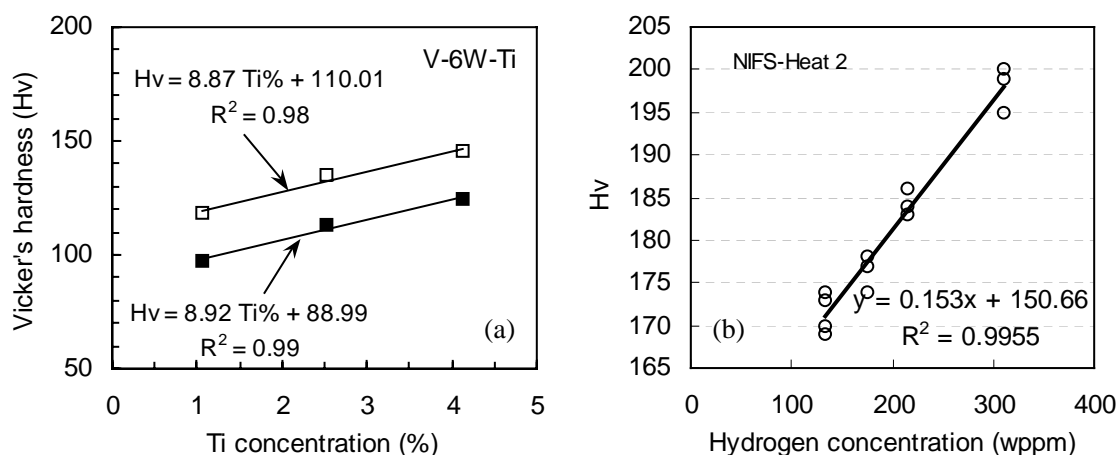


Fig.4.2 (a) Hardness of the V-6W-Ti alloys in solution-annealing state. Solid symbol: contribution of the O and N were subtracted. (b) Hardness dependence of NIFS-Heat 2 on hydrogen concentration.

However, the grain size of the alloys may have certain effect on the hardness, which generally increases with decreasing grain size. The measured mean grain sizes of the alloys for the 1% Ti, 2.5% Ti and 4% Ti alloys shown in Fig. 4.2 (a) were 38, 33 and 37 μm , respectively. The positive deviation of the hardness data of V-6W-2.5Ti from the fitted line may be caused by its relatively smaller grain size.

NIFS-Heat 2 (V-4Cr-4Ti) alloy, in the heat treatment state of $1000^\circ\text{C}/2\text{h}$, was charged hydrogen at 700°C to evaluate the hydrogen embrittlement of the alloy. After the charging, hydrogen concentration and Vicker's hardness of the alloy were measured. Their relation is shown in Fig. 4.2 (b). Obviously the hardness nearly increases linearly with increasing hydrogen concentration, indicating the hydrogen induced hardening is also a solid solution one. From the slope of the fitted straight line, the hardening coefficient of H is about 0.153 Hv/wppm.

Table 4.1 Solid solution hardening coefficient of the major solutes in V-base alloy.

Substitutional solute (Hv/wt%)			Interstitial solute (Hv/wppm)		
Cr	Ti	W	N	O	H
9.55	8.92	7.23	0.12 [106]	0.057 [106]	0.153

The hardening coefficient of major solutes in vanadium alloy is summarized in Table 4.1. Evidently interstitial solutes could strengthen an alloy much stronger than

the substitutional ones.

4.2 Summary

The solid solution hardening by Cr, Ti, W and H was investigated by tensile and hardness tests at room temperature. With the aid of the available literature data of the hardening coefficients of N and O in unalloyed V, the coefficients of Cr, W were obtained. Effects of grain size on the evaluated results were analyzed. As the variation in grain size was not significant, its effects were negligible.

The results could be summarized as follows:

- (1) Cr, Ti and W are strong solid solution strengtheners. Their hardening intensities are similar, based on their contribution in unit of per weight percent.
- (2) Interstitial C, N, O and H are even stronger strengtheners to V-base alloy.

5 Precipitation, cold rolling and their hardening

The interstitial C, N and O solutes in a vanadium alloy are not thermally stable particularly when the alloy contains Ti. Precipitates such as Ti-CON and VC will form during thermo-mechanical process and on annealing at appropriate temperature. The precipitation behavior has been studied before and results showed its significant influence on the mechanical performances. As a result, it seems to be of very importance to stabilize the microstructure of the alloy for stable mechanical properties for a vanadium-alloy structure during high temperature service. For this purpose, commonly a vanadium alloy is annealed at 900~950°C with the formation of most precipitates. These precipitates are usually blocky type in large size, thus the precipitation leads to the decrease in the strength due to the loss of solid solution hardening. The stability of this precipitation will be showed in the present paper for some alloys. On the other hand, it was found that fine precipitates would form at ~700°C for V-4Cr-4Ti in solid solution state, harden the alloy a lot. It is possible to utilize the hardening to obtain a higher-strength alloy. For this purpose, the precipitates should be as fine as possible and be in high number density. For this consideration, alloys were isochronally annealed at various temperatures for 1hr to find the proper precipitation-hardening temperature in the present study. Aging at 600-800°C was also conducted for the same purpose and finally the evolution of aging hardening on time was investigated in order to determine an optimizing process for an ultimate strengthening. Its impact on ductility and its thermal stability were investigated to evaluate its feasibility for engineering application. The role of alloying elements on the behavior was discussed. Besides, hardening by cold rolling and its thermal stability were also studied, with or without the combination hardening by precipitation, in the present paper.

5.1 During isochronally annealing

Alloys in SA state (1100°C/1h annealing) were studied along with the ones in Recrystallization Annealing state (RA-900°C/1h annealing) for comparison. The

alloys were V-4Cr-4Ti, V-4Ti, V-6W-1Ti and V-6W-4Ti. TEM observation shows the alloys in SA state scarcely contain any precipitates (see Fig. 5.1 (a) as an example), indicating that most of the alloying elements and interstitial impurities are in solid solution. For the alloys in RA state, many precipitates of large size were observed. Examples for V-4Cr-4Ti and V-6W-4Ti are shown in Fig. 5.1 (b) and (c). Evidently, V-6W-4Ti contains more precipitates than V-4Cr-4Ti. According to the photos, the area number density of the precipitates is about $2.35 \times 10^{13}/\text{m}^2$ and $8.77 \times 10^{12}/\text{m}^2$ for V-6W-4Ti and V-4Cr-4Ti, respectively. These precipitates make the alloys in RA state contain less alloying elements and particularly interstitials in solution in matrix as compared to the alloys in SA state. Due to this difference, their precipitation and hardening behavior were quite different.

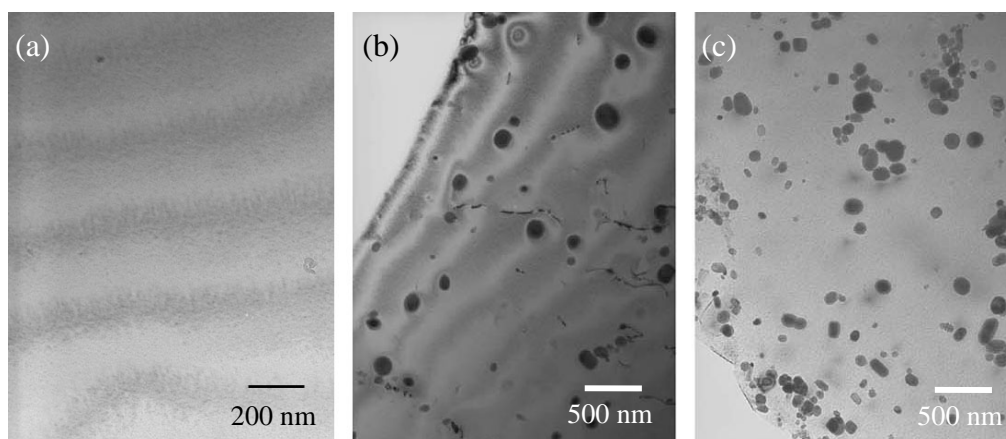


Fig. 5.1 TEM microstructure of the (a) V-6W-4Ti alloy in SA state, (b) V-4Cr-4Ti and (c) V-6W-4Ti in RA state.

Fig. 5.2 shows the hardness after the 1 h isochronally annealing from (a) ~ 400 to 1100°C for alloys in SA state and (b) ~ 400 to 900°C for the same alloys in RA state. For SA alloys, there is notable hardening at ~ 500 - 800°C (see Fig. 5.2 (a)), and peak hardening occurred at a critical temperature (CT) above which the hardening got weaker. The CT for V-4Cr-4Ti is about 700°C , about 100°C higher than that for the other alloys without Cr addition. Besides, the peak hardening for the V-4Cr-4Ti alloy is much stronger than that for the others at the critical temperatures. Invariably, slight softening happened for all of the alloys at 900°C . On the other hand, results shown in

Fig. 5.2 (b) indicate that the RA alloys have much small hardness change over the annealing temperatures, irrespective of the alloys. There was always slight hardening for V-4Cr-4Ti in the temperature range. For others, slight hardening happened at selective temperatures.

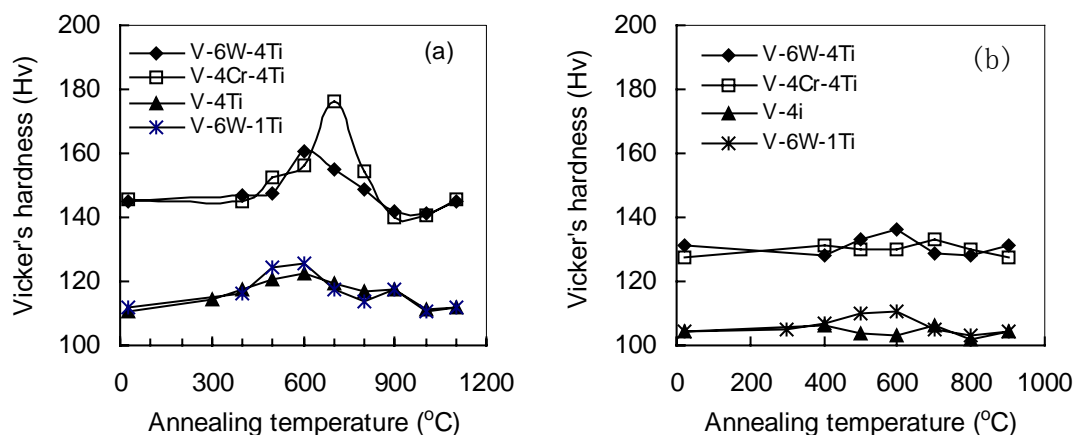


Fig. 5.2 Vicker's hardness as a function of annealing temperature for the alloys in (a) SA state and (b) RA state. Hardness was measured at room temperature.

Fig.5.3 is the TEM photos showing the precipitates in the SA-state V-6W-4Ti alloy after annealing at 500~900°C for 1 h. The hardness data is also included in the figure. Originally, there is no precipitate in the alloy (see Fig. 5.1 (a)). Hardly any precipitates were observed at 500°C and 900°C (see Fig. 5.3 (1) and (6)), where the hardness changed few. At 600°C, fine precipitates appeared in size of ~2 nm and at high number density, resulting in strong hardening at the temperature. The precipitates get coarser with increasing temperature from 600 to 800°C, while the number density decreased. As coarsening precipitates leading to increasing distance between two adjacent precipitates, resistance to dislocation motion became weaker, and the hardness of the alloy decreased. Fig. 5.4 (a) shows the temperature dependence of the size and the number density of the precipitates. At 700°C, in addition to the fine precipitates, some larger ones appeared and grouped in micro-regions (Fig. 5.3 (3)). The data in Fig. 5.4 does not include these grouped large precipitates. The figure indicates that the density almost decreased linearly with increasing temperature, while the precipitates exhibited an increasing coarsening rate. The result of TEM-EDX analysis of the grouped precipitates is shown in Fig. 5.5 (a). Not fully similar to the

large precipitate observed in the RA treated alloy (see Fig. 5.5 (b)), the precipitates contain not only high concentration of Ti and C but also high concentration of V. At 800°C, precipitates were plate-shaped in diameter of ~31.4 nm on average. These precipitates preferentially orientated to the $\langle 100 \rangle$ directions.

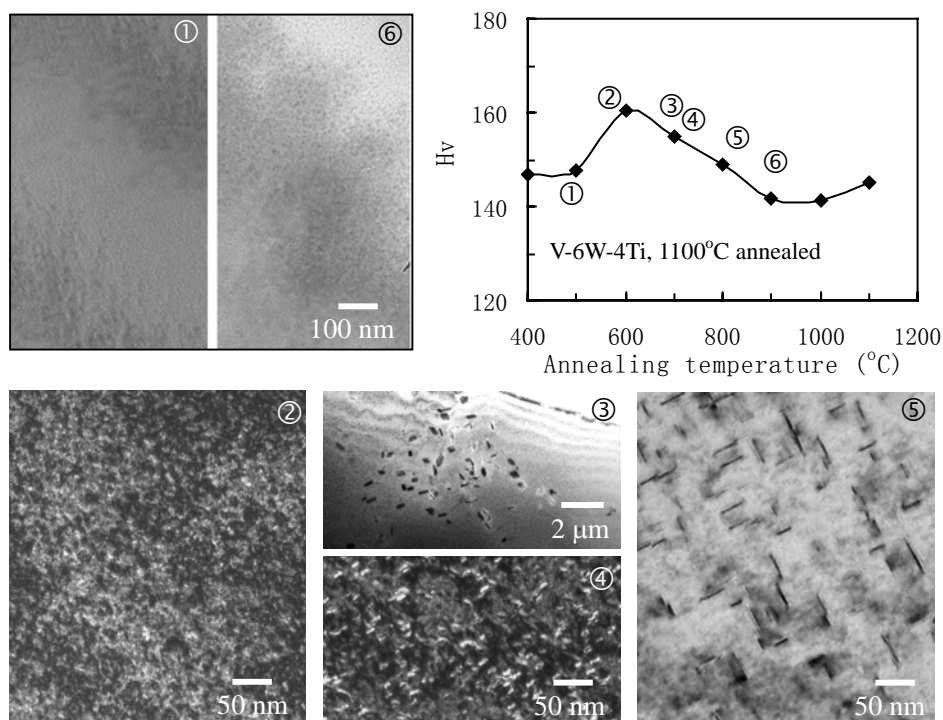


Fig. 5.3 Hardness (Hv) and microstructure at different annealing or aging temperature for the solid solution treated V-6W-4Ti alloys.

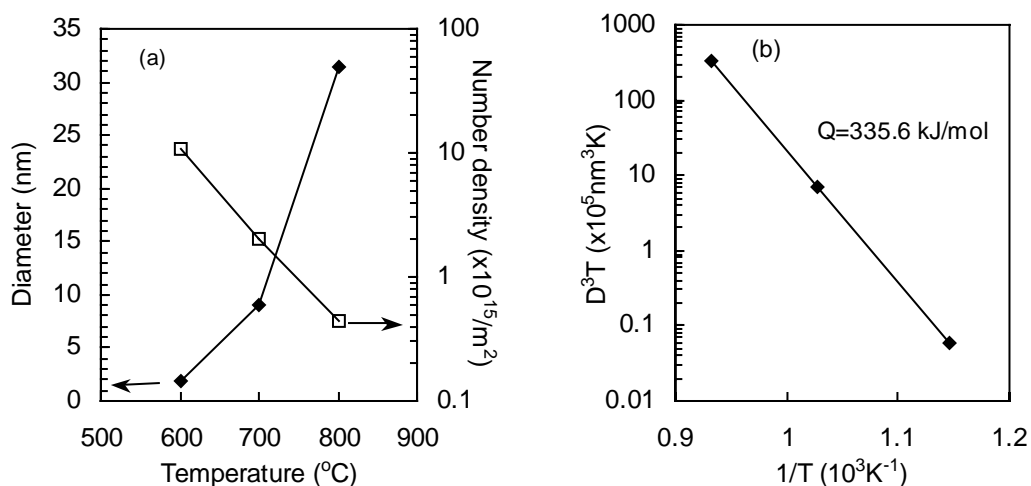


Fig. 5.4 The temperature dependence of (a) the diameter and number density of the fine precipitates appeared in the SA treated V-6W-4Ti alloy, (b) that showing the relationship between the diameter (D) and the reciprocal temperature for activation energy evaluation.

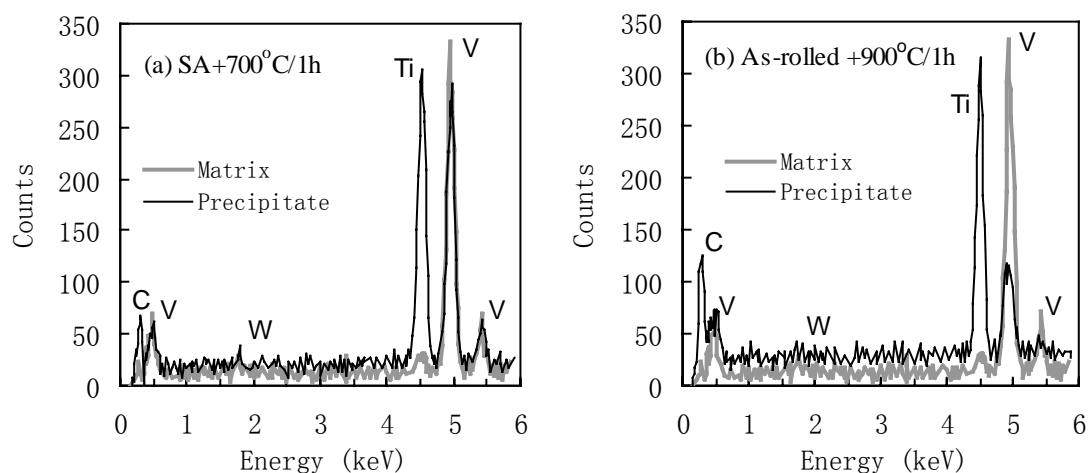


Fig. 5.5 TEM-EDX spectra of the matrix and the precipitate in V-6W-4Ti (a) in SA state after annealing at 700°C for 1 h and (b) in as-rolled state after annealing at 900°C for 1 h.

For the V-6W-4Ti alloy in solid solution annealing state, fine precipitates appeared at 600°C and became larger with increasing temperature in the isochronally annealing. Theoretically the average diameter (D) of the precipitates has a relationship with the temperature as

$$D^3 = D_0^3 + \frac{C}{T} e^{-\frac{Q}{RT}} t, \quad (5.1)$$

where D_0 is the initial diameter of the precipitates, which was taken as zero here. C is constant, Q is the activation energy of the diffusion of solutes forming the precipitates in the matrix, R is a gas constant, T is absolute temperature in unit of K and t is time. This expression is suitable for describing the growth of the precipitates; but the time should not include the incubation time for precipitate nucleation. This incubation time for precipitate nucleation is not measured in the present experiments. As the temperature is high, the time is presumed to be very short and is negligible as compared to the 1 hr annealing. By this approximation the time t is taken as 1hr. Fig. 5.4 (b) is the experimental data showing the relationship, from which the activation energy was calculated to be about 335.6 kJ/mol. It is much higher than the energy of oxygen diffusion in V and V-4Cr-4Ti, 123 and 130 kJ/mol at 300-650°C, respectively [118]. So the growth of the precipitates was not controlled by the diffusion of

interstitials in the matrix. The energy is a little higher than the activation energy of 270 kJ/mol for self-diffusion in pure V at 700-800°C. Considering the precipitates were Ti-CON type, the energy should have strong relation with the Ti solute diffusion. Comparing with V atom, Ti atom has larger atomic size. The diffusion of Ti in V matrix should require higher activation energy than V due to this difference. It is eventually concluded that the growth of the precipitates was controlled by the diffusion of Ti solutes in the alloy.

5.2 During aging

5.2.1 Aging at 600-800°C for 50hrs

To evaluate both the stability of the historical formed precipitates and the precipitation hardening further, V-6W-4Ti and V-6W-1Ti in both SA and RA states were aged at 600-800°C for 50hrs. Hardness was measured after the aging at room temperature. Results are shown in Fig. 5.6. Again it was proven that the microstructure of the RA-state alloys is rather stable since the hardness change after the aging was almost negligible. Nevertheless, the hardness change for the alloys in SA state is quite different from the isochronally annealing results, though likely some similarity in the trend of the temperature dependence. The difference is that the hardness decreased drastically with the increase of the aging temperature. In spite of much stronger hardening at 600°C, softening appeared at and above 700°C though V-6W-1Ti showed slight hardening at 700°C. Therefore, aging temperature should be at or less than 600°C if one wants to strengthen the alloys by aging.

Samples after aging at 600°C were observed in a transmission electron microscope (TEM). Figure 5.7 shows the TEM photos for V-6W-4Ti in SA (a) and RA state (b). It indicates that high number density precipitates formed in the SA-state alloy, resulting in the hardening. Comparing with the photo shown in Fig. 5.3, it clearly shows that the precipitates produced in the aging were bigger than those produced in the isochronally annealing. The alloy in RA state showed low number density but large precipitates after the aging. Compared with the one before the aging

(see Fig. 5.1), clearly the precipitates got larger and fewer. It indicates that the precipitates formed in the historical thermo-mechanical process are also unstable at elevated temperature, but it did affect the hardness insignificantly.

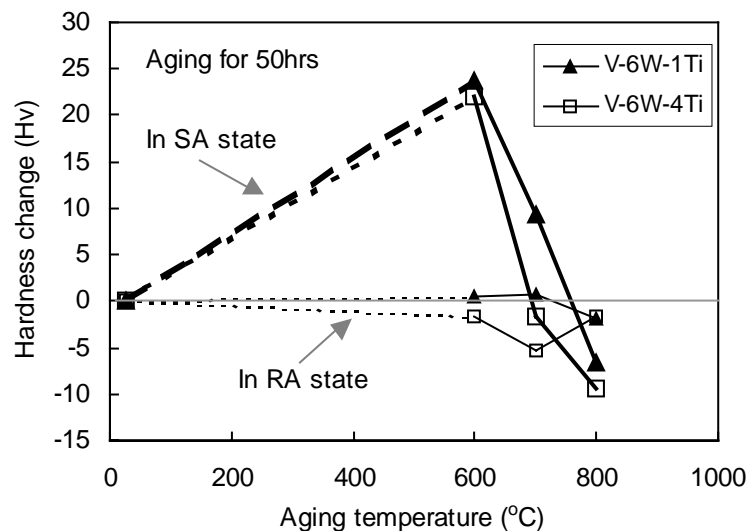


Fig. 5.6 Hardness change of V-6W-1Ti and V-6W-4Ti in SA and RA state after aging at 600-800°C for 50hrs. Hardness was measured at RT.

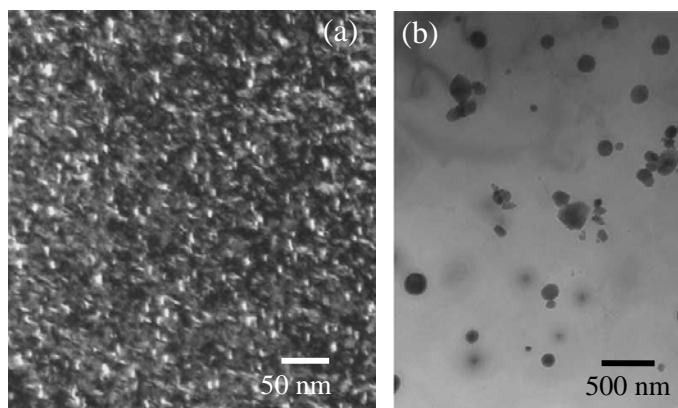


Fig. 5.7 TEM photos showing the precipitates produced in the SA-state (a) and RA-state (b) V-6W-4Ti alloy after aging at 600°C for 50hrs.

5.2.2 Hardening by aging at 600°C for longer time and its thermal stability

Fig. 5.8 (a) shows the hardening of V-6W-1Ti, V-6W-4Ti and V-4Cr-4Ti (SWIP-Heat) by aging at 600°C for 1-393h. The alloys in SA state had hardness of 112, 145 and 146 Hv and mean grain size of 38, 37 and 39 μm , respectively. The figure shows that the hardening approximately increased with the aging time for each

alloy and reaches a peak at ~10 h. The hardening for V-4Cr-4Ti had a lower rate at beginning than the V-W-Ti alloys, but it soon got significantly higher after aging for more than 3 h. Thereafter, the hardening was constant till 135 h, and gets weaker at 393 h for both V-6W-1Ti and V-6W-4Ti. In contrast, the hardening decreases monotonically with increasing aging time after ~10 h for V-4Cr-4Ti. Consequently, the hardening is thermally unstable at the temperature, especially for V-4Cr-4Ti. As for the strength of the hardening, obviously V-4Cr-4Ti is much stronger, while the hardening of V-6W-1Ti and V-6W-4Ti shows little difference. It seems that Ti variation in the range of 1-4mass% does not affect the hardening significantly, but Cr addition makes the alloy have stronger age-hardening capability. For V-4Cr-4Ti, the peak hardening produced about 35% increase of its hardness.

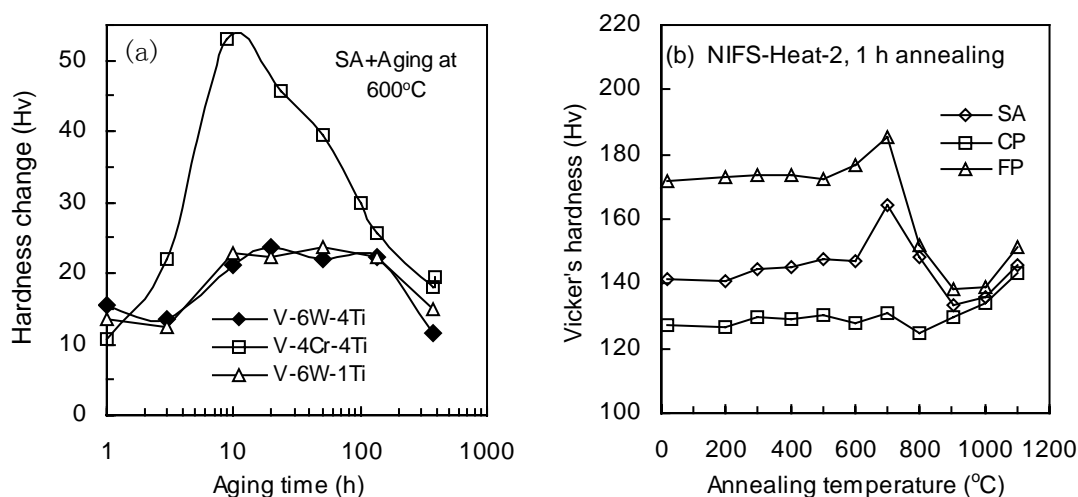


Fig. 5.8 Vicker's hardness increment (ΔH_v) as a function of the aging time for V-6W-4Ti, V-4Cr-4Ti (SWIP-Heat) and V-6W-1Ti alloys (a) and the dependence of the hardness on annealing temperature for the NIFS-Heat 2 alloy after SA, CP and FP treatment (b). Hardness was measured at room temperature.

To study the thermal stability of the hardening by aging, the NIFS heat V-4Cr-4Ti alloy samples in different annealing or aging states were annealed at 200-1100°C for 1h. The states were nominated as SA, FP and CP, denoting the alloy in solid-solution annealing state (1100°C/1hr), containing fine precipitate (SA+600°C/10hr) and containing coarse precipitates (as rolled + 950°C/1hr), respectively. Fig. 5.8 (b) shows the annealing temperature dependence of the hardness measured at room temperature, which could be summarized as follows: (1) The hardness of the alloy in CP state is

stable below 900°C. (2) The alloy in SA state is much harder than that in CP state. The alloy in FP state is even harder due to the hardening by the FP treatment. However, at 900°C and above, the difference almost disappeared. (3) Notably additional hardening appears at 600-700°C for both SA and FP samples. At higher temperature, hardness decreases till 900°C but then increases at 1000-1100°C. (4) In addition to the difference in hardness level of the different heat-treated samples, the annealing produces a 0.5-1.3% increase in hardness for the FP sample and a relatively higher increase of 2-4.2% for the SA sample at 300-500°C. It seems that the harness of the alloy in FP state is quite stable below 500°C, but that in SA state is less stable.

5.3 Effect of aging hardening on tensile properties

The tensile behavior and tensile properties of the V-4Cr-4Ti alloy (SWIP heat) were studied or measured at room temperature. Tensile strain rate was 3.5×10^{-4} /s. Fig. 5.9 (a) illustrates the tensile curves of the aged alloy, along with the one not aged (in SA state). Aging time is also indicated in the figure. Following the elastic regime, load drop due to yield occurred for the alloy in SA state. Instead of this yield behavior, the alloy after aging showed immediate strain hardening. On the other hand, evidently the aged alloy has both higher yield strength and ultimate tensile strength than the non-aged one. The total elongation is obviously decreased by the aging for 24 h.

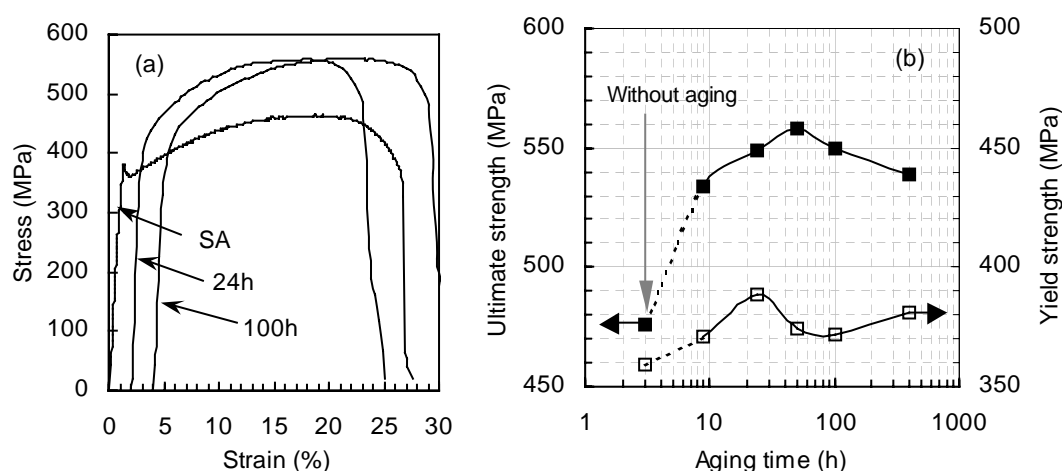


Fig. 5.9 tensile curves for SA treated V-4Cr-4Ti (SWIP-Heat) specimens and those after 24 and 100h aging (a) and tensile strengths of the alloy as a function of the aging time at 600°C (b). All tested at room temperature.

The dependence of the tensile strength on the aging time, especially the ultimate tensile strength (UTS), is just similar to the hardness. Fig. 5.9 (b) and Fig. 5.10 show the tensile properties of the alloy as a function of the aging time. The strength increases with increasing aging time within the initial 10 to 50 h but decreases afterwards. However, the strength, particularly the ultimate tensile strength, remains higher than that of the SA one over the aging time to 393h. The elongation of the alloy changes adversely to the strength with the aging time. Corresponding to the nearly highest strength after 24h aging, both the uniform elongation (UE) and the total one (TE) get to a minimum value (see Fig. 5.10 (a)). However, the loss of the elongations is not significant, about 4.2% and 2.3% for TE and UE, respectively. Both elongations almost recovered completely after 50h-aging. With longer aging time, the uniform elongation decreased. Once more, the decrease is not significant, merely about 1.25%.

Figure 5.10 (b) shows the change of the strain hardening exponent (n) and the absorbed energy (A_e) of the tensile specimen in the tensile tests with the change of the aging time. The exponent is defined by the expression of $S=K\varepsilon^n$, where S is true stress and ε is true strain. It doesn't change much by the aging, ranging from 0.2 to 0.22. A_e is calculated according to the load-displacement curve, represents the static fracture toughness of the alloy. The energy decreases a little at 24h aging but increases much at 50 h and beyond. The increase is more than 10%. So long-time aging could increase the toughness of the alloy.

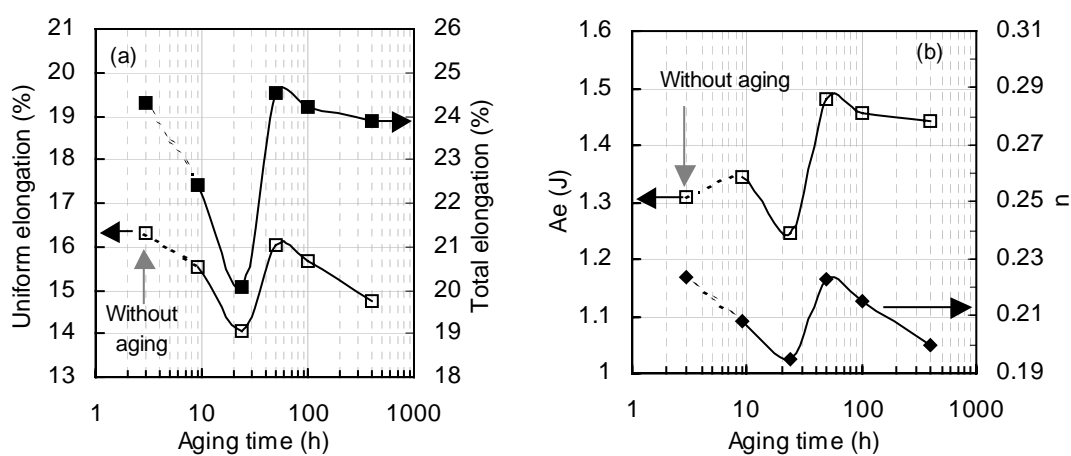


Fig. 5.10 The aging time dependence of (a) elongations and (b) the strain hardening exponent (n) and the absorbed energy (A_e) of the specimen in the tensile test.

Typical fracture morphology of the specimens is shown in Figure 5.11. All exhibited ductile fracture with dimple pattern. However, some of the dimples in the fracture surface of the aged one look smaller than those of the SA specimen. Since high number density of fine precipitates existed in the aged alloy, the nucleation sites for dimples should be of high number density as well. This should account for the smaller but higher number density of the dimples observed.

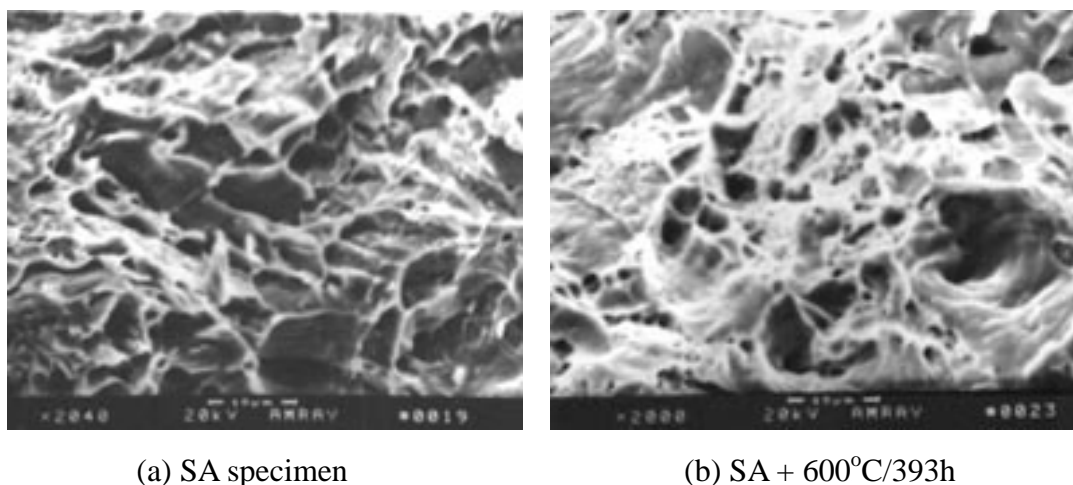


Fig. 5.11 SEM photos showing the morphology of the fracture surface of the tensile specimens tested at room temperature.

5.4 Hardening by cold rolling and its recovery

Figure 5.12 (a) shows the hardness of V-4Cr-4Ti type alloys as a function of the amount of cold work defined as reduction in thickness by cold rolling. As the data was obtained in the past few years in studies for different purposes, the alloy in different amount of cold work has different historical thermo-mechanical treatments [115,86, 119]. The last thermal treatment before the cold rolling is indicated in the figure. In spite of the difference, it could be deduced approximately from the figure that the cold rolling strengthened the alloy significantly and the hardness increased with increasing amount of cold work. Fig. 5.12 (b) shows the hardness recovery curves of the 20%CW cold-rolled V-4Cr-4Ti alloy (NIFS-Heat 2) during isochronally annealing from 200 to 1100°C for 1 h. Comparing with the hardness data shown in Fig. 5.8 (b), it could be found that the contribution of the cold rolling to the hardness differs with

the state of the prior heat treatments. The increase in hardness by the cold rolling was 54 (38%), 51 (40%) and 33 (19%) in Hv for the alloy in SA, CP and FP state at room temperature, respectively. The alloy in FP state having lower hardness increase by the rolling might be resulted from the lowered strain hardening capability due to the 10 h aging (see Fig. 5.10). Even though the smaller hardening, the alloy in FP state displays the highest hardness to more than 200 in Hv after the cold rolling. The hardness recovery curves shown in Fig. 5.12 (b) indicate that the hardening by the cold rolling could be maintained till $\sim 700^{\circ}\text{C}$, irrespective of the previous annealing or aging state. Further more, there is small additional hardening by the annealing at about $300\sim 600^{\circ}\text{C}$ for the cold rolled alloy in SA and FP state. The hardening might be caused by interactions between interstitial solutes and dislocations, which will be discussed hereinafter.

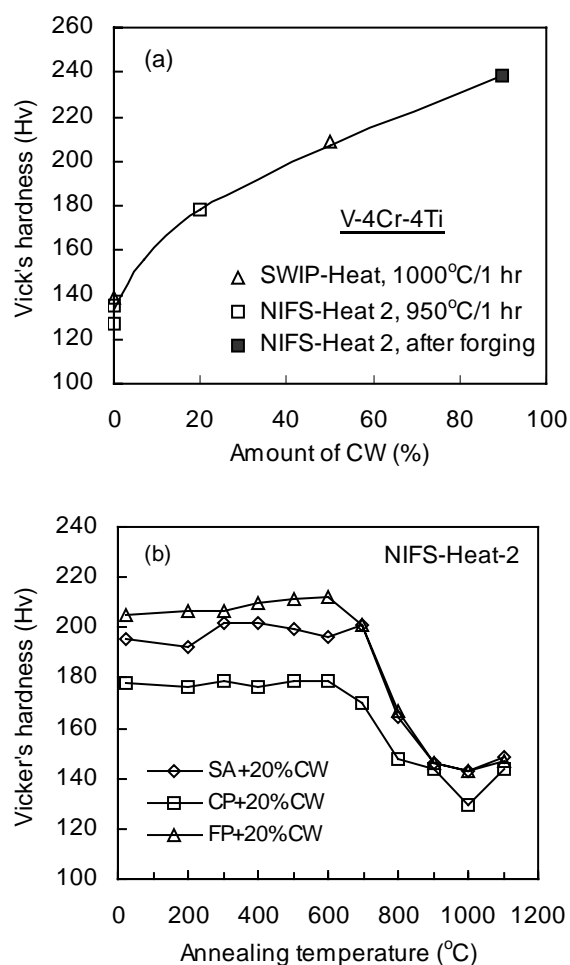


Fig. 5.12 (a) The dependence of Vicker's hardness on the amount of cold rolling rate for V-4Cr-4Ti [115,86, 119], and (b) the hardness recovery curves of the 20%

cold-rolled NIFS-Heat 2 alloy in different heat treatment states during the 1 h isochronally annealing in vacuum. Hardness was measured at room temperature.

5.5 Discussions and summary

5.5.1 Hardening at 600-700°C

Many studies showed that precipitates in V-4Cr-4Ti alloy were Ti-rich and most likely to be Ti- (O, N, C) [66,84,86,120]. Usually two kinds of precipitates were observed, large and fine ones. The large globular-shaped precipitates may be formed during the hot-working process [86]. The fine one was usually thought to be formed during the heat treatment at ~700°C [84]. In the present study, the 1100°C solid solution treated V-6W-4Ti alloy and the additional 900°C annealed one did not show any precipitates. It indicates that 900°C annealing couldn't produce any precipitates in the alloy. Therefore, the large precipitates appeared in the RA treated alloys should be produced in the previous melting, hot-working and heat treatment process. The precipitates are found Ti, C-rich and were presumed to be Ti- (O, N, C) precipitates also. The concentration of interstitial C, N and O in the matrix of the RA treated alloy must be very low due to the pre-existed large precipitates. As a result, precipitation won't occur anymore and hardening couldn't occur or is very small in the following annealing or aging as that shown in Fig. 5.2 (b). Estimated from the temperature dependence of the hardness, the microstructure of the alloy in RA state is thermally very stable at high temperature to 900°C.

The hardening by annealing at 600-700°C and aging at 600°C shown in Fig.5.2 and 5.8 is caused by precipitation for the SA-state alloys. This could be deduced from the good accordance of the hardness change with the characteristic of the fine precipitate shown in Fig. 5.3. However, precipitation would result in the loss of solid solution hardening because of the reduction of the interstitial solute and Ti in solution. As the fine precipitate grew bigger and bigger at higher temperature, the hardness of the alloys decreased due to the weakening of precipitation hardening and the loss of the solid solution hardening. The characteristic of the time dependence of the

hardening in Fig. 5.8 (a) supposes a continuous precipitation in the V-4Cr-4Ti alloy on aging at 600°C till ~10h, followed by precipitate coarsening which causes the loss of the hardening. In Fig. 5.8 (b) for the FP treated NIFS-Heat 2 alloy, additional hardening occurred at 600 and 700°C for the 1 h annealing. Thus the peak hardening of the alloy in the 600°C-aging should appear at a time between 11 to 24 h.

The results showed that the peak annealing hardening of the V-4Cr-4Ti alloy appeared at higher temperature than that of the V-6W-4Ti alloy, both in SA state. N. J. Heo [74] studied another V-4Cr-4Ti alloy, and also found peak hardening at 700°C and the precipitates exhibited a similar growth feature to those observed in the V-6W-4Ti alloy with increasing temperature. The hardening is also a precipitate hardening. Besides, V-4Cr-4Ti alloy showed a much stronger hardening capability than the V-6W-4Ti alloy both in the annealing and in the 600°C aging. It suggests that the fine precipitates produced in V-4Cr-4Ti must be smaller and in higher number density than those in V-6W-4Ti. On the other hand, the annealing induced hardening of the V-6W-4Ti is quite similar to that of the V-4Ti alloy. It indicates that the difference between V-6W-4Ti and V-4Cr-4Ti is caused by Cr other than W in solid solution. Ti and Cr could form an intermetallic phase of TiCr_2 in the Ti-Cr binary system [111]. It is possible that there is a strong interaction between Cr and Ti in V-Cr-Ti system, which may increase the number of the nucleation sites for precipitation and slow down the growth of the precipitates, because the interaction would decrease the mobility of Ti while the growth was proved in the present study to be controlled by the motion of Ti atoms in matrix. Estimated from these hardening behaviors, it is concluded that Cr addition to a V-Ti alloy could enhance the precipitation hardening. However, further investigation for the mutual interaction of Ti and Cr is required.

V-6W-1Ti and V-6W-4Ti displayed equivalent hardening in the aging. Estimating from the C, N and O concentrations in the alloys, 1mass%Ti is enough to exhaust the C, N and O interstitial impurities to form precipitates. Thus further Ti addition in the V-6W-Ti alloy could not change the hardening behavior.

5.5.2 Thermal stability of the precipitates

The results show that the hardening by aging at 600°C in the NIFS alloy is stable at and below 500°C, indicating that the aging-induced precipitates are thermally stable in the temperature range. This nature should be related to the mobility of Ti and other interstitial solutes in the alloy, as the precipitates are Ti-CON type. It is known that the interstitial C, N and O are mobile at ~300°C while Ti is mobile above 500°C [120]. In another word, Ti is relatively immobile below 500°C. Therefore, strong precipitation could only occur above the temperature. On the other hand, the growth of precipitate requires the diffusion of both Ti and the interstitial solutes. Consequently precipitate will not grow below the temperature and be thermally stable. However, the alloy in SA state exhibited some hardening at 300~500°C. It is presumed that at the temperatures interstitial solutes move to Ti and form some clusters, which strengthens the alloy a little. As the free interstitial solutes in FP treated alloy is much less due to the existed fine precipitates, so less cluster will be formed. Eventually, the FP treated alloy is more stable in hardness below 500°C.

Tensile behavior of the aged-alloy exhibited no yield deformation while the alloy in SA state exhibited obvious yield flow. Thus the yield flow in the SA-state alloy should be caused by the interstitial solutes, which pinned the dislocations in the alloy. Precipitation depletes the interstitials in matrix and thus more free dislocation remained. Virtually, the alloy in RA state, contains many large precipitate, also exhibited yield deformation behavior during another tensile test at room temperature, which will be shown in the chapter 6. This difference tells a deduction that the aging depleted more interstitials than the historical thermo-mechanical treatments or the RA treatment. On this point of view, the hardness of the 600°C-aged alloy might be more stable than the RA treated one, of course at temperatures lower than 500°C according to the above statements. Further more, the least free interstitial impurities in the aged alloys promote its priority for low temperature application in fusion reactors since the least interstitials in matrix may make the alloy have strong resistance to neutron irradiation inducing embrittlement as described in the introduction of the present

paper, however, this benefits should be verified further.

As the results have shown that the aging hardened alloy could keep its ductility high and even had better static fracture toughness after ~50 h aging at 600°C, and moreover, the hardening is stable up to 500°C, this hardening should be able to be used to increase the strength of the alloy, and have the potentiality as the structural material for components severed at relatively low temperature (<500°C) without changing the constitutional composition of the alloy.

5.5.3 Thermal stability of the hardening by cold rolling

Figure 5.13 shows the microstructure of the NIFS-Heat 2 alloy with SA+20%CW treatment followed by annealing at 750°C for 1 h. Apart from the dislocation structures shown in Fig. 5.13 (a), large precipitates were observed (see Fig. 5.13 (b)). As the alloy in SA state contains few precipitates [50] and the cold rolling could not produce any precipitate in it, the observed precipitates must be formed during the annealing. At other temperature if suitable for the precipitation, similar microstructure will certainly be observed but surely with different precipitate size and number density. Therefore, the hardness of the alloy contains the contribution of precipitation hardening and the dislocations, both will change with the change of the annealing temperature. To analyze the thermal stability of the hardening by cold rolling solely, the precipitation hardening should be removed.

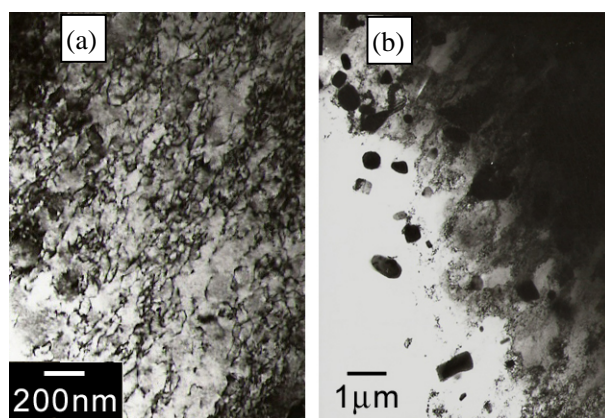


Fig. 5.13 TEM microstructure of the NIFS-Heat 2 alloy in SA+20%CW state after annealing at 750°C for 1 h, (a) dislocations and (b) precipitates.

The precipitation hardening during the 1 h isochronally annealing in the present study is included in the hardness (H_P) shown in Fig. 5.8 (b) for the NIFS alloy. With 20%CW cold rolling, the hardness increases to another value (H_{P+CW}) shown in Fig. 5.12 (b), which changes with the annealing temperature due to precipitation hardening and the recovery of the cold rolling produced dislocation structure. The remained contribution of the cold rolling to the hardness (H_{CW}) after the annealing could approximately be obtained with the expression of $H_{CW} = H_{P+CW} - H_P$. Thus the recovery rate (R) of the hardening (ΔH_{CW}) by the 20%CW cold rolling after the annealing could be expressed as $R = (H_{CW} - \Delta H_{CW}) / \Delta H_{CW}$. Figure 5.14 shows the dependence of R on the annealing temperature. It could be seen from the figure that notable recovery has taken place at 700°C for the NIFS-Heat 2 alloy in any state of SA, CP or FP. That is, the hardening caused by the 20%CW cold rolling could be maintained from RT to 600°C. Moreover, an additional hardening around 500°C for the cold-rolled FP sample and a smaller one at 300~400°C for the cold-rolled SA sample were found.

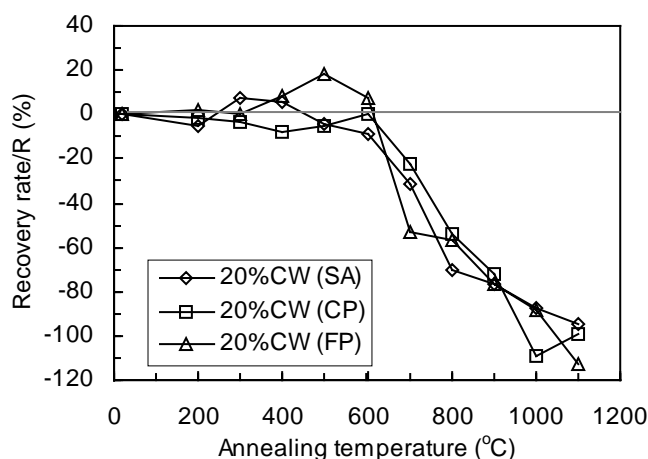


Fig. 5.14 Hardness recovery rate of the 20% cold-rolled NIFS-Heat 2 alloy without the contribution of precipitation hardening caused by the isochronally annealing.

The additional hardening is possibly related to the interaction between interstitial impurities and dislocations. In the annealing process interstitial solutes may diffuse into dislocations, which impede dislocation motion, decrease dislocation recovery and increase the deformation resistance of the alloy in the following hardness test and increase its hardness therefore. Since the alloy in CP state contains many large

precipitates, the effective interstitial C, N and O impurities would be quite few. Such interaction would be very weak and no additional hardening occurred. The stronger additional hardening occurring at 500°C for the 20%CW FP sample than that for the 20%CW SA sample at 300-400°C suggests that the pre-existed fine precipitates in the FP sample resisted the recovery of the dislocation structure, causing a strong appearance of the additional hardening. Otherwise, the additional hardening of the SA sample should be stronger for it contains the most interstitial impurities in solid solution.

5.5.4 Summary

The precipitation behavior in V-6W-4Ti was studied in detail, together with the precipitation hardening in the alloy and in other alloys of V-4Cr-4Ti, V-4Ti and V-6W-1Ti. Just similar to that reported for the V-4Cr-4Ti alloy, the precipitates formed in the V-6W-4Ti alloy during annealing and aging are Ti and C-rich ones. The precipitates got coarsening with increasing annealing temperature, started from ~600°C, leading to the decrease of the precipitation hardening. The growth of the precipitates obeys to thermal activation kinetics with the activation energy of 335.6 kJ/mol and thus is presumably controlled by the diffusion of Ti other than C, N and O interstitial solutes in the matrix of the alloys. Other results could be summarized as follows.

- (1) Due to the strong interaction of Cr-Ti, peak hardening by the precipitation shifts to higher temperature in V-4Cr-4Ti as compared to other alloys without Cr.
- (2) Precipitation hardening by aging at 600°C in V-4Cr-4Ti is very strong and is stable at <500°C. Peak hardening could be obtained by the aging for ~11-24 h. Comparatively, other alloys without Cr addition show weaker precipitation hardening. Cr seems to be able to enhance the precipitation hardening significantly, while Ti in the level of 1~4% mass shows little effect.
- (3) Precipitation hardening by aging at 600°C neither deteriorate the ductility significantly and nor decrease the absorbed energy in the tensile test of the alloy particularly when aging time exceeds ~50 h.

- (4) The precipitation hardening could be utilized to strengthen an alloy, which may be used for the components subject to higher stress levels at relatively low temperature of $\leq 500^{\circ}\text{C}$ considering its thermal stability. This kind of alloy may have strong resistance to neutron irradiation embrittlement as well due to the depletion of interstitial solutes in matrix by the precipitation.
- (5) The alloys containing the most of the large precipitates formed in the historical thermo-mechanical process have very strong thermal stability of microstructure and hardness at $200\text{-}900^{\circ}\text{C}$. For high temperature service above 600°C , alloy in $\sim 900^{\circ}\text{C}/1\text{hr}$ annealing state should be used.

Hardening by cold rolling has been investigated as well. Thermal stability of the hardening is analyzed. It was found the $600^{\circ}\text{C}/10\text{ h}$ aged plus 20%CW has very high strength with its harness of more than 200Hv for V-4Cr-4Ti. The combined hardening is also stable at $\leq 600^{\circ}\text{C}$, and has the potential for application for high strength vanadium structures.

6. Motion of interstitial solutes and DSA

It was reported that C, N and O impurities are mobile below 300°C in V. They migrate to dislocations at high temperature, affecting the higher temperature performance of the metal. Ti has strong affinity to the impurities and could resist the motion or lead the motion take place only at higher temperature. Thus alloying elements may change the performance. H is the smallest solute in an alloys, is mobile even at room temperature. All these motions or the consequent interactions would influence the mechanical performance of an alloy significantly.

6.1 Effect of C, N and O on recovery behavior and role of alloying elements

6.1.1 General behavior

50%CW (amount of cold rolling defined as the reduction ratio in thickness) vanadium alloys were isochronally annealed at 200-1000°C to study their hardness recovery and recrystallization behaviors. Figure 6.1 shows the recovery curves for some of the alloys. Two sets of data from literatures [106,115] for NIFS-heat2 V-4Cr-4Ti and unalloyed V are together plotted in the figure. Hardness recovery almost stopped at 900°C for all of the alloys, indicating a complete recrystallization. Accordingly, alloying elements have little effect on the 1hr-annealing temperature for complete recrystallization. However, the recovery behavior at lower temperature is somehow different between the alloys with and without Ti/Al addition. Typical representatives are V-8W and unalloyed V, those without Ti, for them there appeared additional hardening peaks around 300°C. The hardening looks very strong with a hardness increase by a factor of more than 20%. Moreover, including V-7W-0.3Al, notable hardness recovery occurs at a temperature of 100°C lower than that for the others with Ti addition. The former is about 600°C, while the latter is about 700°C.

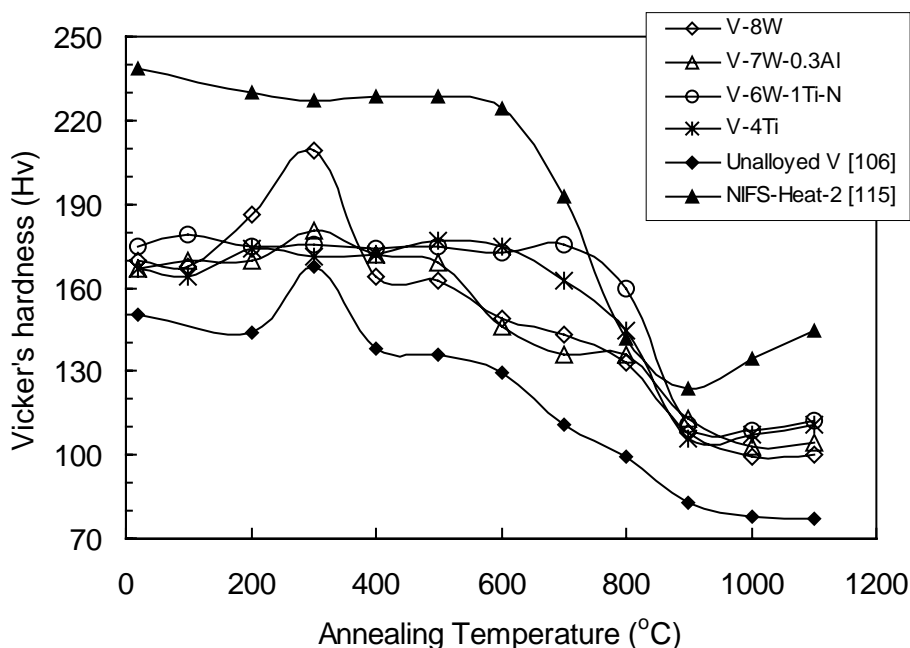


Fig.6.1 The hardness of the isochronally annealed alloys as a function of annealing temperature.

The additional hardening was caused by interactions between interstitial C, N, O impurities and dislocations produced in the previous cold rolling. These impurities are mobile at $\sim 300^{\circ}\text{C}$ [120] and their migrations into the dislocations not only decrease the potential energy of the cold-rolled alloy but also impede dislocation motions. The interaction consequently slowed down the recovery. However, this is impossible to increase hardness. Virtually, the hardness increase was caused by the impurities in the dislocations and their resistance to the dislocation motion not during the high temperature annealing but in the following hardness test at room temperature.

Titanium has strong affinity to the impurities, which, as a result, can hardly move to the dislocation sites at low temperature to produce their interaction and the dislocations, leading to the absence of the additional hardening for the Ti-bearing alloys around 300°C . As the temperature gets higher, Ti becomes mobile above 500°C [120]. The binding Ti-O or those of Ti with other interstitial solutes could be broken by thermal activation of Ti and the impurity solutes. The impurities get free from the binding to move to dislocations to resist their motion and would cause hardness increase in the following hardness tests. However, no notable additional hardening

was observed for these alloys despite of the interactions, indicating the recovery of dislocation structures is bigger as compared to that at low temperature of $\sim 300^{\circ}\text{C}$, which reduced the total hardness increase. It's clear from the results that the interaction makes the alloy with Ti show little hardness recovery at $600\text{-}700^{\circ}\text{C}$.

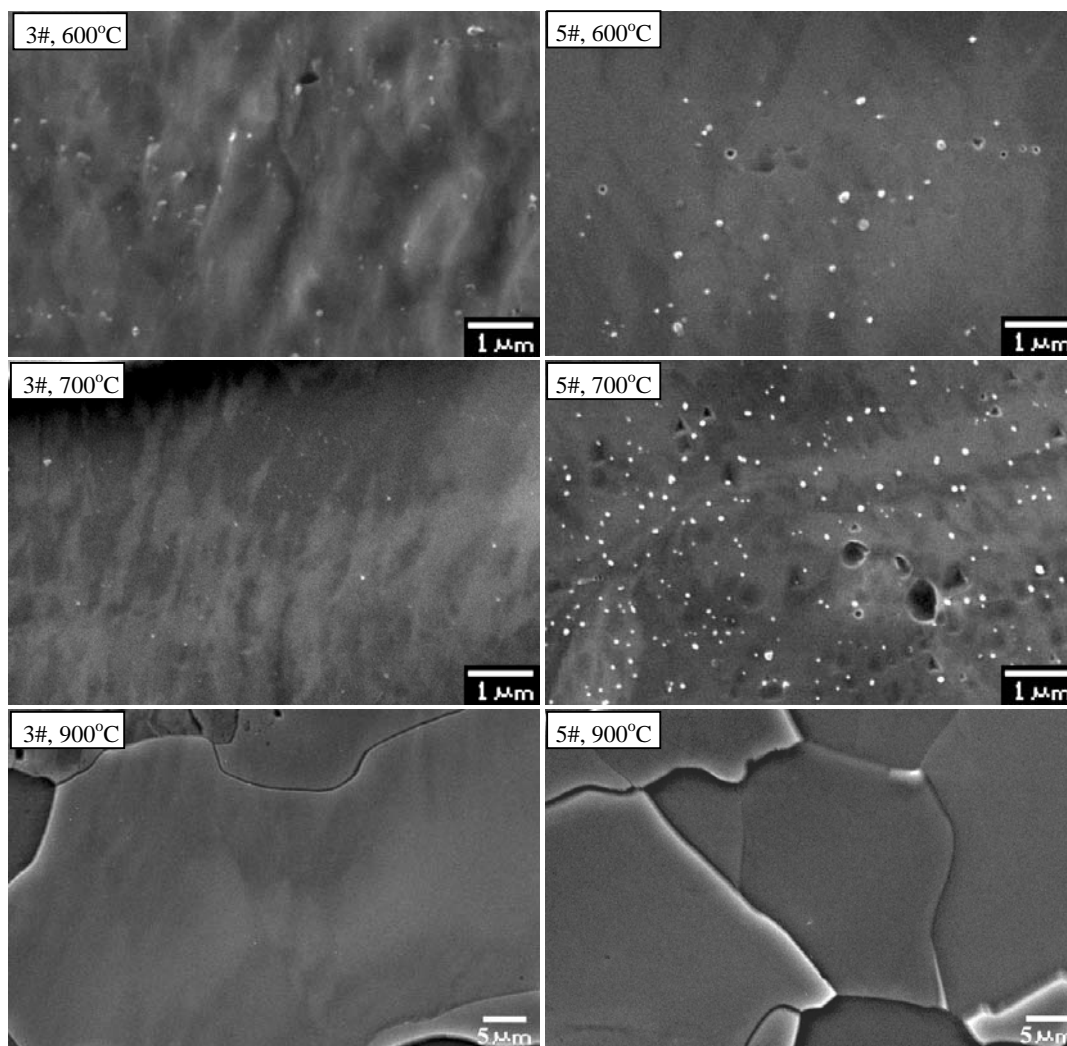


Fig. 6.2 SEM photos showing the precipitates in the alloys annealed at 600°C , 700°C and 900°C , 3#: V-6W-1Ti-N, 5#: V-4Ti.

In addition to the effect of Ti of suppressing the interaction of interstitial impurities with dislocations on the hardness recovery at relatively low temperature, precipitation due to the Ti and the impurities could also have certain effect. SEM observation showed many precipitates in the alloys with Ti at 600 and 700°C , as shown in Fig.6.2, but hardly any precipitate is observed at 900°C . Most of the

precipitates are less than $0.4\mu\text{m}$ in diameter. The precipitates distributed heterogeneously, were found to be much smaller and with less number in V-6W-1Ti-N than those in V-4Ti. This result indicates that the precipitation varies with the alloy composition and the annealing temperature. On the other hand, nearly no or very small numbers of precipitates were observed in the alloys without Ti. Surely the precipitates were formed due to the addition of Ti. For vanadium alloys containing Ti, precipitation of Ti- (CON) precipitate usually occurs at $600 - 800^\circ\text{C}$. This has been described in other part of this paper.

In another annealing of V-6W-4Ti and V-4Cr-4Ti at 800°C , hardness was measured after short time exposure of less than 1 h. Result shown in Fig.6.3 indicates that the hardness recovery had high rate within the initial 20 minutes, following with a quite slow decrease of the hardness with time. Invariably, V-6W-4Ti showed less hardness recovery than V-4Cr-4Ti and the difference got larger with increasing time. It indicates that W rather than Cr has more effect on the recovery behavior. W has high melting point and was thought to have low self-diffusivity in V [121]. Thus the substitutional W could give more resistance to dislocation climb than other alloying elements, which is quite significant to high-temperature recovery of cold-worked alloys. Subsequently, hardness recovery becomes a little more difficult due to W.

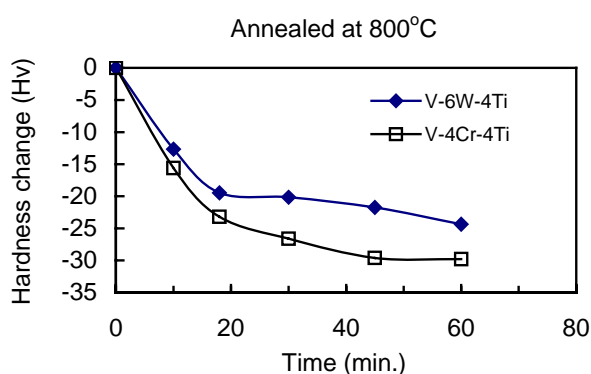


Fig. 6.3 The hardness change of V-6W-4Ti and V-4Cr-4Ti alloys annealed at 800°C as a function of annealing time.

Though the alloying elements have little effect on the complete recrystallization temperature, the recrystallized grain size at 900°C showed certain dependence on

them. As we known, small grain could increase the mechanical strength of a material; the hardness after the recrystallization might contain the contribution of the grain size. Fig. 6.4 shows the grain size of some alloys after the 1 h annealing at 900°C as a function of the sum of the concentrations of their main elements. Here the factor for W was taken as 0.9, while that for others is 1. With this assumption, the grain size of the Ti-bearing alloys shows a good linear dependence on the total concentration. It seems that any addition of Cr, Ti or W could decrease the size, but the grain size data for V-8W located far above the linear dependence line in the figure, indicating that the contribution of W in V-8W is not as big as it in other alloys containing Ti. Though the reason for it is not known, it could roughly be concluded that the combination of more alloying elements is more effective to decrease grain size than a single element besides the base element of V.

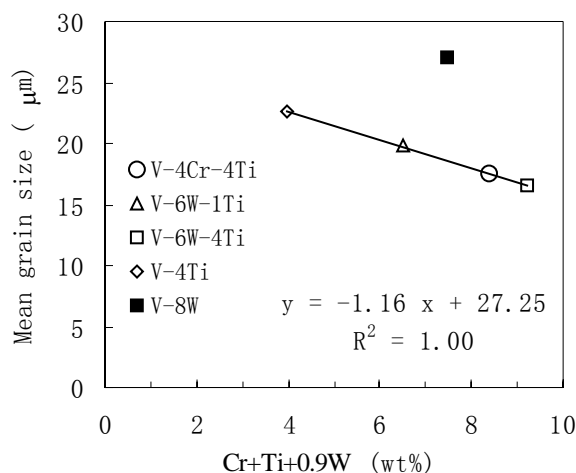


Fig. 6.4 The mean grain size of the alloys after 900°C/1h annealing as a function of a modified total amount of the main alloying elements in weight (wt) concentration.

It was found that the recrystallized grain grows drastically above 900°C. Figure 6.5 shows the image of the recrystallized grains in V-4Ti after annealing at 900°C for 1h and the change of the grain size with the annealing temperature along with other alloys. Clearly the grains are all in equiaxial shape, indicating that recrystallization has completed at the temperature. The grain size increases with increasing temperature greatly. As an example, the size increases from 17 to 39μm for V-4Cr-4Ti in the temperature range. Unlike others, the drastic increase happened above 1000°C

for V-4Cr-4Ti. It seems that the Cr-Ti interaction stated in Chapter 5 is still active at 1000°C, which reduce the grain growth rate. Though the difference in grain size among the alloys is big at 900°C, it becomes small at 1100°C where only V-4Ti shows relatively larger grain size.

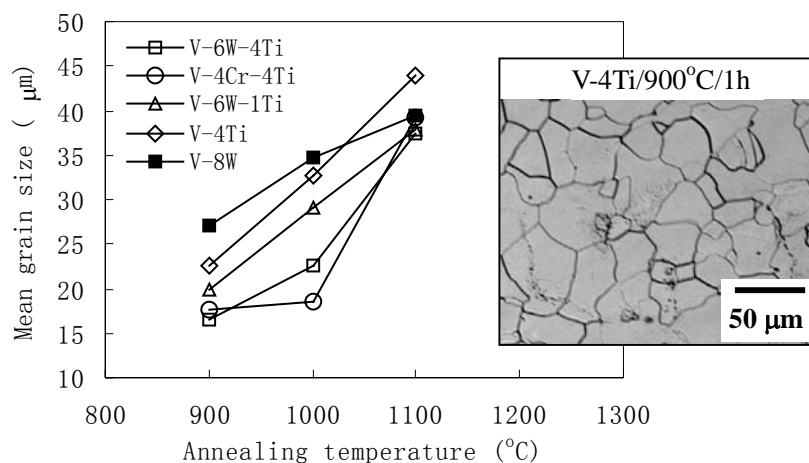


Fig. 6.5 The mean grain size of the alloys as a function of annealing temperature, together with an optical microscopic photo showing the equiaxed grains in V-4Ti after annealing at 900°C for 1h.

6.1.2 Effect of interstitial impurities in matrix

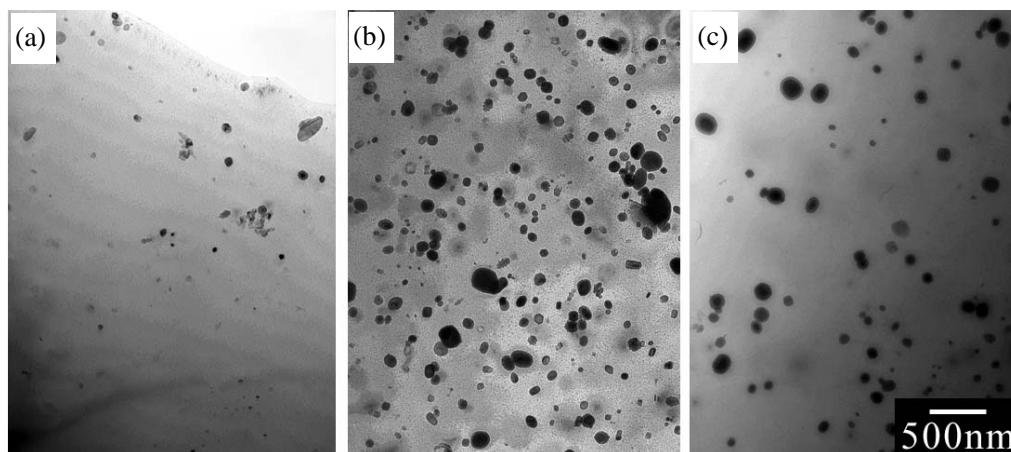


Fig.6.6 TEM microstructure of the 900°C annealed alloys showing the large precipitates, (a) V-6W-1Ti, (b) V-6W-4Ti and (c) V-4Cr-4Ti.

As we know, C, N and O interstitial impurities in the V-X-Ti alloys may form precipitates with Ti. Studies have shown that large size precipitates is formed during the preparation of the alloy in the forging and hot rolling process. As a result, the

amount of the interstitial impurities in matrix will be decreased, which may affect the recovery behavior of the alloys. Figure 6.6 shows the microstructure, which contains many large precipitates, of V-6W-1Ti, V-6W-4Ti and V-4Cr-4Ti alloys, all with 50%CW, after annealing at 900°C for 1 h.

Figure 6.7 shows the dependence of hardness on the 1h isochronal annealing temperature for V-4Ti and NIFS-Heat 2, which were annealed at 900°C and 950°C for 1h for recrystallization in advance, respectively. Similar to the microstructures of those alloys shown in Fig. 6.6, both alloys should also contain many large precipitates prior to this isochronally annealing because both temperatures are not high enough for dissolution of the precipitates. The figure shows there is softening at 800°C for both alloys, indicating the coarse or growth of the precipitates. Above this temperature, their hardness increases with increasing temperature, indicating an increasing solid-solution hardening due to the resolution of the precipitates and the increasing amounts of interstitial C, N and O in matrix.

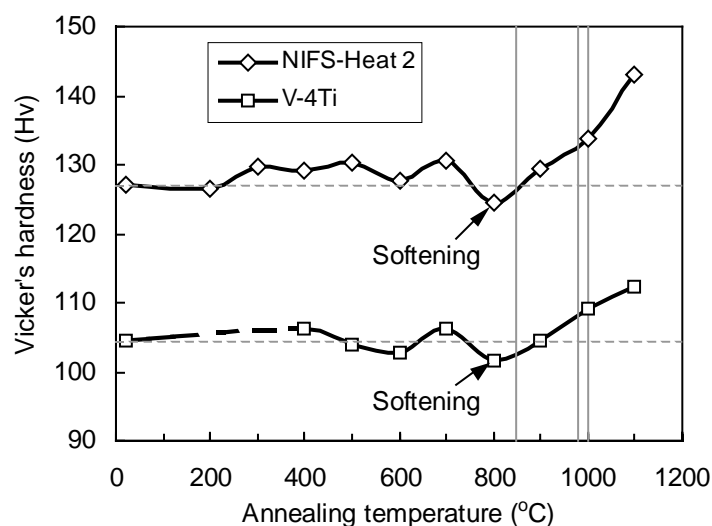


Fig. 6.7 The hardness of V-4Ti (900°C/1h annealed) and V-4Cr-4Ti (NIFS-Heat 2, 950°C/1h annealed) as a function of annealing temperature for the 1h isochronally annealing.

In the present study, the 50%CW cold-rolled alloys, some of which were annealed at 850°C for 1h and some at 980-1000°C for 1h before the cold rolling, were used for the recovery and recrystallization (R&R) experiment. The temperatures are plotted by

vertical lines in grayish color in Fig. 6.7. According to what stated above, the one ever annealed at 980-1000°C would have more interstitials in solid solution than those ever annealed at 850°C. By comparing the R&R behavior of the alloys in both annealing states, the effect of interstitials in matrix on this behavior could be obtained.

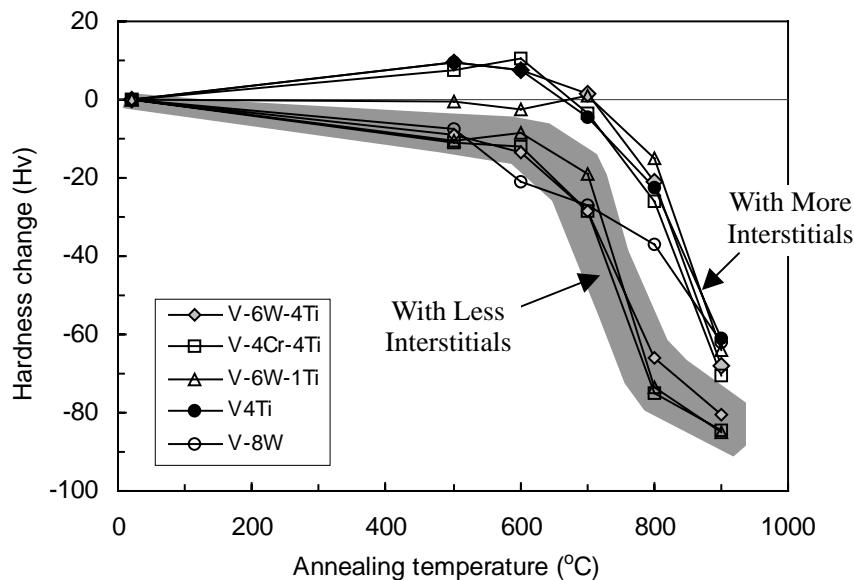


Fig. 6.8 Hardness changes after annealing at 500-900°C for the alloys with less (lines within the shadow area) and more (others) interstitials in matrix.

Figure 6.8 shows the hardness change for the alloys with less or more interstitials after the isochronally annealing. It tells a story that more dislocation recovery and so more hardness loss occurred for the alloys containing less interstitials in matrix. But the alloys containing both 4%Ti in mass and more interstitials in matrix even exhibit certain additional hardening by the 1h-annealing at 500-600°C and their hardness recovered less above the temperature. It has been stated that interstitial C, N and O could migrates towards dislocations and impede their motion, consequently dislocation recovery becomes less and so the hardness could keep high. The additional hardening is caused by the same mechanism as that for the V-8W alloy at 300°C, the resistance of the interstitial solutes in dislocations to their motion during the hardness test. **Therefore, it could be concluded that additional hardening could happen for any of the alloys when they had enough high amount of interstitial C, N and O in their matrixes. The hardening appears at higher**

temperature for the Ti-bearing alloys due to Ti decreasing the mobility of the interstitials at less than 500°C.

V-6W-1Ti that annealed at 980°C before the cold rolling, unlike the 4%Ti alloys, doesn't exhibit the additional hardening at 500~600°C. It seems that the hardening is also affected by the Ti concentration. However, this difference is unlike to be caused by precipitation since the precipitation hardening for the V-6W-4Ti and V-4Cr-4Ti alloys are quite different as described in Chapter 5 but here both alloys show quite similar additional hardening behavior. Theoretically thinking, the interstitials in low Ti alloy should be more mobile and has weaker resistance to dislocation motion than the high Ti alloy at the temperature. Consequently, the hardness recovered more and additional hardening would not occurred at the temperature although interstitials surely have migrated into the dislocations and have similarly resisted dislocation motion in the following hardness test at room temperature as what happened in the alloys with 4%Ti in mass.

Ti decreases the mobility of interstitial solutes in V-base alloys, thus the additional hardening shifts to high temperature. The temperature is about 300°C for alloys without Ti and 500-600°C for the alloys with 4%Ti in mass. Accordingly, the temperature for V-6W-1Ti should appear at a middle temperature. However, this was not occurred for the alloy as shown in Fig. 6.1. It is not understandable and requires further studies.

6.1.3 Summary

The effects of alloying elements, interstitial solutes and their interactions on the recovery and recrystallization of V-base alloy were investigated. Alloys concerned were V-4Cr-4Ti, V-4Ti, V-6W-4Ti, V-6W-1Ti, V-7W-0.3Al and V-8W. Results could be summarized as follows.

- (1) Strong interactions of interstitial impurities with dislocations will take place at ~300°C for alloys without Ti, causing strong additional hardening in the recovery test at the temperature.

- (2) The interactions in the Ti-bearing alloys still exists but occurs at higher temperatures (500-600°C) due to Ti decreasing the mobility of interstitial C, N and O solutes. This characteristic makes the alloys with Ti start the notable hardness recovery at higher temperature than the alloys without Ti. If the free interstitials in matrix is sufficient high, additional hardening will also happen for the Ti-bearing alloys at 500-600°C.
- (3) W seems to have stronger resistance to dislocation recovery at high temperature than Cr. Further investigation is required to understand its mechanism.
- (4) The least temperature for complete recrystallization is about 900°C, irrespective of the variation in alloying elements in the present alloys. However, the grain size was effectively decreased by any addition of Ti, Cr and W, and the combination of more elements than one plays greater role.
- (5) Grain growth rate increases rapidly with increasing temperature from 900°C to 1100°C. Cr-Ti interaction stabilizes the grain size till 1000°C.

6.2 High temperature tensile tests

6.2.1 Tensile properties and fracture characteristics

Fig. 6.9 shows the tensile properties of the tested alloys plotted against test temperature, together with the data of NIFS-Heat-1 (V-4Cr-4Ti) reported by K. Fukumoto [122]. The strength of the V-6W-1Ti is the lowest one among the alloys, indicating weaker solid solution strengthening by its less Ti concentration. At room temperature, V-6W-4Ti had the highest strength among the alloys, which decreased more rapidly than that of the V-4Cr-4Ti (NIFS heat) with increasing temperature. Strengthening happened with increasing temperature above ~400°C for almost any of the alloys, corresponding to the occurrence of DSA (dynamic strain aging). The strengthening stopped at 600°C for V-6W-4Ti but kept increasing till 700°C for V-4Cr-4Ti. Both alloys had similar strength from 400 to 600°C. At 800°C the ultimate

tensile strength of V-6W-4Ti lost much with a very high total elongation of more than 40%. Tensile curve showed that strain hardening ceased after a small amount of plastic deformation for the alloy, indicating the deformation induced by creep at the temperature. For the NIFS Heat, however, this change seems not to have occurred in spite of its less loss in ultimate tensile strength at the temperature. Commonly, the elongation of the alloys decreases with increasing temperature below 600°C.

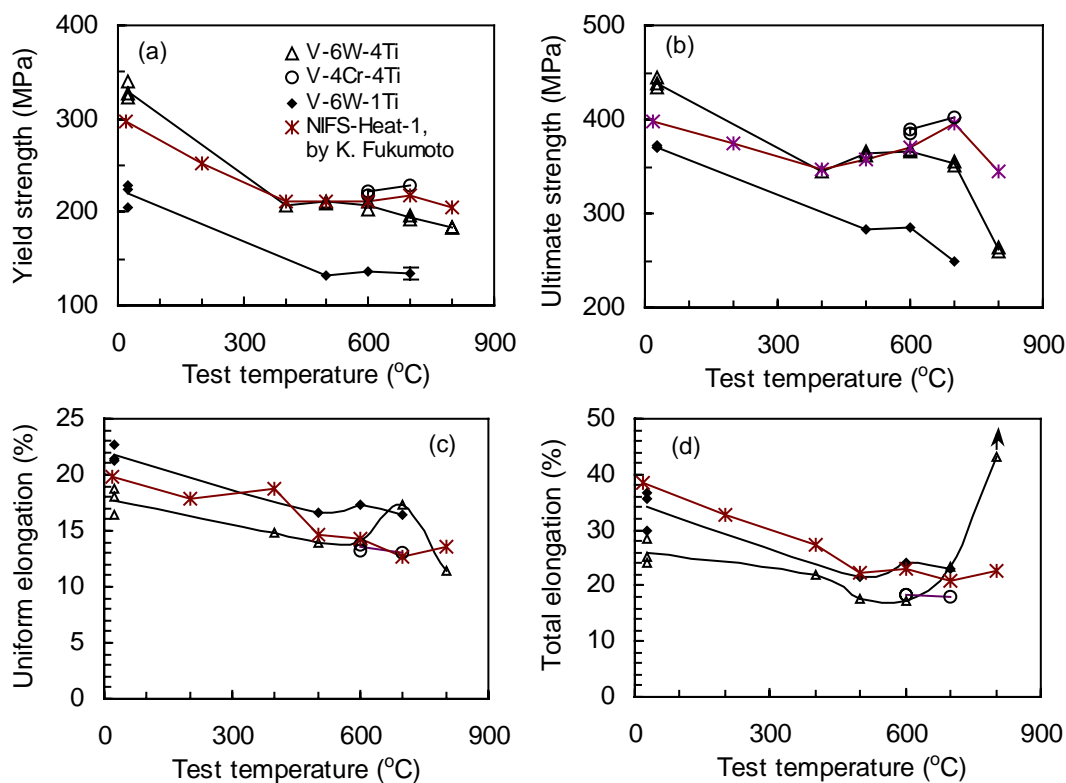


Fig. 6.9 The temperature dependence of (a) yield strength (b) ultimate tensile strength (c) uniform elongation and (d) total elongation.

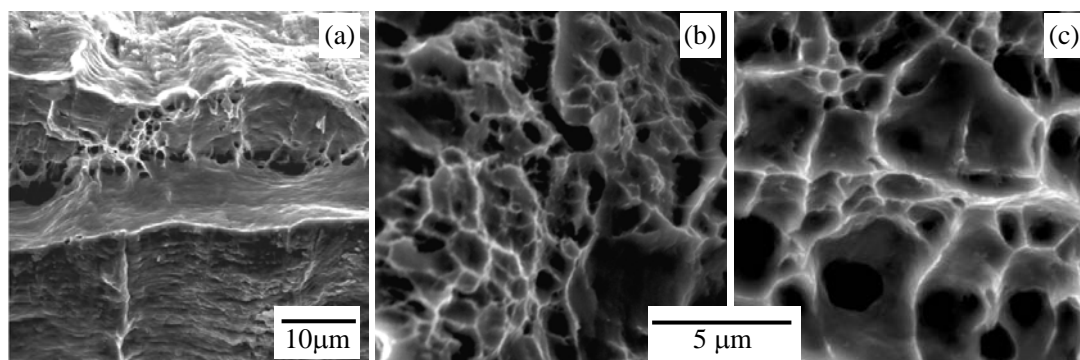


Fig. 6.10 SEM photos showing the fracture patterns of the specimens tested at 600°C and 700°C, (a) V-6W-1Ti/600°C, (b) V-4Cr-4Ti/700°C, (c) V-6W-4Ti/700°C.

SEM observation of the fracture surface showed that all specimens had large reduction in cross section area of more than 90%, indicating that significant necking had taken place before the final fracture. The fractures were commonly in dimple patterns with large portion of shear lips. Examples of the fractographs are shown in Fig. 6.10. It is obvious that the dimples in V-4Cr-4Ti are much smaller than those in V-6W-4Ti, indicating stronger deformation resistance in the former alloy.

6.2.2 Tensile behavior and the appearance of the DSA

Fig. 6.11 (a) illustrates the tensile curves of V-6W-4Ti tested at room temperature (RT) and 400~800°C. Following the elastic regime, Lüders extension occurs at RT without the initial stress drop. The extension seems to get shorter with increasing temperature and thoroughly disappeared at >500°C. The behavior is quite different from other alloys. Results showed that yield or the Lüders extension didn't occur for V-6W-1Ti at any temperature tested. It didn't occur at 600°C but at RT for V-4Ti, the only two temperatures at which the alloy was tested. Obvious Lüders extension was observed for V-4Cr-4Ti tested at both 600 and 700°C. It is thus summarized that only V-4Cr-4Ti, the alloy containing Cr, has the Lüders extension at $\geq 600^\circ\text{C}$ among the alloys.

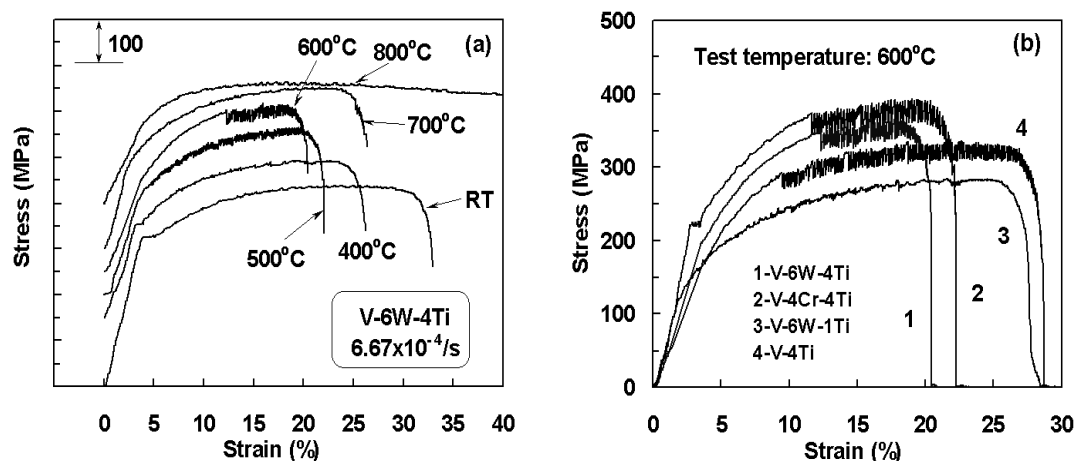


Fig. 6.11 Tensile curves of the V-6W-4Ti alloy at different test temperature (a) and the one together with others at 600°C showing the appearance of DSA behavior (b); Curves in Figure (a) offset on stress axis for clarity.

Serrations of flow curve occurred at about 500~700°C for V-6W-4Ti (Fig. 6.11(a)). The height of the serrations increased with increasing temperature, and the initiation point of serrations changed with temperature. It initiated at the start of plastic deformation at low temperature but shifted toward the end part of the flow curve at higher temperature regime. At 700°C, there were just several serrations appeared shortly after the plastic instability. These serrations are known to be related to DSA phenomena, an interaction between dislocations and interstitial solutes. Being a non-uniform deformation, the behavior is much similar to yield flow and thus could be explained by the following equations, which is used to describe yield deformation.

$$\left(\frac{d\varepsilon}{dt}\right)_p = \rho b v. \quad (6.1)$$

Here $(d\varepsilon/dt)_p$ is plastic strain rate, which could be taken as constant in the present tensile test due to the constant tensile strain rate. ρ is dislocation density, which could be supposed to be approximately constant at a strain. The character b is the Burgers vector of the dislocation and v is dislocation velocity, which is a function of the shear stress (τ) applied on the dislocations and could be expressed as

$$v = \left(\frac{\tau}{\tau_0}\right)^{m'}. \quad (6.2)$$

τ_0 is the shear stress for $v=1$, and m' is called as stress sensitivity exponent. According to Eqn. (6.1), v should keep constant during the tensile test to meet the constant strain rate requirement. When a dislocation was pinned by interstitial solutes, its velocity would decrease. To keep it unchanging, the applied stress must increase according to Eqn. (6.2). The dislocation will get free from the pinning at enough high stress. As a result, the velocity of the dislocation increases and the applied stress should decrease accordingly. When the mobility of the interstitial solutes could match up with the motion of the dislocations, such process will repeatedly take place, leading to the serration of the applied stress-strain curve. Because the motion of dislocations is mainly dependent on strain rate while the mobility of interstitial solutes depend on test temperature, the serration or DSA could occur in specific ranges of strain rate and test temperature. Though interstitial C, N and O are mobile at ~300°C, the mutual

binding of them by Ti in the alloys makes them be mobile at higher temperature of $\sim 500^{\circ}\text{C}$ (at which Ti is mobile). That's why the DSA appeared at $>500^{\circ}\text{C}$.

The tensile curve at 600°C shown in Fig. 6.11 (a) clearly shows that the serrations started with stress drop. It means that interstitial solutes pinning dislocations had occurred before the occurrence of DSA. With the increase of temperature, interstitial solutes become more mobile and the pinning strength gets stronger due to more impurities moving to pin dislocations until a maximum pinning strength is achieved. As a consequence, out-of pinning can take place at higher stress. This should accounts for the delay of the serrations at high temperature. At even higher temperature, interstitial solutes become so mobile that little resistance could they apply on dislocation motion, DSA, thus the serrations, disappear.

The amplitude of the stress drop, i.e., the height of the serration, should reflect the intensity of the dynamic strengthening by interstitial solutes. Comparing the serration height of the alloys from the tensile curves shown in figure 6.11 (b), the strengthening in V-4Ti, V-6W-4Ti and V-4Cr-4Ti is quite similar to each other, but being quite stronger than that in V-6W-1Ti. In fact, no strong serration was observed for V-6W-1Ti at any temperature. This weaker strengthening by interstitial solutes for V-6W-1Ti is in good accordance with the weaker additional hardening observed in the recovery studies stated in section 6.1.2. So once more it is confirmed that interstitial solutes in V-6W-1Ti is more mobile than those in other alloys with 4%Ti in mass. **In another word, it could be concluded that the serration height is temperature and Ti concentration dependent and has little relation with the Cr or W addition in the alloy.**

6.2.3 Effect of alloying elements and interstitials on the tensile strength

Comparing with V-6W-4Ti at $>600^{\circ}\text{C}$, V-4Cr-4Ti exhibited higher strength, not only the yield strength but also the ultimate tensile one. It is seemingly due to the successive increase of the strength of V-4Cr-4Ti but the decrease of the strength of V-6W-4Ti from 600°C to 700°C . This temperature dependence of the tensile strength

looks much similar to the temperature dependence of the precipitation hardening for both alloys in the 1 h isochronally annealing (see Fig. 5.2 (a) in Chapter 5). It has been stated in section 5.5.1 that Ti in V-4Cr-4Ti is less mobile than in V-6W-4Ti due to the strong interaction between Ti and Cr. The slower mobility of Ti in V-4Cr-4Ti will theoretically cause the DSA shifts to higher temperature. DSA has the role to strengthen the alloy, and the shift must have certain contribution to the high temperature tensile strength of V-4Cr-4Ti at 700°C. Furthermore, interstitial solutes in V-4Cr-4Ti, having slower mobility due to mutual binding of the lower mobility Ti to all of them, should provide stronger resistance to dislocation motion than the ones in V-6W-4Ti, thus the strength of V-4Cr-4Ti could keep high at high temperature.

On the other hand, TEM observation showed that the V-6W-4Ti alloy contains more large precipitates than the V-4Cr-4Ti alloy as shown in Fig. 6.6. According to the photos, their area number density is about $2.35 \times 10^{13}/\text{m}^2$ and $8.77 \times 10^{12}/\text{m}^2$, respectively. Considering the similar C, N and O impurity level in both alloys and the precipitates absorbing the interstitial solutes, the solutes in the matrix of V-6W-4Ti is thus much less in amount than those in the matrix of V-4Cr-4Ti. Under the same test condition, more interstitial solutes would make the DSA stronger due to more interstitial solutes could take part in their interactions with dislocations. So at this point of view, the V-4Cr-4Ti alloy should have higher strength than the V-6W-4Ti alloy at high temperature.

6.2.4 Summary

High-temperature tensile properties of V-4Cr-4Ti, V-6W-4Ti, V-6W-1Ti and V-4Ti were investigated with emphasis on the effects of alloying elements and interstitial impurities. Results could be summarized as follows.

- (1) V-6W-4Ti has good high temperature strength below 600°C. However, its strength is inferior to V-4Cr-4Ti at higher temperature.
- (2) DSA occurs for all of the alloys tested at ~500-700°C. The height of the serrations of the load-displacement curve caused by DSA is temperature and

Ti dependent, but shows little relations to Cr and W additions in the alloys.

- (3) Similar to the stronger precipitation hardening property of V-4Cr-4Ti than V-6W-4Ti above 600°C, the better high temperature strength of V-4Cr-4Ti is due to the lower mobility of Ti and interstitial C, N and O in the alloy, caused by the Cr-Ti interactions. Another possible reason may come from the relatively less free interstitial C, N and O in the matrix of V-6W-4Ti than those in the matrix of V-4Cr-4Ti.

6.3 Hydrogen release during tensile loading at room temperature

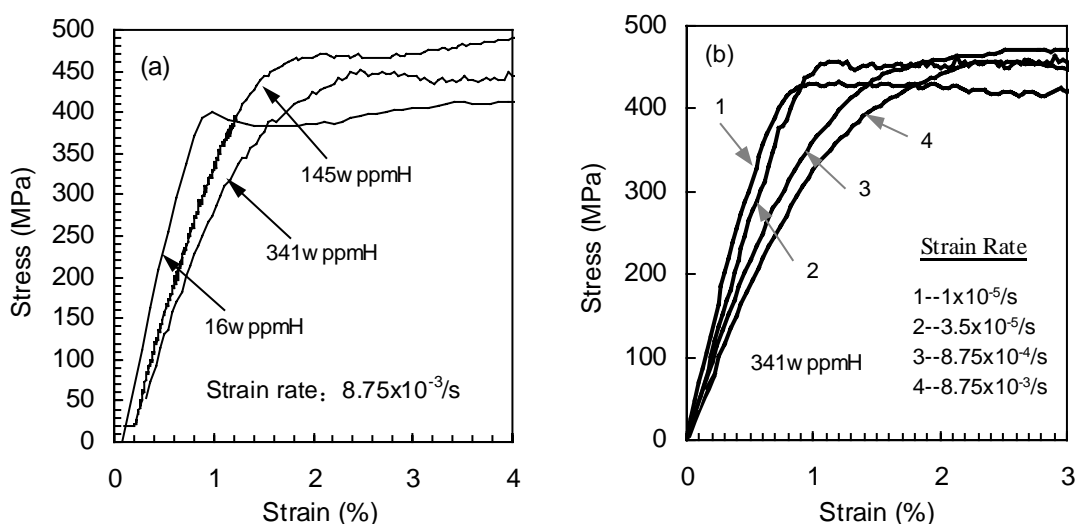


Fig. 6.12 Tensile curves of V-4Cr-4Ti containing (a) 16, 145 and 341 wppmH and (b) 341 wppmH at different strain rate.

The V-4Cr-4Ti alloy containing different hydrogen concentration from 16 to 341 wppm was tensile tested at room temperature at strain rate of 1×10^{-5} - $8.75 \times 10^{-3}/s$. Fig. 6.12 (a) shows the tensile curves at strain rate of $8.75 \times 10^{-3}/s$. The Young's modulus of the alloy could be estimated approximately from the slop of the initial part of the curves in elastic regime. Obviously the modulus decreases with increasing hydrogen concentration. This is because the hydrogen decreased the mutual binding force between the atoms of the alloy while the elastic modulus is proportional to the binding force.

Figure 6.12 (b) is the tensile curves for the alloy containing 341 wppmH tested at

various strain rates at room temperature. In the same way the Young's modulus could be estimated. It is found that the modulus increases with the decrease of the strain rate. Usually elastic modulus would not be affected by tensile rate because elastic wave transfers at sonic speed in the specimen and the strain rate is far low from it. According to the observed dependence of the modulus on the hydrogen concentration, it is presumed that hydrogen release occurred in the tensile test. If hydrogen released at a fixed speed, then the hydrogen in the specimen tested at lower strain rate would release more. So the alloy tested at lower strain rate would show higher elastic modulus.

To confirm the hydrogen release, holding test at fix load within the elastic regime was designed. The change of the length of the specimen was recorded which was converted into strain. The V-4Cr-4Ti alloy with 341wppmH was hold at 370 MPa for more than 1 h. Figure 6.13 shows the dependence of the strain on hold time. The strain decreased with time, in a decreasing rate, to values lower than zero beyond ~20min. The reduction of the strain indicates a continual hydrogen release, which causes the increase of the elastic modulus, due to which the strain gets smaller as the applied load is constant. But the increase of the modulus should have a limit, the maximum one if the hydrogen concentration reached to zero. Even so, the strain is impossible to become negative if only the modulus increase was taken into account.

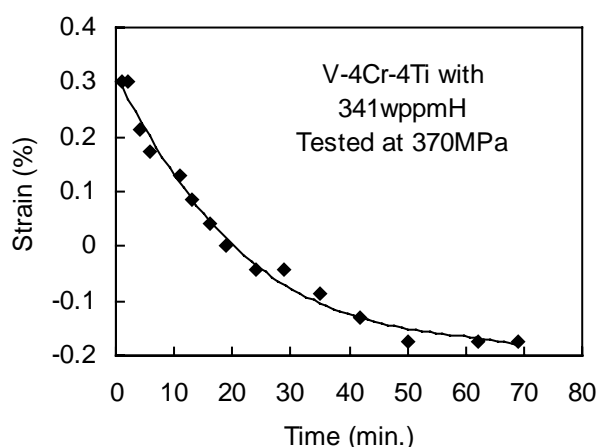


Fig. 6.13 The strain of V-4Cr-4Ti with 341wppmH hold at 370MPa as a function of hold time at room temperature.

Hydrogen atoms in the alloy will stay in the interstitial sites of the BCC crystal.

As the size of the interstitial is less than the atomic size of H, hydrogen into the interstitial will cause expansion of the alloy. When hydrogen release takes place, an opposite process will happen, leads to the shrinkage of the alloy. This should be the true reason for the negative strain shown in Fig. 6.13.

Due to the shortage of material, the hydrogen release study was concentrated on another alloy of V-6W-2.5Ti. The basic tensile property of the alloy with different hydrogen concentration was measured at room temperature at strain rate of 8.3×10^{-4} /s. Table 6.1 reported its tensile properties. It indicates that the hydrogen strengthened the alloy significantly while the strain hardening capability estimated from UE was little affected. During the hold test, tensile strain rate was very low due to the constant load and thus the yield strength of the alloy will be lower than the values listed in the Table. By experience, the strength is about 40 MPa lower. To ensure the specimen to be loaded in the elastic regime, the hold stress was at least 50 MPa lower than the yield strength.

Table 6.1 The tensile properties* of V-6W-2.5Ti alloy containing different hydrogen at RT

H Concentration. (wppm)	YS (MPa)	UTS (MPa)	UE (%)	TE (%)
As-received	253	350	21.5	32
33	295	389	22	38.5
306	346	461	21.5	36.5

*YS: yield strength; UTS: ultimate tensile strength; UE: uniform elongation; TE: total elongation.

Figure 6.14 shows stress-strain curves including the unloading part of the fixed stress holding test of the alloy. When it was not hydrogen charged (shown as “as-received” in Table 6.1 and “without H” in the figure, respectively), the hold test at 200MPa showed no change of the strain during the 5 h loading. For unknown reason, the specimen showed certain residual plastic deformation produced during the loading to the hold point. On the contrary, the alloy containing 306wppmH showed notable

decrease of the strain when hold at 250MPa. Once more, specimen shrinkage was observed due to hydrogen release. The strain became negative when the holding time exceeded 1h.

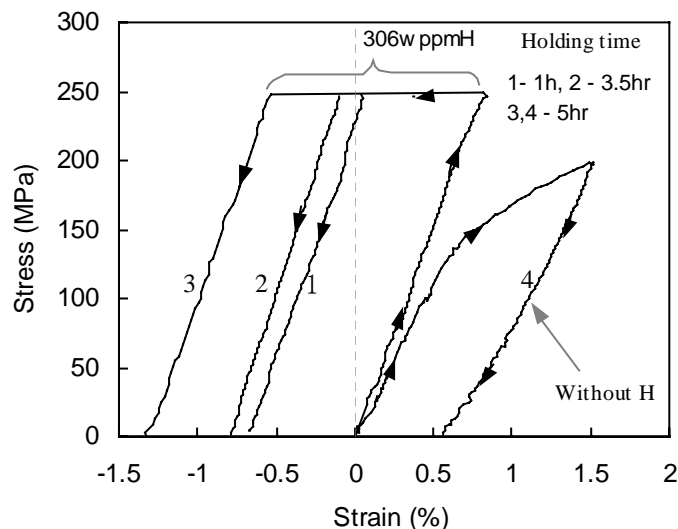


Fig. 6.14 The Stress-strain curves of the V-6W-2.5Ti alloy with 306wppmH hold at 250MPa for 1-5hrs and the one without hydrogen charging hold at 200 MPa for 5 hrs.

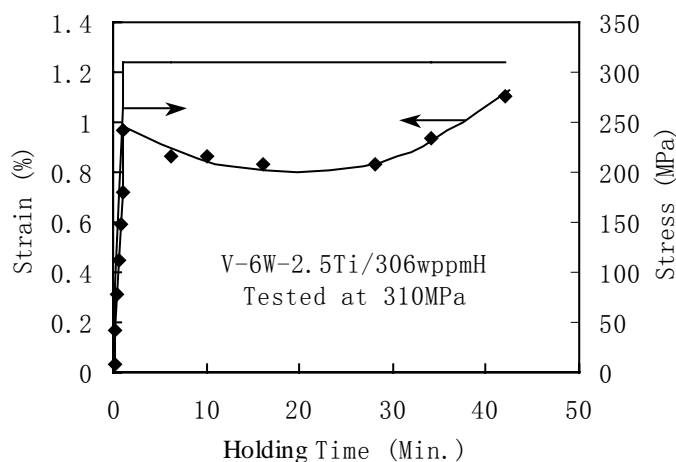


Fig. 6.15 Deformation behavior of V-6W-2.5Ti hold test at 310MPa, showing the transition from strain decrease to increase with hold time.

When the hold stress is near to but a little lower than the yield strength, the behavior is somehow different. Figure 6.15 shows the result of the test at 310 MPa for the V-6W-2.5Ti alloy with 306 wppmH. Initially, similar to what observed above, the strain decreased with time. But beyond ~20minutues, the strain began to increase. Hydrogen release caused the former decrease in strain, meanwhile would cause the

decrease of the yield strength of the alloy. When it got lower than the hold stress, then plastic deformation will occur. Therefore, the later increase of the strain should be caused by the plastic deformation, which should be higher than the shrinkage caused by hydrogen release that took place at the same time.

The Hydrogen release behavior was also observed in the alloy with much low hydrogen concentration. This time the specimens were hydrogen charged at 600°C for 5h, but the measured hydrogen concentration was merely 33wppmH. The hold test was conducted at ~100 MPa and ~200 MPa, for the purpose to study the effect of the applied stress. Results are shown in Fig. 6.16. Similar results were obtained to the case for the alloy with 306wppmH, but the total reduction of the strain seems to be a little lower. However, the effect of the applied stress level looks very small. Moreover, the test at lower stress seems to have a little more decrease of the strain. Perhaps it is caused by the error of the measurement system. More tests are required to evaluate the effect.

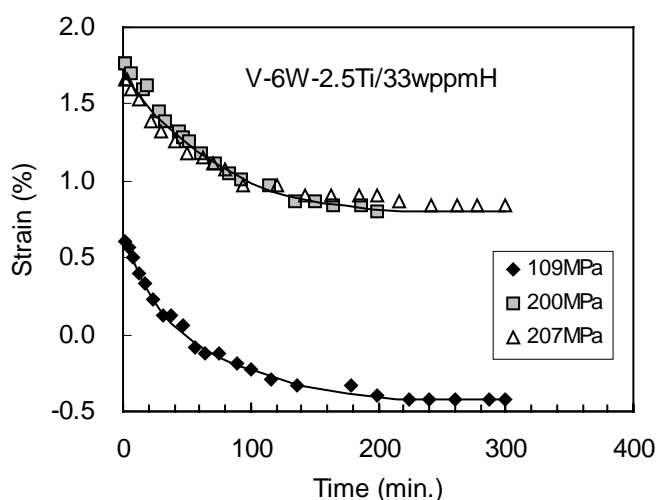


Fig. 6.16 Response of strain on time for V-6W-2.5Ti with 33wppmH loaded at ~100-200MPa.

According to the strengthening by hydrogen, hydrogen release would result in the loss of the tensile strength. Table 6.2 reports the measured yield and ultimate tensile strength of the alloy with 33wppmH before and after the constant stress holding test at room temperature. Tensile strain rate is also $8.3 \times 10^{-4}/s$. From the table, it could be found that the strength, both the yield and the ultimate one, was decreased

due to the hold tests. However, the decrease is not so significant, in the range of 2-3MPa for the yield strength and 9-13MPa for the ultimate tensile strength.

Table 2 The strength of V-6W-2.5Ti with 33wppmH after constant stress holding test at different stress for 5hrs.

Holding Stress (MPa)	0	109	198	207
Yield Strength (MPa)	295	292	/	293
Ultimate tensile strength (MPa)	389	377	376	380

The hydrogen concentration of the specimens after the hold test was measured to determine the amount of hydrogen released. For the alloy with 306wppmH tested at 250MPa, the measured hydrogen concentration ranged from 199 to 268wppm. So the hydrogen release produced a hydrogen concentration reduction of the alloy in the range of 107 to 38wppm. However, there found no clear dependence of the amount of the hydrogen released on the hold time despite a seemingly tendency of the increasing hydrogen release with the time up to 5 hrs.

After all, hydrogen release was observed for vanadium alloys during tensile tests at room temperature. It could be concluded that the hydrogen release will occur even at tensile stress as low as 100MPa and even when the primary hydrogen concentration is as low as 33wppm. The release not only increases the elastic modulus of the alloy, but also causes the shrinkage of tensile specimen. Derived from this result, it is predicative that hydrogen charging will cause the expansion of the specimen. This dimension change due to hydrogen charging and hydrogen release will cause problems such as structural instability, additional stress in the structure and so on. So more attentions and studies should be placed on the hydrogen release behavior in future.

6.4 Discussions and summary

It has been investigated the recovery and recrystallization, high temperature tensile properties and the related DSA phenomena, hydrogen release and its effect on tensile strength of several V-base alloys containing various combination of Cr, Ti, W

and Al. With these investigations, solute mobility, interstitial impurities and alloying elements and their interactions, and the interaction of interstitial solutes with dislocation were assessed. Emphasis was put on their effects on mechanical performance of V-base alloys. Results are summarized as follows.

- (1) Interstitial impurities of C, N, O and H have great effects on the materials performance of V-base alloys. They increase the resistance to dislocation motion, thus increase strength and mitigate dislocation recovery of cold-rolled alloys.
- (2) Interaction between interstitial impurities (C, N and O) and dislocations plays a very important role to affect mechanical properties of vanadium alloys. At appropriate temperature, the interstitials are mobile and migrate to pin dislocations, greatly enhance the contribution of the interstitial impurities to the strength of vanadium alloys. In high temperature tensile test, the interaction causes phenomena of DSA, which increases high temperature strength. In recovery test of cold-rolling hardened alloys, the interaction brings about additional hardening and suppresses the hardness recovery at high temperature.
- (3) Due to the strong affinity of Ti to C, N and O impurities, Ti in vanadium alloys decreases their mobility. As a result, interactions between the impurities and dislocations, including the DSA, shift to higher temperature, improving high-temperature mechanical performances of a V-base alloy.
- (4) Cr has strong interaction with Ti. This interaction decreases the mobility of Ti solutes, sequentially decreases the mobility of interstitial C, N and O solutes. According to what mentioned above, the high temperature strength of V-base alloy will be further improved. That's the reason for the better high temperature tensile strength of V-4Cr-4Ti than V-6W-4Ti. However, this effect on hardness recovery was not observed in the annealing of cold-rolled alloys, perhaps due to much slow motion of dislocations in these alloys in the process. The force driving a dislocation to move in cold rolled alloys is from other dislocations, thus is smaller than the force to drive a dislocation to move for

plastic deformation in a tensile test. Besides, the dislocation motion in a tensile testing specimen requires satisfying the strain rate requirement and hence is in high velocity.

- (5) W seems to have stronger resistance to dislocation recovery than Cr at high temperature. Further investigation is required to understand its mechanism.
- (6) Hydrogen release will take place at room temperature on tensile loading V-base alloy. The release increases the elastic modulus and decreases the strengths of hydrogen containing alloys. And being of most importance, the release will cause dimensional instability of a vanadium structure, resulting in other crucial problems, such as causing additional stress.
- (7) W, Ti and Cr, particularly their combination, could effectively decrease the grain size of a vanadium alloy, and would improve the mechanical performances of the alloy since metals with smaller grain size usually have higher strength and better fracture toughness.

7. Degradation of mechanical properties by hydrogen

7.1 Hydrogen induced ductility loss and the embrittlement

V-4Cr-4Ti of NIFS-Heat2 was used in the annealing state of 1000°C for 2 h. Tensile tests were performed at room temperature. Fig. 7.1 shows the dependences of uniform and total elongations on hydrogen concentration. The total elongation, exhibited a negative dependence, decreases with the hydrogen monotonically from ~31.7% to ~17% in the H concentration range of <215 wppm. The ductility of the alloy

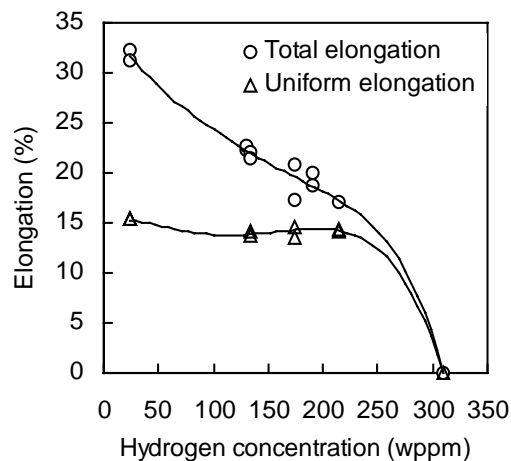


Fig. 7.1 Total and uniform elongations of the V-4Cr-4Ti alloy (NIFS-Heat 2) as a function of hydrogen concentration.

was entirely lost at 310 wppm H, indicating a complete brittle fracture. The critical hydrogen concentration (CHC) required to embrittle the alloy in this static tension loading condition is thus between 215 and 310wppm. On the other hand, the uniform elongation behaved differently. It had a value of ~15% and was nearly unchangeable at the hydrogen concentration of less than 215 wppm. It seemed that hydrogen effect on ductility was solely to reduce the non-uniform deformation in the necking area of a tensile specimen at hydrogen level of lower than the CHC.

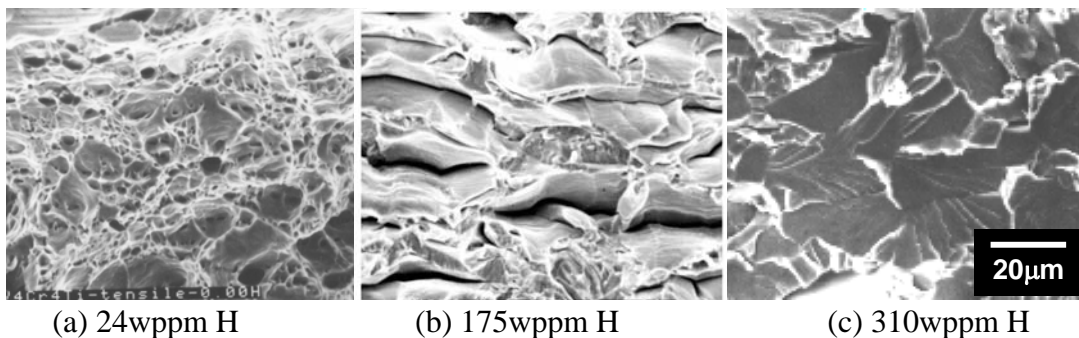


Fig. 7.2 SEM photos showing fracture characteristics of the NIFS-V4Cr4Ti alloy with different hydrogen concentration.

K. Natesan et al. [123] reported that the critical hydrogen concentration required to embrittle the U.S V4Cr4Ti alloy (heat #832665) is about 360wppm based on their tensile test results. The alloy had an oxygen concentration of 310 wppm. In the present study, the critical hydrogen concentration was a little lower than that for the U.S. heat. One of the reasons is the comparably higher oxygen concentration in the present hydrogen charged specimens. In a study reported by H.D. Rohrig et al. [107], similar to what found here, the uniform elongation of their studied V-4Cr-4Ti alloy was not affected by hydrogen in less than ~450 wppm while the total elongation decreased.

Fracture mechanism is analyzed to reveal the hydrogen embrittlement of the alloy. SEM observation showed that ductile fracture with many dimples was the major feature for the non-hydrogen charged specimens, corresponding to the high ductility of the as-received alloy. However, with the hydrogen doped, the fracture changed much. The specimens showed quasi-cleavage fractures along with many secondary cracks at H concentration of 113-215 wppm. The number of the cracks decreased with increasing hydrogen concentration. At 310wppm H, no crack appeared and the fracture changed into a complete cleavage one. Figure 7.2 is the SEM photos illustrating the change of the fracture mode with the hydrogen concentrations.

The secondary cracks have a direction parallel to the width of the specimen. This orientation is related to orientation of precipitate distribution generated in the historical rolling process as reported in Ref. [86]. That is, cracking along precipitates is easier than in the matrix.

7.2 Effect of specimen thickness on hydrogen induced ductility loss

Generally, the measured ductility of a material appears to decrease with thickening the test specimen. The behavior shown

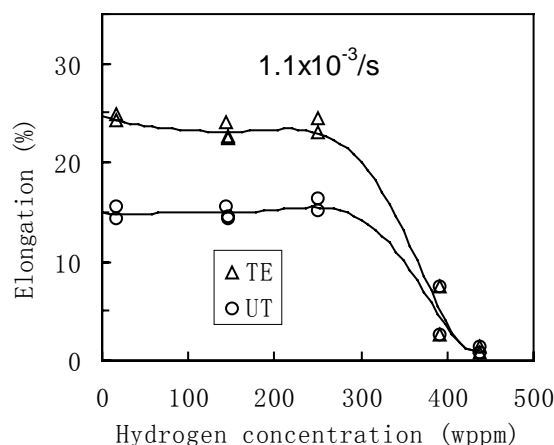


Fig.7.3 Tensile elongations as a function of H concentration for V-4Ti tested at RT.

in Section 7.1 is from the results obtained with a 1.9 mm thick specimen. With more tests for other alloys, it was found that the monotonic decrease of the total elongation seems not to happen for thinner specimens. As an example, Fig. 7.3 shows the tensile elongations of V-4Ti on hydrogen concentration; here the tensile specimens were 0.5 mm in thickness. Besides the little change in uniform elongation (UE) within the hydrogen range from 14 to 249 wppm, evidently the total elongation (TE) didn't change significantly as well. So the dependence of the total elongation on the hydrogen seems to be dependent on specimen thickness, while the uniform one could be little affected.

In a tensile test, following the elastic regime, plastic deformation and strain hardening will occur. As a result, further deformation requires increasing load constantly. However, beyond certain strain level with full development of cell-shape dislocation structures, the hardening will become weaker. When it cannot catch up with the reduction rate of specimen cross section, non-uniform deformation (necking of the specimen) will occur. In this condition, plastic deformation will concentrate within the necking area. As the forced strain rate is constant, the true strain rate in the necking area would become much higher. Besides, the necking would cause three-directional stress state in the region and plastic deformation become more difficult. The thicker the specimen, the stronger the three-directional stress state. According to the effect of the thickness on hydrogen dependence of the total elongation, it suggests that the stress state and possibly the accelerating strain rate in the necking area could enhance the hydrogen-induced ductility loss.

7.3 Fracture toughness, impact property and the possible mechanisms

7.3.1 Response of J_{1c} and the absorbed energy to hydrogen

The CT (compact tension) specimens for measuring J_{1c} contain pre-fatigue cracks, thus the effect of crack on hydrogen embrittlement could be evaluated. Figure 7.4 (a) shows the response of the fracture toughness of the NIFS-Heat 2 alloy to hydrogen

concentration at room temperature. A specimen compliance change rate method [124] was used to determine the crack initiation point and it was found that the point located at the maximum load point for all of the specimens. The corresponding J integral was then taken as J_{1c} when it satisfies the validity criterion of Eqn. (3.4). Most of the data shown in the Fig. 7.4 (a) meets the criterion except that for the specimen without hydrogen charged, which, however, had much high J integral of 594.7kJ/m^2 , indicating that the as-received alloy is very tough. The figure showed that the alloy with hydrogen of more than 130 wppm had very low fracture toughness. J_{1c} was less than 50kJ/m^2 and was little affected by the hydrogen concentration in the regime from 130 to 190 wppm. Accordingly, the critical hydrogen concentration to induce brittle crack propagation initially must be less than 130 wppm in the alloy with cracks. At 310wppm H, complete brittle fracture happened with J_{1c} reaching to the lowest value of $\sim 4\text{kJ/m}^2$.

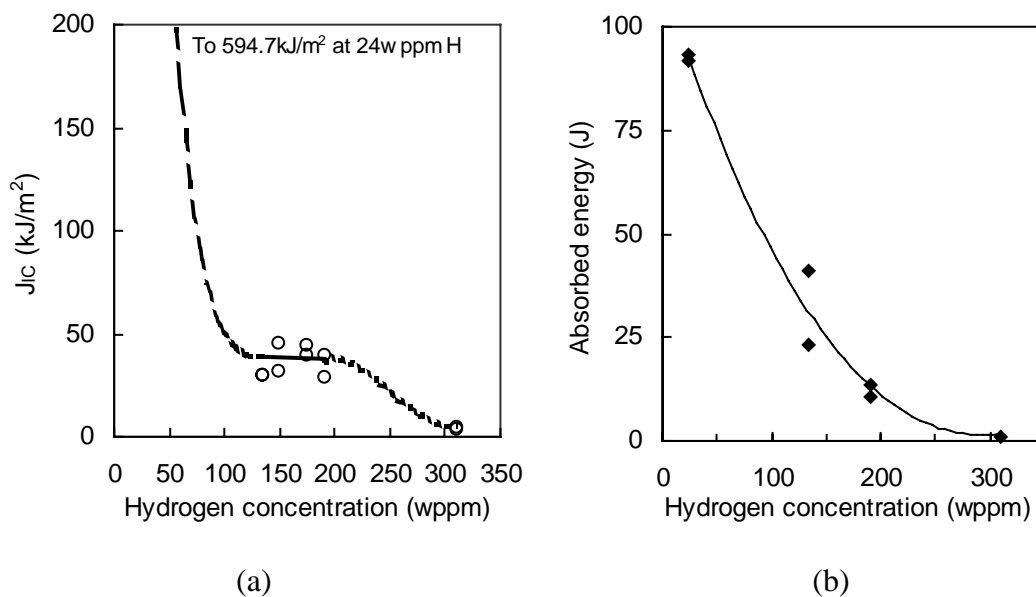


Fig.7.4 The hydrogen concentration dependence of the (a) J_{1c} for the V4Cr4Ti alloy and (b) absorbed energy of the impact specimen. Test temperature: room temperature.

Fig.7.4 (b) shows that the absorbed energy of the half-size Charpy specimen decreased drastically with increasing hydrogen concentration. At 130wppm H the energy is less than half of the non-hydrogen charged one. It could be concluded from the figure that more than 190wppm H is needed to bring about complete brittle fracture. If one defines the hydrogen concentration at which one half of the energy

was lost as the transition one from ductile to brittle failure (nominated as DBTHC: Ductile-Brittle Transition Hydrogen Concentration), just as the case to determine DBTT (ductile-brittle transition temperature), then DBTHC is less than 130 wppm for the alloy.

7.3.2 Fracture of the specimens

CT specimen showed a typical cleavage fracture with a few tearing ridges in the initial cracked region (see Fig. 7.5) at low hydrogen concentration, followed by quasi-cleavage fracture with many secondary cracks as that appeared of a fractured tensile specimen. Being quite different, ductile dimple fracture dominated the fracture of the impact specimen with a few cleavage fracture regions. Further observation revealed that both the amount of the secondary cracks in the CT specimen and the dimples in the impact one decreased with the increase of hydrogen concentration, but the fracture mode in the initial cracked region in the CT specimens was hardly affected by the hydrogen of less than 190wppm in concentration. It may account for the non-affected J_{Ic} in the hydrogen concentration range. At higher hydrogen concentration, intergranular fracture occurred in a few micro-regions of the CT specimen. At 310wppm H, the CT specimen fractured in a completely brittle manner. However, even at 310wppm H, there were still a few regions showing dimple fracture pattern for the Charpy specimen. Figure 7.6 shows the change of the fracture feature for both CT and Charpy specimens with hydrogen.

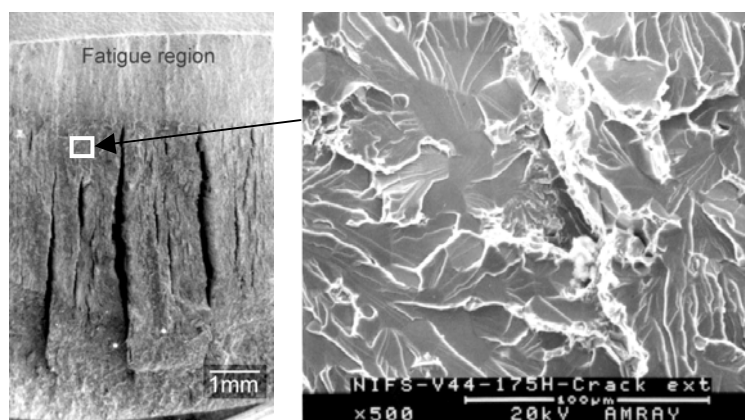
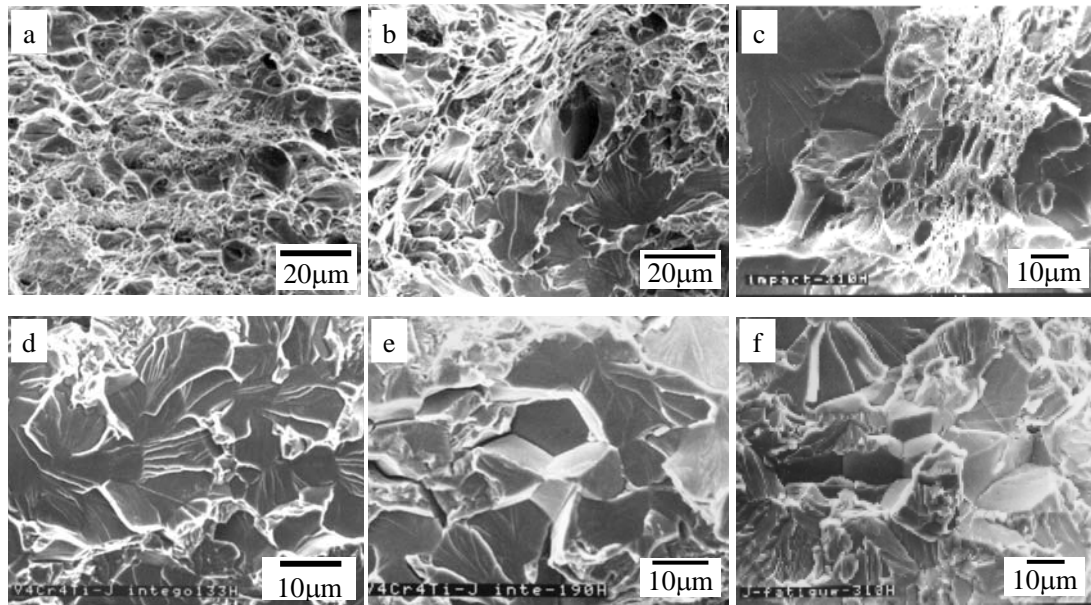


Fig. 7.5 SEM photos showing the fractography of the CT specimen containing 175wppm H.



Fig, 7.6 SEM photos showing the change of the fracture mode with the hydrogen for impact specimen (a, b and c) and CT specimen within the initial cracked region (d, e and f). Hydrogen concentration: a and d: 133wppm, b and e: 190wppm, c and f: 310wppm.

7.3.3 DBTHC or CHC decreases due to the change of stress state and loading rate

Employing the method to explain DBTT, an illustration of the effect of crack or notch and impact loading on hydrogen embrittlement is analyzed. Figure 7.7 schematically shows the change of the fracture stress that causes the separation of crystal planes (cleavage fracture) and the yield strength of an alloy as a function of hydrogen concentration.

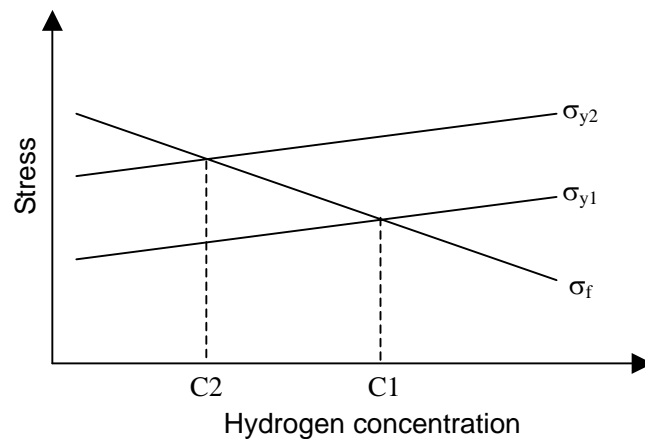


Fig.7.7 A schematic diagram showing the change of fracture stress (σ_f) and yield stress (σ_y) with hydrogen concentration.

As we know, the fracture stress will decrease with increasing hydrogen

concentration due to hydrogen weakening the mutual atomic binding force. On the contrary, yield stress will increase with hydrogen because of solid solution hardening. As a result, the two lines that show the change will intersect at a critical hydrogen concentration as shown in the figure as C1, beyond which brittle fracture will happen due to the higher yield stress than the fracture stress. C1 is the DBTHC or CHC theoretically.

When there is a crack in a specimen as that in a CT specimen, a strong three-directional stress state will be developed around the crack tip during tensile loading if the specimen is thick. To an ultra extent when the dimension of the specimen meets plane strain condition, the yield stress just ahead of the crack tip will be high up to about $3\sigma_y$. Analogously, similar stress state will exist around the notch root in the Charpy specimen but the stress concentration will be much weaker. On another hand, fast loading like the impact will also increase the yield stress of the specimen. In Fig. 7.7, σ_{y1} and σ_{y2} represent the yield stress without and with those effects of crack, notch, impact loading or their combinations, respectively. Obviously the intersection point shifts to lower value of hydrogen concentration due to the increase of the yield stress in the latter case. That is, DBTHC becomes lower and the alloy shows higher sensitivity to hydrogen embrittlement. This is just what was obtained in the present study.

The situation for the tensile specimen after necking is just similar to the Charpy specimen. Both have notch and high loading rate, though the shape of the notch and the rate is different. Looks Like a coincidence, the hydrogen dependence of the absorbed energy of the Charpy specimen and that of the total elongation is quite similar. In fact, their philosophy is basically the same as that shown in Fig. 7.7.

7.3.4 Low but stable J_{1c} at 133-190wppm H

Though what stated above could give a good explanation of the high sensitivity of J_{1c} to hydrogen, but the stable J_{1c} at 133-190 wppm H seems to be out of reasoning. It

is known that the binding force of atoms will be weakened by hydrogen, which decreases the surface energy of an atomic plane. On the other hand, fracture toughness is closely related to this surface energy in terms of the classical fracture mechanics. Therefore, more hydrogen should decrease the toughness more. That is just in opposite to the result of J_{1c} . It is thus supposed that something happened around the crack tip during the testing. One possibility is the stress gradient assisted hydrogen enrichment around the crack tip. Another possibility is the formation of hydride in the area.

Hydrogen atom is very small and thus could have much high diffusion or migration rate in the alloy. If the stress in the specimen is not homogeneous, hydrogen will migrate to the high tension-stress region. In an early work reported by S. Yano et al. [125], it was found that the stress concentration at Lüders bands promoted the formation of hydride, which led to the loss of the capability of a V-15Cr-15Ti alloy against hydrogen embrittlement. Of course, the formation of the hydride requires hydrogen enrichment in the region. In the present tests, high stress concentration existed near the crack tip in the CT specimen. Calculated with the assumption of plain strain condition, the stress at the crack tip would reach to 700~800 MPa just before the initiation of the crack. The nearby hydrogen would diffuse into the region under the driving of the stress gradient. The hydrogen enrichment at the crack tip increases the difficulty of the regional plastic deformation. Consequently, cleavage fracture became easier to take place. The fracture toughness was thus in much low value.

However, even based on the stress-gradient assisted hydrogen enrichment theory, the hydrogen concentration around the crack tip will proportionally differ with the bulk concentration. As a result, the J_{1c} should change with hydrogen concentration. So it is presumed that hydrides were formed around the crack tip due to the hydrogen enrichment. It is the hydride that resulted in the low but stable J_{1c} in the hydrogen range.

The case in the necking area of a tensile specimen is just similar to this situation in the CT specimen but with weaker stress concentration. This should account for the strong effect of the hydrogen on the necking process rather than the uniform

deformation. The stress assisted hydrogen diffusion would not occur in the impact specimen although there was also stress concentration ahead of the notch root, simply because of the fast loading process. The hydrogen in the specimen had scarcely time to diffuse into the high stress region when the fracture took place. It may be one of the main reasons for the large numbers of dimples on the fracture surface. The diffusion of the hydrogen was not measured in this study and may need further study of its effects on the hydrogen embrittlement behaviors considering the effects may be very strong.

7.4 Effect of alloying elements

7.4.1 Experimental results

Various alloy plates in thickness of 0.5 mm were used. It was also found that neither TE nor UE changed much with the hydrogen until a critical hydrogen concentration (CHC) was reached, beyond which the elongations decreased drastically. Figure 7.8 shows the response of UE to hydrogen concentration. Comparing the results, CHC tends to decrease with reducing Ti content in an alloy: V-4Ti has the highest CHC while that for V-8W is the lowest one among the alloys, about 400 and 100 wppm, respectively. Evidently, the property is also benefited from the doped aluminum. Despite of the small Al content in V-7W-0.3Al, its C_{CH} is much higher than that of the V-8W alloy.

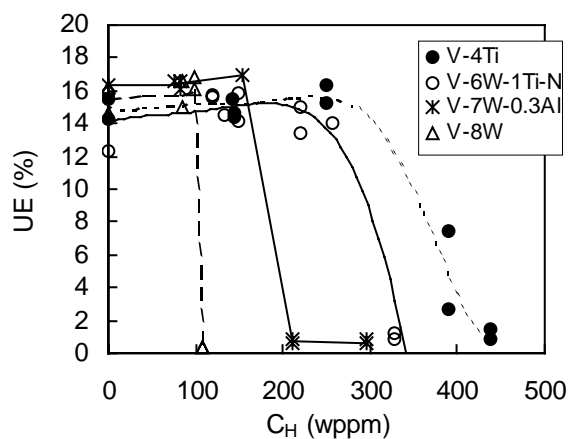


Fig. 7.8 Dependence of uniform elongation (UE) on hydrogen concentration (C_H) for V-base alloys at RT.

It was observed that hydrogen induced hardening happened for any of the alloys. Figure 7.9 is an example showing the hydrogen concentration dependence of the yield

strength and ultimate tensile strength for V-7W-0.3Al. The yield strength nearly increased linearly with the hydrogen at the level below 212wppm, a hydrogen concentration at which brittle fracture occurred (see Fig. 7.8). On the other hand, the ultimate tensile strength increased in the low hydrogen concentration region but started to decrease around the CHC, which is between 154 and 212wppm H for the alloy. When the hydrogen concentration got higher than the CHC, there is a trend that both strengths decrease with increasing hydrogen concentration.

Other alloys showed similarly in the hydrogen-induced hardening behavior. Fig.

7.10 shows the dependence of yield strength on hydrogen concentration for all alloys investigated, including that for the US V44 reported by H. D. Rohrig [107] for which the CHC is in the range of 558-673 wppm. Both the NIFS V44 and the US V44 are V-4Cr-4Ti alloy. The tensile strain rate was also shown in the figure. Approximately, all exhibited linear increase in yield strength with the

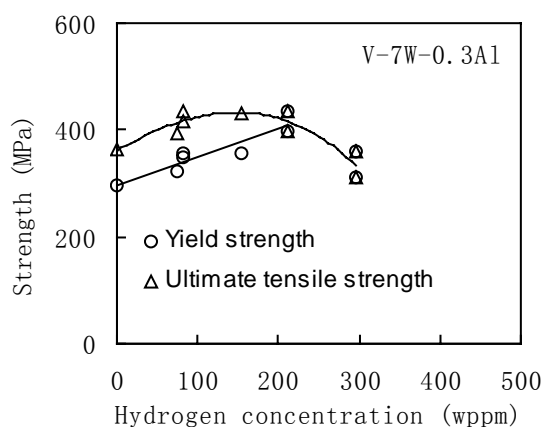


Fig. 7.9 The dependence of the yield strength and the ultimate tensile strength on the hydrogen concentration for V-7W-0.3Al tested at RT at strain rate of 1.1×10^{-3} /s.

hydrogen concentration. However, the increasing rate is quite different from one another. It looks like that the hardening is likely related to the Ti addition in the alloy and is strongly affected by the tensile strain rate. The alloys with Ti addition, such as V-6W-1Ti, V-4Ti and the US V44, have much smaller hardening rate than those without Ti. It is about half or even less as compared to the latter one. Al seems to have similar role as for V-7W-0.3Al, which has slightly lower hardening rate as compared to V-8W. The effect of strain rate seems to be quite significant. If no other factor is considered, the decrease in strain rate from 1.1×10^{-3} /s to 4.4×10^{-4} /s produced a 1.37 times increase in the hardening rate, from 0.3 to 0.71 MPa/wppmH for V-4Cr-4Ti (US V44 and NIFS V44). However, the dimension of the specimens for the US V44 and NIFS V44 are of big difference, which may have certain effects on the behavior.

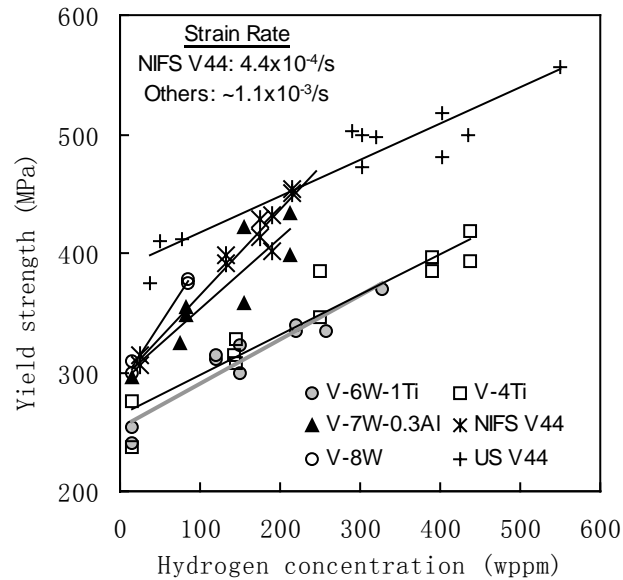


Fig. 7.10 Increase of yield strength with hydrogen concentration for each alloy. Data for the US V44 is from Ref. [107]. Here V44 is an abbreviation of V-4Cr-4Ti.

The results could be summarized as that either Ti or Al addition was helpful in increasing the abilities of the alloys against hydrogen embrittlement. This benefit should partially come from the fact that the addition decreases the hydrogen induced hardening (see Fig. 7.10). The linear increase of the yield strength with hydrogen indicated a solid solution strengthening by the doped hydrogen of less than CHC for any of the alloys. It should account for the little change of the uniform elongation in the hydrogen range.

7.4.2 Mechanism

Substitutive atoms in an alloy seem not only to increase its strength but also to influence the hydrogen distribution in the matrix, changing the hydrogen induced hardening performance. At first, the substitutive atom in the alloy is not likely to be the same size as V. The difference not only causes lattice distortions around the substitutive atoms but also changes the quadrilateral interstitial size in the alloy. Fig.7.11 is the schematic drawing of the atoms in the (101) crystal plane of a V-Ti alloy. Clearly some big interstitials will form along the two closed-packed atom directions of $\langle 111 \rangle$ due to the addition of Ti. Supposing there is a rigid ball in the

interstitial, the radius of the ball is calculated to be 0.4106\AA , which is larger than that in the pure V crystal (about 0.38\AA). Hydrogen atoms will preferentially stay in these large interstitials to produce smaller crystal distortion. As a result, its resistance to the dislocation motion could be decreased and the alloy with big quadrilateral interstitial size would show weak hydrogen-induced hardening.

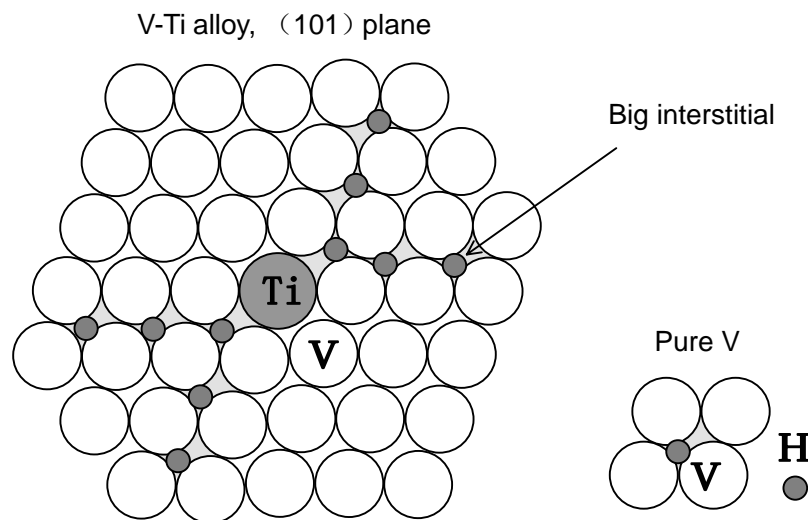


Fig. 7.11 Atoms in (101) crystal plane in a V-Ti alloy, showing the large quadrilateral interstitial sites that H atoms like to dwell in.

Now that the substitutive atom has strong effects on the hydrogen hardening behavior, it is necessary to evaluate how strong the effect is. Since large interstitial has stronger sink strength for hydrogen atom, the hardening could be lessened by increasing the interstitial size. Fig. 7.12 shows the calculated radius of the maximum rigid ball that could be placed in the interstitial for various substitutive atoms in the vanadium crystal. The radius decreases with decreasing the difference between the sizes of V atom and substitutive atom. Consequently, selecting such kind of substitutive atoms that have big difference to V in atomic size could lessen the hardening.

From Fig. 7.12, it is evident that alloying V with Al and Ti could cause much larger quadrilateral interstitial in the crystal than with W. Therefore, the hydrogen-induced hardening in the former alloy would be weaker than the later one. That is what observed in Fig. 7.10 for V-4Ti, V-6W-1Ti, V-4Cr-4Ti, V-7W-0.3Al and

V-8W. Surely, stronger hardening could cause higher sensitivity to hydrogen embrittlement.

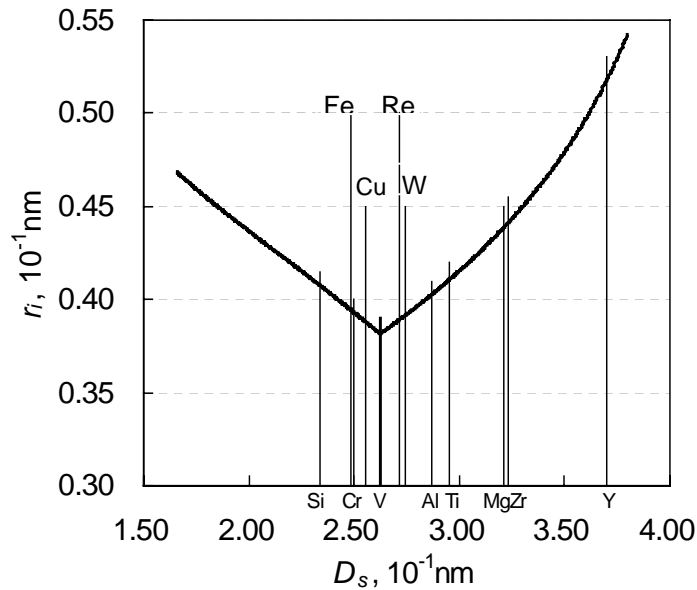


Fig. 7.12 The dependence of the quadrilateral interstice size (r_i) on the diameter of the substitutional atom (D_s) in a V crystal.

7.5 Effect of tensile strain rate and specimen dimension on hydrogen induced hardening

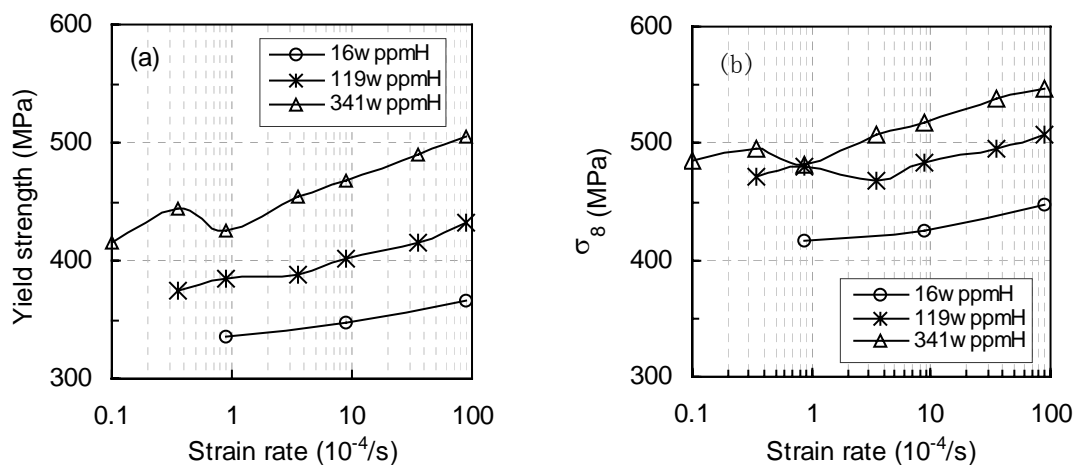


Fig. 7.13 The yield strength (a) and the flow stress at 8% strain (b) as a function of strain rate for the V-4Cr-4Ti alloy containing different amount of hydrogen. Tensile test was performed at RT.

Another possibility for the better resistance of the V-Ti alloys than others without Ti might be the strong affinity of Ti to hydrogen. H has been proven to be mobile at

RT and will migrate to dislocations as the binding could decrease the potential of the dislocation. As a result, it may exert certain resistance to dislocation motion in the tensile test. Due to the strong affinity, Ti will decrease the mobility of hydrogen and thus weaken the hydrogen-induced hardening. To evaluate the possibility, tensile test at serial strain rate was performed. It is presumed that more hydrogen atoms will move to dislocation at lower strain rate and the hardening may become stronger.

Figure 7.13 shows the dependence of yield strength and the flow stress at 8% strain (σ_8) on strain rate for V-4Cr-4Ti. Hydrogen concentration is range from 16wppm (for the alloy without hydrogen charging) to 341wppm. Though a variation around $3.5 \times 10^{-5}/s$, the strength or the flow stress almost decreases with decreasing strain rate. Evidently the expected adverse increase of the strength due to strain rate decreasing is not happened. So the effect of Ti on the mobility of H should have little effect on the hydrogen-inducing hardening behavior.

On the other hand, result in 7.3.1 has shown the strain rate having significant effect on the hydrogen-induced hardening and the hydrogen embrittlement behaviors by comparing the result of US V44 and the NIFS V44. For the US V44, another study by K. Natesan et al showed that the critical hydrogen concentration required to embrittle the alloy is less than 360 wppm [123], which is quite lower than that reported by H. D. Rohrig (558-673wppm) [107]. The former study utilized a much lower tensile strain rate of $1.8 \times 10^{-4}/s$, while that for the latter is $1.1 \times 10^{-3}/s$. It seems to be definite that lower strain rate could enhance hydrogen embrittlement. However, according to what stated above, this should be a coincidence. Then what should account for the different hydrogen embrittlement behavior?

It is noted that the dimension of the specimen gauge section is quite different for these studies related to NIFS V44 and US V44 by K. Natesan and H. D. Rohrig. Table 7.1 reported the gauge dimensions, the ratio (R) of surface area to volume, the strain rate and the CHC obtained from the studies. If taking R as a variable for the CHC, then it could be found that the CHC increases with the increase of the ratio, almost proportionally.

Table 7.1 Parameter of the specimen tested and the corresponding CHC

Alloy	NIFS V44		US V44	
Studies	This study	By Natesan	By Rohrig	
Strain rate (/s)	4.4×10^{-4}	1.8×10^{-4}	1.1×10^{-3}	
Dimension (mm ³)	19x4x1.9	19x4.5x1	7.62x1.52x0.76	
R	1.55	2.44	3.95	
CHC (wppm)	215-310	240-360	558-673	

As what has been stated in section 6.3, hydrogen will release during the room-temperature tensile test. Theoretically thinking, the release will be proportional to the surface area for unit of specimen volume, the R. At higher R, hydrogen will release more and thus the specimen would show better ductility than the one with lower R at the same value of the initial hydrogen concentration. Consequently, the one having higher R appears better property against the hydrogen embrittlement. But actually, the CHC should be lower than the evaluated value if no hydrogen release. On the other hand, thicker specimen should have higher plastic deformation resistance, which should have certain effect on the behavior.

7.6 Oxygen increasing the sensitivity of the alloy to hydrogen embrittlement

All the alloys concerned here have high O concentrations of 700-1100 wppm (see Table 2.1).

J.R. DiStefano et al. reported [126] that when oxygen was excluded, hydrogen concentration up to ~400wppm produced only a small reduction in ductility for V4Cr4Ti alloy; however, above 500wppm the ductility fell precipitously. The grain size had slightly affected the total elongation and the critical hydrogen concentration required to embrittle the alloy. The concentration seems to shift to lower levels and the total elongation decreased with increasing grain size. Fracture due to hydrogen embrittlement was predominantly transgranular cleavage [108]. In this study, some alloys have high oxygen concentrations ranging from 700 to 1100 wppm. Their hydrogen effects on mechanical performance should take the synergistic effects of oxygen into consideration. Fig. 7.14 showed that their elongation decreased quickly with increasing hydrogen in low concentration level. It must be the oxygen that

enhanced the hydrogen embrittlement of the alloy. The CHC for the high O V-4Cr-4Ti is lower than 100 wppm according to the figure. V4Ti-O alloy exhibited better ductility than other alloys at the hydrogen concentrations of ≥ 50 wppm.

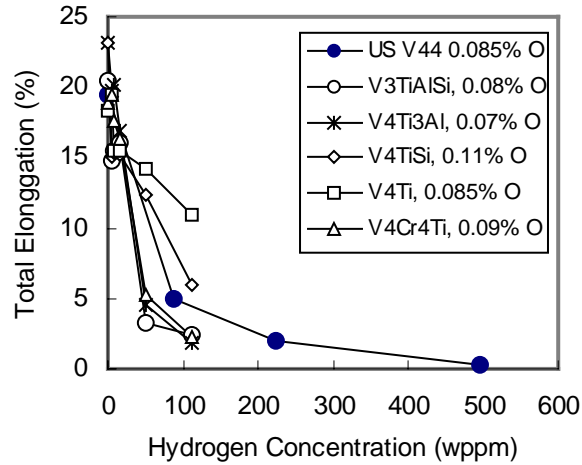


Fig. 7.14 Effect of hydrogen plus oxygen on the total elongations of the vanadium alloys.

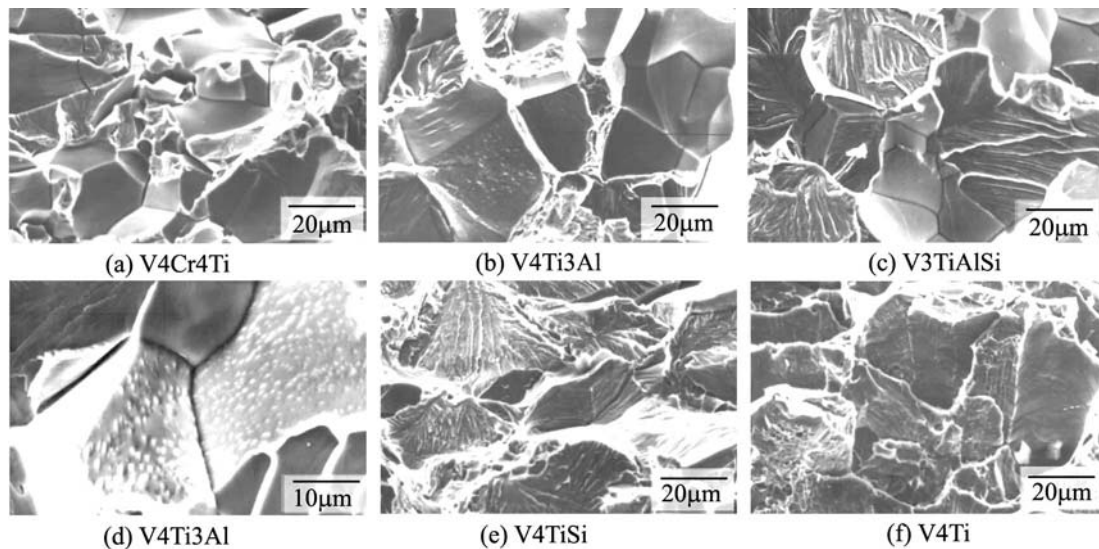


Fig. 7.15 SEM photos showing the fracture patterns of the high O content alloys with 50wppmH.

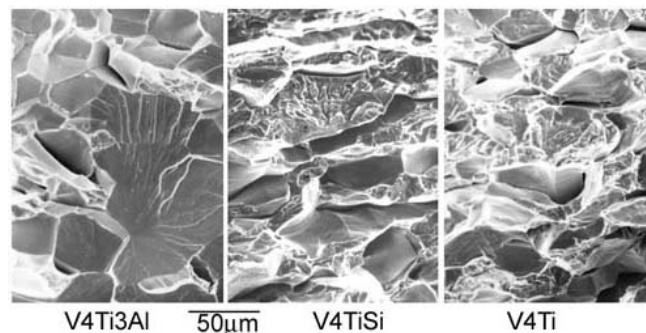


Fig. 7.16 SEM fractographs showing the fracture features for the alloys with 113wppm H

The hydrogen embrittlement fracture surfaces were observed to be mainly transgranular cleavage under a scanning electron microscope. However some intergranular fractures were found for the V4Ti3Al, V3TiAlSi and V4Cr4Ti alloys at 50wppm H (see Fig. 7.15 a-d). Many precipitates in diameter of lower than 1 μ m were found on the surface of the grain of V4Ti3Al alloy (Fig. 7.15 (d)), which may weaken the grain boundary of the alloy. V4Ti and V4TiSi alloys were found to be fractured in a quasi-cleavage manner with many secondary cracks (see Fig. 7.16) even at 113wppm H, indicative of more energy was exhausted during the fracture process. Therefore, the critical hydrogen concentration for V4Ti and V4TiSi alloys must exceed 113wppm while that for other alloys must be less than 50wppm according to the fracture modes. It gave the reason for the better property of V4Ti and V4TiSi alloys against hydrogen embrittlement.

The vanadium alloys in this study have high oxygen concentration due to the absence of protection during the forging and hot-rolling process. According to the result reported by J.R. DiStefano [126], the oxygen was most likely distributed along the grain boundaries. It weakened the grain boundary and led the alloy to a higher trend to intergranular fracture. When hydrogen was taken in, the grain boundary of the alloys would be further weakened. As a result, intergranular fracture becomes easier to occur, particularly for the high strength alloy for which the grain boundary strength is comparably easier to get lower than the grain strength as compared to the low strength alloy, since the grain strength will decrease with the decrease of the alloy's strength level.

7.7 Summary

The effects of hydrogen on the mechanical properties of several V-base alloys, some in high oxygen concentration, were investigated. The tensile properties, fracture toughness, Charpy impact energy were measured, along with the observation of the fracture morphology. With these results, it was evaluated the hydrogen induced ductility loss and strengthening, hydrogen embrittlement, effects of loading rate and

specimen thickness, effects of crack and notch, and the effects of alloying elements including oxygen. Results are summarized as follows.

- (1) Hydrogen embrittlement, a common phenomenon for vanadium alloys, occurs at critical hydrogen concentrations (CHC). The CHC varies a lot for different alloys; alloys with Ti and Al addition have higher CHC than others without them. The difference may be several hundreds wppm hydrogen.
- (2) In the tensile test, the NIFS-Heat 2 alloy could stand high-level hydrogen concentration of more than 215wppm without significant loss in ductility. However, other test results showed that the fracture toughness J_{1c} and impact toughness (evaluated by the absorbed energy of a Charpy specimen) are strongly affected by the hydrogen and the critical hydrogen concentration required to embrittle the alloy may be less than 130wppm. Therefore, assessment of hydrogen embrittlement of an alloy is greatly influenced by the evaluating methods.
- (3) Crack in a structure will surely enhance the hydrogen embrittlement due to the 3-directional state at the crack tip, the hydrogen enrichment ahead of the tip because of the stress gradient there and possibly the enhanced formation of hydrides.
- (4) Specimen thickness also has big effect on the CHC. CHC evaluated by thicker specimen may show lower value due to the smaller amount of hydrogen release and the bigger constraint of the thickness to plastic deformation.
- (5) Hydrogen induced strengthening, being a solid solution type below the CHC, varies a lot with the alloying elements. Ti/Al-bearing alloys have weaker strengthening compared to the ones without them. This should account for the better properties of the former alloys against hydrogen embrittlement.
- (6) Hydrogen, extremely small atom, will preferentially stay in the quadrilateral interstitial of the V crystal and causes local lattice distortion. This distortion increases dislocation motion resistance and thus strengthens the alloy. Substitutional atoms in V will change the size of the interstitial, those with bigger difference in atomic size to V will produce larger interstitials, and

hence decreases the distortion caused by the dwelling of H, making the alloy have low hydrogen inducing strengthening and eventually good resistance to hydrogen embrittlement.

- (7) Increasing oxygen concentration will greatly enhance the hydrogen embrittlement of an alloy due to oxygen preferentially distributing along grain boundaries and reducing the grain boundary strength.
- (8) The fracture of the hydrogen embrittled alloy is usually transgranular cleavage, but may be intergranular for alloy with high oxygen concentration. When hydrogen concentration is not so high up to CHC, fracture is mainly a quasi-cleavage type with many secondary cracks. The number of cracks decreases with increasing hydrogen concentration.

8. Plastic flow at constant stress at RT

8.1 Behavior of plastic flow at room temperature

It has been reported in section 6.3 that hydrogen release will result in the shrinkage of a tensile specimen when it is hold at fixed stresses lower than yield stress. But when the hold stress is close to the yield stress, extension of the tensile specimen will appear after ~20min. for the V-6W-2.5Ti alloy containing 306wppmH (see Fig. 6.15). It was presumed that the extension was caused by lowering the yield strength to a level lower than the hold stress due to hydrogen release. However, there is another possibility of constant plastic flow. To verify it, more tensile hold tests were performed at stresses higher than yield strength.

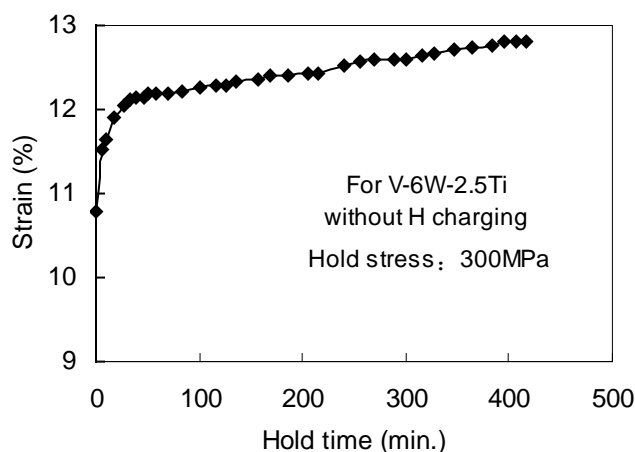


Fig. 8.1 Dependence of strain on hold time for the hold test at 300MPa. Loading rate to the hold stress was about 3.59 MPa/s.

To eliminate the effect of H on the behavior, the as received V-6W-2.5Ti alloy (in 1000°C/1h annealing state) was used. Fig. 8.1 shows a result of the alloy specimen hold at 300MPa for 7hrs. The loading rate to 300 MPa was 3.59 MPa/s. The tensile properties of this alloy could be found in Table 6.1, its yield and ultimate tensile strength were 253 and 350MPa, respectively. Obviously the hold stress is 47MPa higher than the yield strength. The result shows that the strain of the specimen increased with increasing hold time, quickly at the beginning and got steady after ~70

min. The steady state plastic flow rate is about $1.11 \times 10^{-3}/h$.

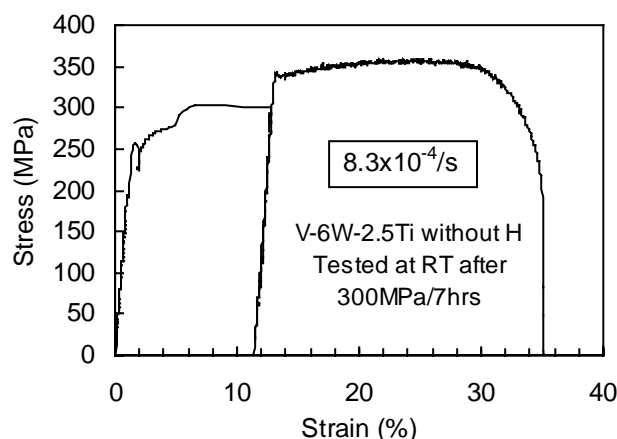


Fig. 8.2 The plastic flow together with the tensile curve of the as-received V-6W-2.5Ti after the hold test at 300 MPa for 7hrs.

After the hold test, tensile test was performed at RT to determine its tensile properties. Stress-strain curve for the whole process of the hold and tensile tests is shown in Fig. 8.2. Estimated from tensile test part, the ultimate tensile strength of the alloy is about 356 MPa (calculated with the primary cross-section area before the hold test), 6 MPa higher than the one before the hold test. The uniform and the total elongation of the hold tested specimen decreased. But if adding the plastic deformation in the hold test to the elongations, both were scarcely affected. Therefore, it could be concluded that the tensile strength of the alloy could be increased slightly by the plastic flow at constant-stress. From the figure one more thing could be obtained. After unload from the hold test at 300 MPa, the specimen was loaded again at a strain rate of $8.3 \times 10^{-4}/s$. As the rate is quite higher than steady state plastic flow rate ($1.11 \times 10^{-3}/h$), the flow stress increased from the 300 MPa in the hold test to 338 MPa in the tensile test. So it is reasonable to think that the yield strength and the ultimate strength of the alloy deformed at constant stress should be about 38 MPa lower than the measured ones by tensile test.

8.2 Effect of hold stress and hydrogen on plastic flow rate

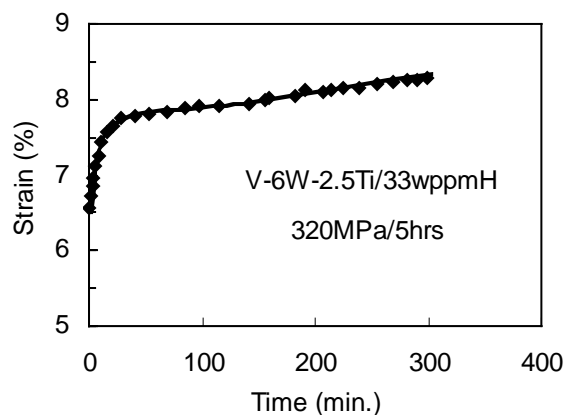


Fig. 8.3 Dependence of strain on hold time for V-6W-2.5Ti containing 33wppmH, the hold test was performed at RT and at 320MPa. Loading rate to the hold stress was about 0.34MPa/s.

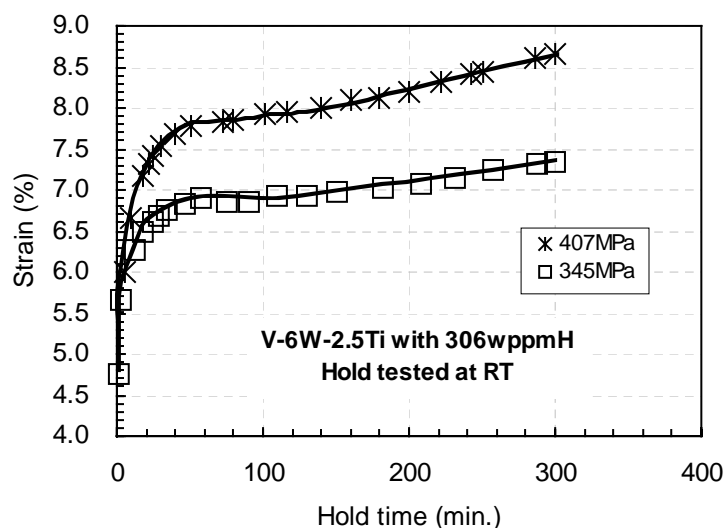


Fig. 8.4 Dependence of strain on hold time for V-6W-2.5Ti containing 306wppmH, the hold test was performed at RT and at 345 and 407MPa, respectively. Loading rate to the hold stress was about 4.3MPa/s.

Fig. 8.3 and 8.4 show the plastic of the V-6W-2.5Ti with 33 and 306 wppmH, respectively. Their yield strengths are 295 and 346 MPa at each hydrogen concentration, respectively. So the hold stress is well above the yield points considering the reduction of the yield strength due to the quite slow strain rate in the hold test. Comparing with Fig. 1, the plastic flow behaved more obviously in three stages, like a creep deformation. The 1st stage, taken as the primary plastic flow, took about 30-60 minutes in which the flow rate decreased with time. The 2nd stage was very short, took about 1 hr and had a very slow flow rate. Following this stage, the

plastic flow went into the 3rd stage, a stage took longer time than the total time of the 1st and 2nd stages. Furthermore, the plastic flow became steady in this stage and the flow rate became higher than the one in the 2nd stage. Here we call it the steady plastic flow rate. From Fig. 8.4, it could be roughly seen that the steady plastic flow rate got higher with the increase of the hold stress.

It is not easy to compare the results to obtain the effect of hydrogen concentration on the behavior since the hold stress and the strength of the alloy varied with the change of the hydrogen concentration. To evaluate the effect, a hold stress location factor (F_H) shown the position of the hold stress between the yield strength and the ultimate tensile strength is defined as

$$F_H = \frac{(\sigma_H - \sigma_Y)}{(\sigma_{UT} - \sigma_Y)}. \quad (8.1)$$

Here σ_H , σ_{UT} and σ_Y are the hold stress, ultimate tensile strength and yield strength, respectively. Since the yield strength and the ultimate tensile strength of a material will change with strain rate, the measured strengths of the alloy could not be used here. But it was found the differences between the stress levels in the tensile test and the hold test were 38, 41 and 54 MPa for the as-received alloy, the one with 33 and 306wppmH, respectively. Thus the strengths under the hold test could be obtained by subtracting the differences from the data reported in Table 6.1. In this way the factor F_H could be obtained. Table 8.1 shows the factor and the corresponding steady plastic flow rate.

Table 8.1 The F_H and the corresponding steady plastic flow rates for the V-6W-2.5Ti with various hydrogen concentrations.

Alloy state	As-received	With 33wppmH	With 306wppmH	
F_H	0.88	0.70	0.46	0.96
Plastic flow rate ($10^{-3}/h$)	1.11	1.21	1.5	3.30*

*Averaged value by two data.

The steady plastic flow rates are plotted against the hold stress location factor (F_H) in Fig. 8.5. When F_H is zero, the plastic flow rate should be zero according to the previous results that specimen shrinkage will take place when F_H is negative. The

figure tells us that the plastic flow rate is hydrogen concentration dependent. It increases with the hydrogen concentration. Besides, it seems that the rate is linearly proportional to the factor of F_H , i.e., increases with increasing hold stress. However, due to the limited data, more tests are required to build the relationship.

This room temperature plastic flow is a phenomenon not only for V-6W-2.5Ti, but also for V-4Cr-4Ti. Fig. 8.6 is the plastic flow curve for V-4Cr-4Ti with 341 wppmH, which is hold-tested at 470MPa at room temperature. The plastic flow behavior is quite similar to that of the V-6W-2.5Ti. The steady plastic flow rate is about $1.76 \times 10^{-3}/h$.

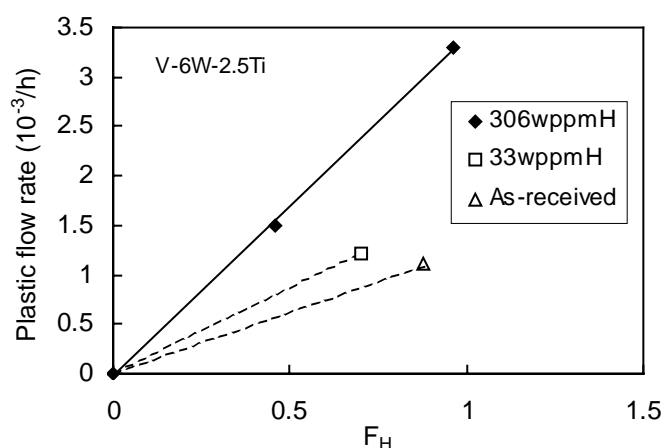


Fig. 8.5 The plastic flow rate data plotted against the hold stress location factor (F_H) for V-6W-2.5Ti.

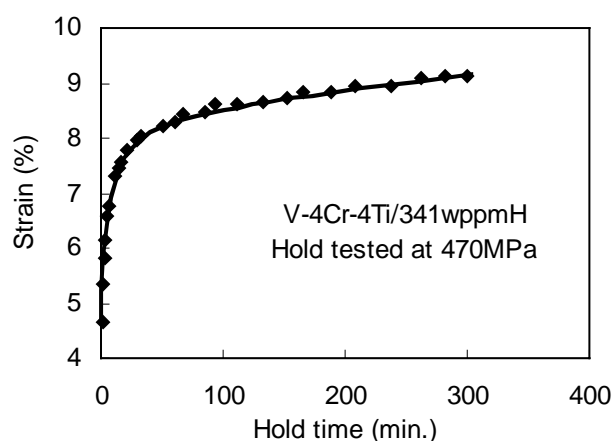


Fig. 8.6 plastic flow curve for V-4Cr-4Ti alloy containing 341wppmH at room temperature.

8.3 Discussions and summary

As the plastic flow occurs at hold stress higher than the yield strength, it could be deduced that the occurrence of the plastic flow requires certain number of dislocations in the alloy. Thus it could be presumed that the plastic flow is related to dislocation motions. At room temperature, dislocation climb is impossible because it needs the motion of atoms and is a thermal activation process. So the plastic flow should be dislocation glide assisted.

The specimen was loaded at certain loading rate to the hold stress. Virtually the strain rate was very high after the yield point. The applied stress must increase to overcome the increasing resistance of dislocation motion for successive deformation, which is known as strain hardening. Under the driving of the increasing load, dislocations could move at certain speed. As the stress reached to the prior set one, the applied stress stopped increasing. At that moment, the applied stress should be equal to the resistance of the dislocation motion. As a result, the dislocation should move at a constant velocity. However, further motion of the dislocations means the increase of the resistance. Thus the velocity will decrease with time. That's what was observed in the 1st stage. With the increasing resistance, dislocations were nearly unable to move and the deformation rate became almost zero or very small in the 2nd stage. Therefore, the deformation in both the 1st and the 2nd stages is produced by the inertia of dislocation motion.

However, when time went into the 3rd stage, something took place and made the dislocation move faster. The driving force was not increased due to the fixed hold stress. Thus it is solely caused by the decrease of dislocation motion resistance. At the temperature, only cross glide of dislocations and motion of hydrogen atoms are possible to decrease the resistance. Cross glide causes the extinguishments of negative and positive dislocation pairs, reducing dislocation density and/or release the clogged dislocation to other easily moving planes. The resistance coming from the interaction of dislocations could be decreased due to the decrease of the number density. As a result, further deformation becomes easy. On the other hand, for the alloy with hydrogen, the hydrogen atoms would prefer to stay in the dislocations and impedes dislocation motion. As it was found that hydrogen could release from a tensile loaded

specimen, the resistance could also be reduced due to hydrogen release. These should account for the increasing plastic flow rate with the increase of the hydrogen concentration in the alloy.

To verify the hydrogen release, tensile test was performed after the hold test. It was found the ultimate tensile strength of the hydrogen charged alloy was reduced due to the hold test. It has been stated that the ultimate strength will increase slightly due to the hold test for the as-received V-6W-2.5Ti. Therefore, the loss of the ultimate strength of the alloy that was hydrogen charged should be caused by hydrogen release, because hydrogen induced strengthening decreases with hydrogen loss. As an example, Fig. 8.7 shows the tensile curve of the alloy containing 306wppmH without the hold test (dashed line) and the one followed a hold test (solid line). It is evident that the ultimate tensile strength is decreased. For the alloy containing 33 wppmH, the ultimate tensile strength also had a loss of ~3MPa. Although the loss is very small, it is in contrary to the slight increase of the strength for the as-received alloy.

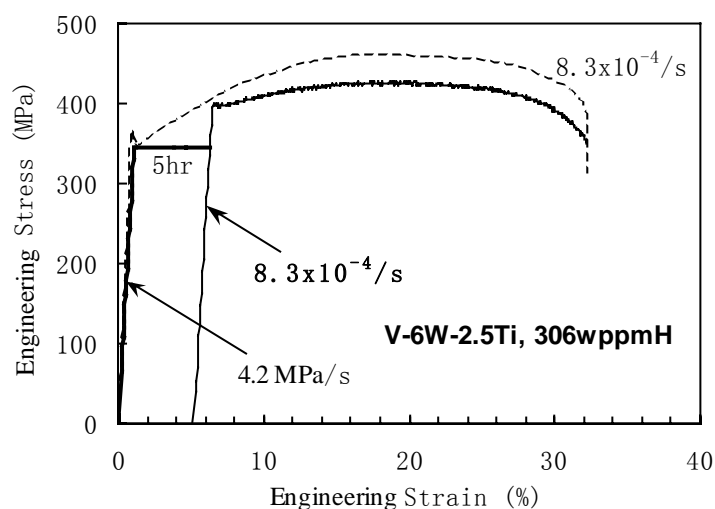


Fig. 8.7 The tensile curve (in dashed line) and the relation between the stress and strain in both the hold test and the following tensile test.

There are reports on creep deformation (primary creep) for steels [127], various metals and alloys [128] at room temperature. Generally, cubic metals demonstrate very low creep rate. In contrast, hcp metals and alloys such as Ti-6Al-4V demonstrate significant primary creep. The creep rate was also found to increase with the increase of applied stress. However, the reported creep tests were performed at stress level

lower than proof stress. According to the result showing in 6.3, it is impossible for the vanadium alloy investigated in the present paper to have this primary creep deformation behavior at room temperature. Although the present hold tests and the deformation behavior are similar to this kind of creep, the plastic flow can only occur at high stress level higher than the yield strength of the tested alloys. This is also significant for understanding the basic deformation behavior of vanadium alloys, and may be of engineering importance since stress at local region (such as the region with stress concentration) of a vanadium structure may exceed the yield stress of the alloy.

The results in this chapter could be summarized as follows:

- (1) A special room temperature plastic flow behavior was found for V-6w-2.5Ti and V-4Cr-4Ti, much similar to creep deformation. Its particularity is that the plastic flow merely takes place at stresses above the yield strength of the alloys.
- (2) The plastic flow exhibits a three-stage behavior with the initial two stages to be mostly caused by the inertia of the tensile deformation during the loading to the hold stress and thus be very short. The 3rd stage shows a steady plastic flow.
- (3) The steady plastic flow is most likely dislocation-glide assisted. The plastic flow rate increases with increasing stress level.
- (4) Hydrogen in the alloys seems to enhance the plastic flow due to hydrogen release that decreases dislocation motion resistance.
- (5) Considering its importance and the limited data obtained, further investigation is necessary for better understanding the deformation mechanism.

9 Summary and conclusions

Various V-base alloys for fusion blanket application were prepared for the purpose to study the effects of solutes and their interactions on mechanical properties. The recovery and recrystallization, the hardening by both precipitation and cold rolling, thermal stability of the hardening, tensile properties at room and elevated temperature, fracture toughness, impact energy absorption, hydrogen release and room temperature plastic flow behavior were investigated of the alloys with and without hydrogen charged. Based on these measured results and certain microstructure analysis by SEM, TEM and optical microscope observations, the effects of interstitial C, N, O and H on these properties or behaviors were studied. Emphasis was placed on the possible interactions between the solutes, particularly the one between Cr and Ti, that seems to have not been studied before, and the interaction between the interstitials with dislocations, as well as the mutual effects among the interactions. These interactions should be entirely studied considering their great effects on mechanical performances and other behaviors.

Major experimental results or achievements in the present study could be summarized as follows.

- (1) Alloy development: Many model vanadium alloys have been fabricated with good control of interstitial C, N and O impurities. Alloying elements covered Ti, Cr, W, Al and Si, in concentration of ~1-8% in mass. Alloying V with W was proven to be feasible with very thin W sheet to promote its dissolution into the melted V. Adding Al to V has the role to mitigate oxygen contamination during hot working.
- (2) Hardness Recovery: Notable hardness recovery occurs at $>600^{\circ}\text{C}$ for the 50%CW cold-rolled alloys containing Ti. For others without Ti, it starts at $\sim 500^{\circ}\text{C}$ with additional hardening at $\sim 300^{\circ}\text{C}$. For alloys with 4%Ti in mass, if the interstitial C, N and O concentration in their matrix is high, additional hardening will take place at $500\text{-}600^{\circ}\text{C}$.

- (3) Recrystallization: The least temperature for complete recrystallization of the cold-rolled alloys is $\sim 900^{\circ}\text{C}$ for the 1 h annealing, irrespective of the alloying elements. But the Ti, W and Cr additions, especially their combination, somehow reduce the grain size significantly. The size increases drastically with increasing temperature above 900°C for alloys without Cr but above 1000°C for V-4Cr-4Ti.
- (4) Solid-solution hardening: Almost all of the alloying elements, particularly the interstitial C, N and O solutes (should be taken as alloying elements as well), are strong solid solution strengtheners. The hardening ability of the substitutional Ti, W and Cr are similar to each other, but are quite lower than the interstitial solutes.
- (5) Precipitation and its hardening: When alloys containing Ti are in solid solution state, precipitation will occur at $500\text{-}800^{\circ}\text{C}$, resulting in peak hardening at $600\text{-}700^{\circ}\text{C}$, where the formed precipitates are ultra fine and their growth is controlled by Ti diffusion. The precipitates are most likely Ti- (CON). The hardening in V-4Cr-4Ti appears at higher temperature than that in other alloys without Cr, and the peak hardening for V-4Cr-4Ti is much stronger. Strong hardening could be obtained by ageing V-4Cr-4Ti at 600°C for 11-24 h by a hardness increase of more than 35%. Though the precipitation is related to Ti, the precipitation hardening capability doesn't vary much with the change of Ti concentration in the range of 1-4% in mass.
- (6) Effect of the precipitation hardening on ductility: No significant reduction in ductility will be caused by the precipitation. Particularly, when aging time exceeds ~ 50 h at 600°C , the toughness defined as the absorbed energy of a tensile specimen during tensile test could even be improved by the hardening.
- (7) Thermal stability of the precipitation hardening: The growth of the precipitates is controlled by diffusion of Ti in matrix with thermal activation energy of 335.6 kJ/mol. The hardening by the aging at 600°C is proven to be stable at $\leq 500^{\circ}\text{C}$ based on the temperature dependence of the hardness during the 1 h isochronally annealing.

- (8) Hardening by cold rolling: Cold rolling can harden the V-4Cr-4Ti alloy considerably. A 20% CW by cold rolling could increase the hardness of the NIFS-Heat 2 alloy in 950°C/1h state by a factor of 40%. But its contribution to the precipitation-hardened alloy is much smaller. The hardening is thermally stable below 600°C due to role of Ti.
- (9) Feasibility to utilizing the hardenings for fusion reactor: The hardenings could be utilized to strengthen the vanadium alloy that may be used for the components subject to higher stress levels at relatively low temperature of $\leq 500^\circ\text{C}$ considering its thermal stability and little effect on tensile ductility. The precipitation-hardened alloy may have strong resistance to neutron irradiation embrittlement due to the depletion of interstitial solutes in matrix by the precipitation. It is suggested to use the hardened alloy at relatively lower temperature and the alloy in RA ($\sim 900\text{-}950^\circ\text{C}$, 1 h annealing) state at high temperature for its good high-temperature thermal stability.
- (10) High temperature performance: V-6W-4Ti has higher or equivalent strength to V-4Cr-4Ti at RT - 600°C, but inferior tensile strength at higher temperature. At 500-700°C, DSA causes load-displacement serrations, whose height is temperature and Ti concentration dependent, and has little relation to both Cr and W addition in the alloy.
- (11) Hydrogen behavior: The V-base alloys with addition of Ti have higher hydrogen absorption rate. Hydrogen in the alloys is unstable even at room temperature. Hydrogen release will occur during tension loading at RT, causing the shrinkage of the tensile specimen and increase in elastic modulus. This dimensional instability will be a big concern for the vanadium alloy as blanket structural material, which serves in a hydrogen or its isotope environment.
- (12) Hydrogen induced hardening and the embrittlement: Hydrogen embrittlement, a common phenomenon for vanadium alloys, occurs at critical hydrogen concentrations (CHC). The CHC varies a lot for different alloys: alloys with Ti and Al have higher CHC than those without them. CHC for V-4Ti is about 400

wppm H, but merely 100 wppm H for V-8W. Hydrogen induced strengthening, being a solid solution type at H concentration below the CHC, varies a lot with the alloying elements. Ti/Al-bearing alloys have weaker strengthening compared to the ones without them. This should account for the better properties of the former alloys against hydrogen embrittlement. Oxygen in V-base alloys enhances the hydrogen embrittlement. The high-O V-4Cr-4Ti has a CHC of less than 50 wppm in the present study, while the CHC for the NIFS-Heat-2 alloy is more than 215 wppm. The fracture of the hydrogen embrittled alloy is usually transgranular cleavage, but may be intergranular for alloy with high oxygen concentration. When hydrogen concentration is not so high up to CHC, fracture is mainly a quasi-cleavage type with many secondary cracks. The number of cracks decreases with increasing hydrogen concentration.

(13) Effect of crack, loading rate and thickness on hydrogen embrittlement: All things of crack, increasing loading rate and thickening specimen will enhance hydrogen embrittlement significantly. Though the CHC for the NIFS alloy is more than 215 wppm according to then tensile results, it would be less than 130 wppm based on either the fracture toughness evaluated with compact specimens with pre-fatigue cracks or the absorbed energy obtained by impact tests of Charpy specimens.

(14) Room temperature plastic flow: Room temperature plastic flow occurs for V-base alloys at hold stress higher than yield strength. The plastic flow is dislocation-glide assisted and could be enhanced by the hydrogen in the alloy. The plastic flow rate increases with the increase of applied stress.

Following is a description of the mechanisms for the effect of solutes and their interactions on the mechanical properties of vanadium alloys.

- Whether the interstitial impurities or substitutional solutes concerned in the present paper are strong solid solution strengtheners. They increase friction

resistance of dislocation motion.

- With increasing temperature, the solutes gradually become mobile. Interstitial C, N and O are small atoms in unalloyed V and are mobile at 200~300°C, while Ti in V is mobile at and above 500°C. It is the interstitials that could diffuse towards dislocations to produce an interaction between interstitials and dislocations. The interaction further increases the resistance of the interstitials to dislocation motion. That's why the additional annealing hardening at ~300°C for the cold-rolled alloys without Ti.
- Ti has strong affinity to interstitial C, N and O impurities and could bind them. This interaction greatly reduce the mobility of the interstitial solutes, which is the main reason for the absence of additional hardening at ~300°C for the cold-rolled vanadium alloy containing Ti for Ti is relatively immobile at <500°C. In this case, the interstitial solutes are able to move at higher temperature, where the interaction of interstitials with dislocations could notably take place. That should account for the higher temperature (500-600°C) additional hardening of the cold-rolled alloys containing 4%Ti in mass. The DSA appeared at high temperature of 500-700°C in Ti-bearing alloys should attribute to this interactions as well. If the amount of free interstitial impurities in matrix is high enough, then precipitation and its hardening could happen at temperatures sufficient high for a prominent mobility of Ti, that is, higher than 500°C. Due to these interactions and the feature of the Ti mobility, the hardening by precipitation and cold rolling is stable below 500°C. The growth of the Ti-CON precipitates is controlled by Ti diffusion, which is more difficult than the diffusion of the interstitial solutes in matrix.
- Cr has strong interaction with Ti at high temperature and the presence of Cr in an alloy could have the role to reduce the mobility of Ti due to the interaction. Because of this interaction, other interactions described above will work at higher temperature. That's why the V-4Cr-4Ti alloy have better high temperature strength above 600°C and stronger precipitation hardening than

the V-6W-4Ti alloy, since W has no such role as to interact with Ti.

- Hydrogen could lower the mutual binding force of atoms, thus will cause hydrogen embrittlement.
- Hydrogen is extremely small atom and is mobile at room temperature with the aid of tensile stress. As a result, hydrogen release takes place during tensile test at room temperature. On the other hand, if there is a strong tensile stress gradient in a vanadium structure, hydrogen would diffuse towards the high stress region and enhance the hydrogen embrittlement.
- Hydrogen, extremely small atom, will preferentially stay in the quadrilateral interstitial of the V crystal and causes local lattice distortion. This distortion increases dislocation motion resistance and thus strengthens the alloy. Substitutional atoms in V will change the size of the interstitial, those with bigger difference in atomic size to V will produce larger interstitials, and hence decreases the distortion caused by the dwelling of H, making the alloy have low hydrogen inducing strengthening and eventually good resistance to hydrogen embrittlement. The stronger resistance of Ti/Al-bearing alloys to hydrogen embrittlement than the other alloys in the present study is a sufficient evidence for this mechanism.
- Increasing oxygen concentration will greatly enhance the hydrogen embrittlement of an alloy due to oxygen preferentially distributing along grain boundaries and reducing the grain boundary strength.
- Cross glide of dislocations is the major mechanism for the room temperature plastic flow at constant stress higher than yield strength. Since hydrogen release could reduce the amount of hydrogen to resist the dislocation motion, it enhances the room temperature plastic flow.

The conclusions of the present study are as follows.

- (6) The effect of solutes and solute interactions on mechanical properties of vanadium alloys was significant. All of the solutes concerned were solid solution

strengtheners. The hardening coefficient for interstitial solutes was much higher than that for substitutional solutes.

- (7) Ti and the interstitial C, N and O were necessary and were responsible for higher high-temperature strength and keeping the cold-rolling hardening at elevated temperature. Additionally they were the cause of precipitation, and the resulting hardening could be utilized for enhancing strength of the vanadium alloy for relatively low temperature application. For these properties, Cr also provided large positive contribution by its effect to reduce the mobility of Ti due to their mutual interaction.
- (8) The growth of the precipitate in V- (W/Cr) -Ti alloys is controlled by Ti diffusion because the precipitate is Ti-CON and Ti diffusion is more difficult than the diffusion of the interstitial solutes in matrix.
- (9) A critical new issue of room temperature plastic flow at constant stress higher than yield strength was found for which more studies should be addressed.
- (10) As for the hydrogen effect, the hydrogen embrittlement could be a great concern for the fusion application due to the strong sensitivity of the fracture toughness. In addition, the hydrogen release could cause dimensional instability. Oxygen in vanadium alloys enhanced the embrittlement significantly. Alloying V with species that had relatively large difference in atomic size to V could improve the property.
- (11) All these results showed interactive role of interstitial and substitutional solutes on mechanical properties of vanadium alloys through solid solution hardening, mutual binding or trapping, interaction with dislocations, precipitation and precipitate resolution.
- (12) Finally, it is highly suggested for further investigation of the interaction of Cr-Ti, and the hydrogen release behavior at room temperature in the future.

Acknowledgement

The author expresses his appreciations to many colleagues in Japan and China who provided assistance in the experiments, testing and preparing this thesis. Thanks NIFS in Japan, SWIP and NPIC in China for their support to this research work.

Most of the alloys were prepared in China. Nanjing University has provided the furnace for alloy melting. Thanks Prof. Lu Quan in the University for his aid in preparing the ingot. His experience in alloy melting, especially the melting of V-W alloys, has helped the preparation a lot. Alloy plates were fabricated in NPIC, China. Besides, many mechanical tests were performed with the support of NPIC. The author would like to greatly appreciate the efforts of Prof. Qiu Shaoyu, Li Cong, Chen Yong and Liang Bo in NPIC in preparing the cold rolling plates, mechanical tests and so on. Thanks colleagues in Chengdu Airplane Engine Co. for their aids in chemical composition and H concentration analysis.

Most of the studies were fulfilled and results were obtained in NIFS, Japan. High temperature tensile tests were performed in IMR, Japan. The author greatly thanks Dr. Takeo Muroga for his help in arranging experiments and testing in NIFS and IMR, his support to the study plan, his many good proposals, his help in TEM analysis, and his help in reviewing this thesis. Dr. Takuya Nagasaka has aided the studies a lot in recovery and recrystallization and so forth, including the fruitful discussion on DSA phenomena. Thanks Dr. Teruya Tanaka in NIFS for his aid in activation analysis of the V-6W-4Ti alloy. Thank Dr. Matusi in IMR for his support in the high temperature tensile tests. The collaboration research belongs to the China-Japan CUP program, which has supported this study a lot.

Thank SWIP and my colleagues in SWIP for the aid to the vanadium researches. Without the great support from SWIP, this study could not be fulfilled.

Part of the study was conducted with the support of the Nature Science Foundation of China in recent years. The project No. is 50271025.

References

- [1] Jose Goldemberg, “The promise of clean energy”, *Energy Policy*, 2005, in press.
- [2] BP Statistical Review of World Energy, June 2001, p. 38.
- [3] Mamdouh G. Salameh, *Applied Energy* 75 (2003) 33–42.
- [4] Klaus R.G. Hein, “Future energy supply in Europe—challenge and chances”, *Fuel* 84 (2005) 1189–1194.
- [5] Donald L. Klass, “A critical assessment of renewable energy usage in the USA”, *Energy Policy* 31 (2003) 353–367.
- [6] R. Toschi, “Nuclear fusion, an energy source”, *Fus. Engin. & Des.*, 36 (1997) 1-8.
- [7] The promise of fusion energy,
http://fusioned.gat.com/images/pdf/promise_of_fusion.pdf.
- [8] Charles C. Baker, Robert W. Conn, Farrokh Najmabadi, Mark S. Tillack, Status and prospects for fusion energy from magnetically confined plasmas, 23 (7/8) 1998 649-694.
- [9] Dan Finkenthal, Rick lee, Steve Rodecker, John Ray, Dave Schissel, Pete Taylor, Fusion — Nature’s Fundamental Energy Source, General Atomics, 1996.
- [10] J. D. Lawson, *Proceedings of physical society*, 70, 1957, 445.
- [11] M. D. Williams, D-T operation on TFTR, *Fus. Eng. Des.* 36 (1997) 135-142.
- [12] H. Kishimoto, Plasma confinement improvement in negative shear plasmas, JT-60U Experimental Report No. 36, JAERI, Naka, Japan, 1996.
- [13] M. Keilhacker, M.L. Watkins, JET Team, D-T experiments in the JET tokamak, *J. Nucl. Mater.*, 266-269 (1999) 1-13.
- [14] P.-H. Rebut, ITER: the first experimental fusion reactor, *Fus. Eng. Des.* 27 (1995) 3-16.
- [15] R. Aymar, The ITER reduced cost design, *Fus. Eng. Des.*, 49-50 (2000) 13-25.
- [16] R. Aymar, Status of ITER, *Fus. Eng. Des.* 61-62 (2002) 5-12.
- [17] Y. Shimomura, The present status and future prospects of the ITER project, *J. Nucl. Mater.* 329-333 (2004) 5-11.

-
- [18] W.D. D'haeseleer, The development of fusion development towards a future energy source, *Fus. Eng. Des.* 66-68 (2003) 3-15.
- [19] Satoshi, Konishi, Use of fusion energy as a heat for various applications, *Fus. Eng. Des.* 58-59 (2001) 1103-1107.
- [20] G. Federic, J.P. Coad, A.A. Haasz, G. Janeschitz, N. Noda, V. Philipps, J. Roth, C.H. Skinner, R. Tivey, C.H. Wu, Critical plasma-wall interaction issues for plasma-facing materials and component in near-term fusion devices, *J. Nucl. Mater.* 283-287 (2000) 110-119.
- [21] V. Barabash, G. Federic, M. Rodig, L.L. Snead, C.H. Wu, Neutron irradiation effects on PFMs, *J. Nucl. Mater.*, 283-287 (2000) 138-146.
- [22] H. Bolt, V. Barabash, W. Krauss, J. Linke, R. Neu, S. Suzuki, N. Yoshida, Materials for the plasma-facing components of fusion reactors, *J. Nucl. Mater.* 329-333 (2004) 66-73.
- [23] A. Miyahara and J. B. Whitley, "Thermal effects and other critical issues of plasma facing components", *J. Nucl., Mater.* 179-181 (1991) 19-24.
- [24] M. Seki, M. Guseva, G. Vieider, J. Whitley, ITER related R&D on low-Z plasma facing materials for divertor and first wall, *J. Nucl. Mater.* 179-181 (1991) 1189-1192.
- [25] D.E. Dombrowski, Manufacture of beryllium for fusion energy applications, *Fus. Eng. Des.* 37 (1997) 229-242.
- [26] C. Boudot, I. Bobin-Vastra, P. Lorenzetto, D. Conchon, A. Cottin, J. Jacquinet, D. Cauvin, M. Febvre, Manufacture of two primary first wall panel prototypes with beryllium armor for ITER, *Fus. Eng. Des.* 66-68 (2003) 347-353.
- [27] Karl Ehrlich, E.E. Bloom, T. Kondo, International strategy for fusion materials development, *J. Nucl. Mater.* 283-287 (2000) 79-88.
- [28] Blanket, Top Level Documents for ITER-Technical Basis for the ITER-FEAT Outline Design, G A0 RI 2 00-01-18 R1.0.
- [29] L.V. Boccaccini, L. Giancarli, G. Janeschitz, S. Hermsmeyer, Y. Poitevin, A. Cardella, E. Diegele, Materials and design of the European DEMO blankets, *J. Nucl. Mater.* 329-333, 2004, 148-155.

- [30] S. Nishio, S. Ueda, R. Kurihara, T. Kuroda, H. Miura, K. Sako, H. Takase, et al., Prototype tokamak fusion reactor based on SiC/SiC composite material focusing on easy maintenance, *Fus. Eng. Des.* 48 (2000) 271-279.
- [31] Farrokh Najmabadi, Overview of ARIES-RS tokamak fusion power plant, *Fus. Eng. Des.* 41 (1998) 365-370.
- [32] H.M Chung, B.A. Loomis, D.L. Smith, Development and testing of vanadium alloys for fusion applications, *J. Nucl. Mater.* 239 (1996) 139-156.
- [33] T.V. Kulsartov, V.P. Shestakov, I.L. Tazhibaeva, E.A. Kenzhin, Hydrogen permeation through vanadium alloy V-4Cr-4Ti 'in situ' of reactor irradiation, *J. Nucl. Mater.* 283-287 (2000) 872-875.
- [34] K. Natesan, M. Uz, Oxidation performance of V-Cr-Ti alloys, *Fus. Eng. Des.* 51-52 (2000) 145-152.
- [35] D.R. Harries, G. J. Butterworth, A. Hishinuma, F.W. Wiffen, Evaluation of reduced-activation options for fusion materials development, *J. Nucl. Mater.* 191-194 (1992) 92-99.
- [36] D.L. Smith, H.M, Chung, B. A. Loomis, H. Matsui, S. Votinov, W. Van Witzenburg, Development of vanadium-base alloys for fusion first-wall-blanket applications, *Fus. Eng. Des.* 29 (1995) 399-410.
- [37] E. T. Cheng, Waste management aspect of low activation materials, *Fus. Eng. Des.* 48 (2000) 455-465.
- [38] Karl Ehrlich, Materials research towards a fusion reactor, *Fus. Eng. Des.* 56-57 (2001) 71-82.
- [39] E.V. Dyomina, P. Fenici, V.P. Kolotov, M. Zucchetti, Low-activation characteristics of V-alloys and SiC composites, *J. Nucl. Mater.* 258-263 1784-1790.
- [40] H.M. Chung, B.A. Loomis, D.L. Smith, Properties of V-4Cr-4Ti for applications as fusion reactor structural components, *Fus. Eng. Des.* 29 (1995) 455-464.
- [41] K. Natesan, W.K. Soppet, A. Purohit, Uniaxial creep behavior of V-4Cr-4Ti alloy, *J. Nucl. Mater.* 307-311 (2002) 585-590.
- [42] S. Jitsukawa, K. Shiba, The reduced activation ferritic/Martensitic steel as a

- structural materials for the test blanket modules, Materials Assessment Report, Material documents for ITER.
- [43] R. Lindau, A. Moslang, M. Schirra, Thermal and mechanical behavior of the reduced-activation-ferritic-martensitic steel EUROFER, *Fus. Eng. Des.* 61-62 (2002) 659-664.
- [44] S. J. Zinkle, N.M. Ghoniem, Operating temperature windows for fusion reactors structural material materials, *Fus. Eng. Des.* 51-52 (2000) 55-71.
- [45] S.J. Zinkle, L.L. Snead, Thermo-physical and mechanical properties of SiC/SiC composites, in *Fusion Materials Semiannual. Progress. Report for period ending June 30 1998*, DOE:ER-0313:24, Oak Ridge National Lab, 1998, pp. 93–100.
- [46] R.H. Titran, M. Uz Effects of thermo-mechanical processing on the microstructure and mechanical properties of Nb-1Zr-C alloys, The 4th specialist conference on “Nuclear Power Engineering in Space Materials Fuel”, Podolsk, Russia, September 21-24, 1993.
- [47] J.R. Distefano, H.E. McCoy, Mechanical properties of T-111 at low to intermediate temperatures, *Inter. J. Ref. Met. & Hard Mater.* 20 (2002) 381-387.
- [48] R. Lindau, M. Schirra, First results on the characterization of the reduced-activation-ferritic-martensitic steel EUROFER, *Fus. Eng. & Des.* 58-59 (2001) 781-785.
- [49] T.S. Bray, H. Tsai, L.J. Nowicki, M.C. Billone, D.L. Smith, W.R Johnson, P.W. Trester, Tensile and impact properties of V-4Cr-4Ti alloy heats 832665 and 832664, *J. Nucl. Mater.*, 283-287 (2000) 633-636.
- [50] A. Nishimura, A. Iwahori, N.J. Heo, T. Nagasaka, T. Muroga, S. -I. Tanaka, Effect of precipitation and solution behavior of impurities on mechanical properties of low activation vanadium alloy, *J. Nucl. Mater.* 329-333 (2004) 438-441.
- [51] B.G. Gieseke, C.O. Stevens, M.L. Grossbeck, Fatigue and crack growth behavior of V-Cr-Ti alloys, *J. Nucl. Mater.* 233-237 (1996) 488-491.
- [52] P. Marmy, Y. Ruan, M. Victoria, The tensile and fatigue properties of type 1.4914 ferritic steel for fusion reactor applications, *J. Nucl. Mater.* 179-181 (1991)

- 697-701.
- [53] R. Lindau, A. Moslang, Low-cycle fatigue properties of the helium-implanted 12%Cr steel 1.4914 (MANET), *J. Nucl. Mater.* 179-181 (1991) 753-756.
- [54] A. Nagasha, M. Valsan, R. Kannan, K. Bhann Sankara Rao, S.L. Mannan, *Inter. J. Fatigue*, 24 (2002) 1285-1293.
- [55] J. S. Park, S. J. Kim, C.S. Lee, Effect of W addition on low cycle fatigue behavior of high Cr ferritic steels, *Mater. Sci. & Engin.* 298 (2001) 127-136.
- [56] B. van der Schaaf, D.S. Gelles, S. Jitsukawa, A. Kimura, R.L. Klueh, A. Moslang, G.R. Odette, Progress and critical issues of reduced activation ferritic/martensitic steel development, *J. Nucl. Mater.* 283-287 (2000) 52-59.
- [57] S. Jitsukawa, A. Kimura, A. Kohyama, R.L. Klueh, A.A. Tavassoli, A. van der Schaaf, G.R. Odette, J.W. Resman, M. Victoria, C. Petersen, Recent results of the reduced activation ferritic/martensitic steel development, *J. Nucl. Mater.* 329-333 (2004) 39-46.
- [58] E.E. Bloom, S.J. Zinkle, F.W. Wiffen, Materials to deliver the promise of fusion power – progress and challenges, *J. Nucl. Mater.* 329-333 (2004) 12-19.
- [59] A.-A.F. Tavassoli, Present limits and improvements of structural materials for fusion reactors – a review, *J Nucl. Mater.* 302 (2002) 73-88.
- [60] K. Shiba, M. Enoeda, S. Jitsukawa, Reduced activation martensitic steels as a structural material for ITER test blanket, *J. Nucl. Mater.* 329-333 (2004) 243-247.
- [61] T. Muroga, Perspective of V/Li-TBM in Japan, IEA/JUPITER-II Workshop on Critical Issues of Vanadium Alloy Development for Fusion Reactor Applications, National Institute for Fusion Science, Toki-shi, Gifu-ken, Japan, December 15-16, 2003.
- [62] I.R. Kirillov, Lithium-vanadium breeding blanket activity in the RF, IEA/JUPITER-II Workshop on Critical Issues of Vanadium Alloy Development for Fusion Reactor Applications, National Institute for Fusion Science, Toki-shi, Gifu-ken, Japan, December 15-16, 2003.
- [63] Charles C. Baker, Advances in fusion technology, *J. Nucl. Mater.* 283-287 (2000) 1-9.

- [64]D. L. Smith, S. Majumdar, M. Billone, R. Mattas, Performance limits for fusion first-wall structural materials, *J. Nucl. Mater.* 283-287 (2000) 716-720.
- [65]T. Muroga, M. Gasparotto, S.J. Zinkle, Overview of materials research for fusion reactors, *Fus. Eng. Des.* 61-62 (2002) 13-25.
- [66]R. J. Kurtz, K. Abe, V.M. Vhernov, V.A. Kazakov, G.E. Lucas, H. Matsui, T. Muroga, G.R. Odette, D.L. Smith, S. J. Zinkle, Critical issues and current status of vanadium alloys for fusion energy applications, *J. Nucl. Matr.* 283-287 (2000) 70-78.
- [67]R.J. Kurtz, K. Abe, V.M. Vhernov, D.T. Hoelzer, H. Matsui, T. Muroga, G.R. Odette, Recent progress on development of vanadium alloys for fusion, *J. Nucl. Mater.* 329-333 (2004) 47-55.
- [68]A. Hasegawa, A. Koyama, R. H. Jones, L.L. Snead, B. Riccardi, P. Fenici, Critical issues and current status of SiC/SiC composites for fusion, *J. Nucl. Mater.* 329-333 (2004) 128-137.
- [69]Chung HM, Gazda J, Smith DL. Irradiation-Induced Precipitation and Mechanical Properties of Vanadium Alloys at 430°C [R]. Fusion Materials Semiannual Progress Report, 1998, DOE/ER-0313/24: 49-60.
- [70]D.S. Gelles. Microstructural examination of V-(3-6%)Cr-(3-5%)Ti irradiated in the ATR-A1 experiment [R]. Fusion Materials Semiannual Progress Report, 1998.6, DOE/ER-0313/24, 41-48.
- [71]T. Chuto, M. Satou, K. Abe, Defect microstructure and deformation behavior of V-Ti-Cr-Si-Al-Y alloy irradiated in ATR, *J. Nucl. Mater.* 283-287 (2000) 503-507.
- [72]M. Satou, T. Chuto, K. Abe, Improvement in post-irradiation ductility of neutron irradiated V-Ti-Cr-Si-Al-Y alloy and the role of interstitial impurities, *J. Nucl. Mater.* 283-287 (2000) 367-371.
- [73]T. Chuto, M. Satou, A. Hasegawa, K. Abe, T. Muroga, N. Yamamoto, Effects of small amount of additional elements on control of interstitial impurities and mechanical properties of V-4Cr-4Ti-Si-Al-Y alloys, *J. Nucl. Mater.* 326 (2004) 1-8.
- [74]N. J. Heo, T. Nagasaka, T. Muroga, H. Matsui, Effect of impurity levels on

- precipitation behavior in the low-activation V-4Cr-4Ti alloys, *J. Nucl. Mater.* 307-311 (2002) 620-624.
- [75] B. A. Loomis, D.L. Smith, F.A. Garner, Swelling of neutron irradiated vanadium alloys, *J. Nucl. Mater.* 179-181 (1991) 771-774.
- [76] Chung HM, Loomis BA, Nowicki L, et al. Irradiation-Induced Density Change and Microstructural Evolution of Vanadium-Base Alloys [R]. *Fusion Materials Semiannual Progress*, 1993, DOE/ER-0313/15, 223.
- [77] L.K. Mansur, A.F. Rowcliffe, R.K. Nanstad, S.J. Zinkle, et al, Materials needs for fusion, Generation IV fission reactors and spallation neutron sources — similarities and differences, *J. Nucl. Mater.* 329-333 (2004) 166-172.
- [78] T. Kondo, IFMIF, its facility concept and technology, *J. Nucl. Mater.* 258-263 (1998) 47-55.
- [79] R.J. Kurtz, K. Abe, V.M. Chernov, D.T. Hoelzer, H. Matsui, T. Muroga, G.R. Odette, Recent progress on development of vanadium alloys for fusion, *J. Nucl. Mater.* 329-333 (2004) 47-55.
- [80] B. Riccardi, L. Giancarli, A. Hasegawa, Y. Katoh, A. Koyama, R.H. Jones, L.L. Snead, Issues and advances in SiCf/SiC composites development for fusion reactors, *J. Nucl. Mater.* 329-333 (2004) 56-65.
- [81] H.M. Chung, H.-C. Tsai, D.L. Smith, R. Peterson, C. Curtis, C. Wojcik, Fabrication of 500-kg heat of V-4Cr-4Ti, *Fusion Materials Semiannual Progress Report for Period Ending 30th September 1994*, DOE/ER-0313/17, p. 178-182.
- [82] W.R. Johnson, J.P. Smith, Fabrication of a 1200 kg ingot of V-4Cr-4Ti alloy for the DIII-D radiative divertor program, *J. Nucl. Mater.* 258-263 (1998) 1425-1430.
- [83] T. Muroga, T. Nagasaka, A. Liyoshi, A. Kawabata, S. Sakurai, NIFS program for large ingot production of V-Cr-Ti alloy, *J. Nucl. Mater.* 283-287 (2000) 711-715.
- [84] T. Muroga, T. Nagasaka, K. Abe, V.M. Chernov, H. Matsui, D.L. Smith, Z.-Y. Xu, S.J. Zinkle, Vanadium alloys – overview and recent results, *J. Nucl. Mater.* 307-311 (2002) 547-554.
- [85] M.M. Potapenko, V.A. Grobishev, V.Y. Filkin, I.N. Gubkin, et al., Manufacture of semifinished items of alloys V-4Cr-4Ti and V-10Ti-5Cr for use as a structural

- material in fusion applications, *J. Nucl. Mater.* 233-237 (1996) 438-441.
- [86] T. Nagasaka, N.J. Heo, T. Muroga, M. Imamura, Examination of fabrication process parameters for improvement of low-activation vanadium alloys, *Fus. Eng. Des.* 61-62 (2002) 757-762.
- [87] H. Kurishita, T. Kuwabara, M. Hasegawa, S. Kobayashi, K. Nakai, Microstructure control to improve the resistance to radiation embrittlement in vanadium, *J. Nucl. Mater.* 343 (2005) 318-324.
- [88] M. Koyama, K. Fukumoto, H. Matsui, Effects of purity on high temperature mechanical properties of vanadium alloys, *J. Nucl. Mater.* 329-333 (2004) 442-446.
- [89] M.L. Grossbeck, J.F. King, D.J. Alexander, P.M. Rice, G.M. Goodwin, Development of techniques for welding V-Cr-Ti alloys, *J. Nucl. Mater.* 258-263 (1998) 1369-1374.
- [90] M.L. Grossbeck, J.F. King, T. Nagasaka, S.A. David, Gas tungsten arc welding of vanadium alloys with impurity control, *J. Nucl. Mater.* 307-311 (2002) 1590-1594.
- [91] T. Nagasaka, T. Muroga, M.L. Grossbeck, T. Yamamoto, Effects of post-weld heat treatment conditions on hardness, microstructures and impact properties of vanadium alloys, *J. Nucl. Mater.* 307-311 (2002) 1595-1599.
- [92] T. Nagasaka, N.J. Heo, T. Muroga, A. Nishimura, H. Watanabe, M. Narui, K. Shinozaki, Impact properties of NIFS-HEAT-2 (V-4Cr-4Ti) after YAG laser welding and neutron irradiation at 563 K, *J. Nucl. Mater.* 329-333 (2004) 1539-1543.
- [93] H.M. Chung, J.-H. Park, R.V. Strain, K.H. Leong, D.L. Smith, Mechanical properties and microstructural characteristics of laser and electron-beam welds in V-4Cr-4Ti, *J. Nucl. Mater.* 258-263 (1998) 1451-1457.
- [94] D.L. Smith, K. Natesan, J.-H. Park, C.B. Reed, R.F. Mattas, Development of electrically insulating coatings on vanadium alloys for lithium-cooled blankets, *Fus. Eng. Des.* 51-52 (2000) 185-192.
- [95] A.V. Verkov, V.A. Evtikhin, I.E. Lyublinski, Self-healing electrical insulating coating processes for vanadium alloy – lithium systems, *Fus. Eng. Des.* 58-59

- (2001) 731-735.
- [96]D.L. Smith, J.-H. Park, I. Lyublinski, V. Evtikhin, A. Perujo, H. Glassbrenner, T. Terai, S. Zinkle, Progress in Coating development for fusion systems, Fus. Eng. Des. 61-62 (2002) 629-641.
- [97]B. A. Pink, L.D. Chitwood, J.R. DiStefano, Long-term stability of ceramics in liquid lithium, J. Nucl. Mater. 289 (2001) 52-56.
- [98]B.A. Pink, P.F. Tortorelli, A. Jankowski, J. Hayes, T. Muroga, A. Suzuki, O.I. Yeliseyeva, V.M. Vhernov, Recent progress in the development of electrically insulating coatings for a liquid lithium blanket, J. Nucl. Mater. 329-333 (2004) 119-124.
- [99]Z. Yao, A. Suzuki, T. Muroga, K. Katahira, Chemical formation of erbium oxide layer on V-4Cr-4Ti during exposure to liquid doped with erbium, J. Nucl. Mater. 329-333 (2004) 1414-1418.
- [100]T. Muroga, J.M. Chen, V.M. Chernov, K. Fukumoto, D.T. Hoelzer, R.J. Kurtz, T. Nagasaka, B.A. Pint, M. Satou, A. Suzuki, Watanabe, Advances in development of vanadium alloys and MHD insulator coatings, to be presented at 12-ICFRM, Dec. 4-9, 2005, California, USA.
- [101]D.R. Diercks, B.A. Loomis, Alloying and impurity effects in vanadium-base alloys, J. Nucl. Mater. 141-143 (1986) 1117-1124.
- [102]B.A. Loomis, A. B. Hull, D.L. Smith, Evaluation of low-activation vanadium alloys for use as structural material in fusion reactors, J. Nucl. Mater. 179-181 (1991) 148-154.
- [103]D.L. Smith, H.M. Chung, H. Matsui, A.F. Rowcliffe, Progress in vanadium alloy development for fusion application, Fus. Eng. Des. 41 (1998) 7-14.
- [104]D.t. Hoelzer, A.F. Rowcliffe, Investigating solute interactions in V-4Cr-4Ti based on tensile deformation behavior of vanadium, J. Nucl. Mater. 307-311 (2002) 596-600.
- [105]V.A. Evtikhin, I.E. Lyublinski, A.V. Vertkov, S.N. Votinov, A.I. Dedyurin, Influence of alloying and impurity element contents on V-Ti-Cr alloy properties, J. Nucl. Matr. 307-311 (2002) 591-595.

- [106] T. Nagasaka, H. Takahashi, T. Muroga, T. Tanabe, H. Matsui, Recovery and recrystallization behavior of vanadium at various controlled nitrogen and oxygen levels, *J. Nucl. Mater.* 283-287 (2000) 816-821.
- [107] H.D. Rohrig, J.R. DiStefano, L.D. Chitwood, Effect of hydrogen and oxygen on the tensile properties of V-4Cr-4Ti, *J. Nucl. Mater.* 258-263 (1998) 1356-1360.
- [108] J.R. DiStefano, J.H. De Van, D.H. Rohrig, L.D. Chitwood, Reactions of hydrogen with V-Cr-Ti alloys, *J. Nucl. Mater.* 273 (1999) 102-110.
- [109] A.Kh. Klepikov, O.G. Romanenko, Y.V. Chikhray, I.L. Tazhibaeva, Hydrogen release from irradiated vanadium alloy V-4Cr-4Ti, *Fus. Eng. Des.* 51-52 (2000) 127-133.
- [110] S. Ohnuki, T. Yasuda, T. Suda, S. Watanabe, B.M. Oliver, Effect of alloying elements and neutron-irradiation on hydrogen behavior in V alloys, *J. Nucl. Mater.* 329-333 (2004) 481-485.
- [111] T.B. Massalski, *Binary Alloy Phase Diagrams*, ASM, 1986.
- [112] M. Fujiwara, K. Natesan, Oxidation of V-4Cr-4Ti alloys containing Al, Si and Y, *Fusion Materials Semiannual Progress Report*, DOE/ER-0313/27, 1999, 45-48.
- [113] CHEN Ji-ming, XU Ying, DENG Ying, XU Zeng-yu, "The effect of Al, Cr on the oxidation behavior of a V-4Ti alloy", *Plasma Sci. & Tech.*, 5 (1) 2003, 1661-1668.
- [114] H. Bleichert, H. Wenzl, *Phys. Stat. Sol. B* 144 (1987) 361.
- [115] N.J. Heo, T. Nagasaka, T. Muroga, Recrystallization and precipitation behavior of low-activation V-Cr-Ti alloys after cold rolling, *J. Nucl. Mater.* 325 (2004) 53-60.
- [116] J. Chen, S. Qiu, L. Yang, Z. Xu, Y. Deng, Y. Xu, Effects of oxygen, hydrogen and neutron irradiation on the mechanical properties of several vanadium alloys, *J. Nucl. Mater.* 302 (2002) 135-142.
- [117] C. Nishimura, T. Ozaki, M. Komaki, Y. Zhang, Hydrogen permeation and transmission electron microscope observations of V-Al alloys, *J. Alloys Comp.* 356-357 (2003) 295-299.
- [118] M. Uz, K. Natesan, V. B. Hang, Oxidation kinetics and microstructure of V-(4-5)

- wt% Cr-(4–5) wt% Ti alloys exposed to air at 300–650°C, *J. Nucl. Mater.* 245 (1997) 191-200.
- [119] J.M. Chen, T. Nagasaka, T. Muroga, Y. Xu, S.Y. Qiu, Y. Chen, The recovery and recrystallization of cold-rolled V- Cr (W)-Ti alloys with different Pre-heat treatment, Presented at the 13th Inter. Conf. on Nucl. Eng. (ICONE 13), May 16-20, 2005, Beijing, China.
- [120] D. T. Hoelzer, M. K. West, S. J. Zinkle, A. F. Rowcliffe, Solute interactions in pure vanadium and V–4Cr–4Ti alloy, *J. Nucl. Mater.* 283-287 (2000) 616.
- [121] B.A. Loomis, G. Wiggins, Corrosion and oxidation of vanadium-base alloys, *J. Nucl. Mater.* 122 (1984) 693-697.
- [122] K. Fukumoto, T. Yamamoto, H. Matsui, et al, Proc. 5th IEA and JUPITER Joint Workshop on Vanadium Alloys for Fusion Applications, Oct. 30~Nov. 1, P. 96~105.
- [123] K. Natesan, W.K. Soppet, Performance of V–Cr–Ti alloys in a hydrogen environment, *J. Nucl. Mater.* 283-287 (2000) 1316-1321.
- [124] T. Kobayashi, I. Yamamoto, M. Niinomi, Evaluation of dynamic fracture toughness parameters by instrumented Charpy impact test, *Eng. Fract. Mech.* 24 (1986) 773-782.
- [125] S. Yano, M. Tada, H. Matsui, Hydrogen embrittlement of MFR candidate vanadium alloys, *J. Nucl. Mater.*, 179-181 (1991) 779-782.
- [126] J.R. DiStefano, B.A. Pint, J.H. DeVan, H. D. Röhrig, L. D. Chitwood, Effects of oxygen and hydrogen at low pressure on the mechanical properties of V–Cr–Ti alloys, *J. Nucl. Mater.* 283-287 (2000) 841-845.
- [127] N. Tsuchida, E. Baba, K. Nagai, Y. Tomota, Effects of interstitial solute atoms on the very low strain-rate deformations for an IF steel and an ultra-low carbon steel, *Acta Materialia* 53 (2005) 265-270.
- [128] T. Yamada, K. Kawabata, E. Sato, K. Huribayashi, I. Jimbo, Presences of primary creep in various phase metals and alloys at ambient temperature, *Mater. Sci. Eng. A* 387-389 (2004) 719-722.

List of the published papers

- 1 **J.M. Chen**, T. Nagasaka, T. Muroga, Y. Xu, S.Y. Qiu, Y. Chen, “The recovery and recrystallization of cold-rolled V- Cr (W)-Ti alloys with different Pre-heat treatment”, Presented at ICONE-13 (13th International Conf. on Nuclear Energy), May 16-20, 2005, Beijing, China.
- 2 **J.M. Chen**, T. Muroga, T. Nagasaka, S. Y. Qiu, F. Zhang, C. Li, B. Liang, Z.Y. Xu, “Aging and its impact on tensile properties of V-4Cr-4Ti”, Presented at JCS8, Oct. 3-9, 2004, Sendai, Japan.
- 3 **J.M. Chen**, T. Muroga, T. Nagasaka, Y. Xu, C. Li, S. Y. Qiu, Y. Chen, “Precipitation behavior in V-6W-4-Ti and V-4Cr-4Ti alloys”, J. Nucl. Mater., 2004, 334, 159-165.
- 4 **J.M. Chen**, S.Y. Qiu, T. Muroga, Y. Xu, Y. Chen, Y. Deng, Z.Y. Xu, “The hydrogen induced ductility loss and strengthening of V-base alloys”, J. Nucl. Mater., 2004, 334, 143-148.
- 5 **J.M. Chen**, T. Muroga, S.Y. Qiu, T. Nagasaka, W.G. Huang, M.J. Tu, Y. Chen, Y. Xu, Z.Y. Xu, “The development of advanced vanadium alloys for fusion applications”, J. Nucl. Mater., 2004, 329-333 PA, 401-405.
- 6 **CHEN Jiming**, Takeo Muroga, Qiu Shaoyu, XU Ying, DEN Ying, XU Zengyu, “Hydrogen embrittlement of a V4Cr4Ti alloy evaluated by different test methods”, J. Nucl. Mater., 325, 2-3, (2004), 79-86.
- 7 **J.M. Chen**, “V-W-Ti alloys”, Presented at the 7th IEA and JUPITER-II Joint Workshop on the Critical Issues for Vanadium Alloys for Fusion Application, Dec. 15~16, 2003, Toki, Gifu, Japan.
- 8 T. Muroga, T. Nagasaka, **J.M. Chen**, Z.Y. Xu, Q.Y. Huang and Y.C. Wu, “Characterization of Fusion Candidate Vanadium Alloys”, Plasma Sci. & Tech.,

- 6(4), 2004, 2395-2399.
- 9 T. Muroga, T. Nagasaka, A. Nishimura, **J.M. Chen**, “Improvement of vanadium alloys by precipitate control for structural components of fusion reactors”, Science Forum, 475-479, 2004, P. 1449.
- 10 **Jiming Chen**, Takeo Muroga, Takuya Nagasaka, Ying Xu, Shaoyu Qiu, “The recovery and recrystallization of cold rolled V-W-Ti alloys”, J. Nucl. Mater., 2003, 322, 73-79.
- 11 **Chen Jiming**, Xu Ying, Deng Ying, Yang Lin, Qiu Shaoyu, “The synergetic effects of hydrogen and oxygen on the strength and ductility of vanadium alloys”, Plasma Sci. & Tech., 5 (6) 2003, 2051-2056.
- 12 **CHEN Ji-ming**, XU Ying, DENG Ying, XU Zeng-yu, “The effect of Al, Cr on the oxidation behavior of a V-4Ti alloy”, Plasma Sci. & Tech., 5 (1) 2003, 1661-1668.
- 13 **CHEN Jiming**, YANG Lin, QIU Shaoyu, XU Zengyu, “Hydrogen embrittlement and high temperature oxidation behavior of vanadium alloys for fusion application”, Rare Metal Materials and Engineering, 2003, 32 (2), 113~116 (in Chinese).
- 14 **Jiming Chen**, Ying Xu, Shaoyu Qiu, T. Muroga, Ying Deng, Zengyu Xu, “Hydrogen embrittlement of a V4Cr4Ti alloy”, Proc. of the 7th China-Japan Symp. on Materials for Advanced Energy Systems and Fission & Fusion Engineering, July 29~Aug. 2, 2002, Lanzhou, China, P. 421-428. (ISBN 981-238-424-3).
- 15 **Jiming Chen**, Zengyu Xu, Lin Yang, “The influence of hydrogen on tensile properties of V-base alloys developed in China”, J. Nucl. Mater. 2002, 307-311, 566-570.
- 16 **Jiming Chen**, Shaoyu Qiu, Lin Yang, Zengyu Xu, Ying Deng and Ying Xu, “Effects of oxygen, hydrogen and neutron irradiation on the mechanical

- properties of several vanadium alloys”, *J. Nucl. Mater.* 2002, 302 (2-3), 135-142.
- 17 **CHEN Jiming**, “Effects of neutron irradiation on strength and ductility of vanadium alloys and its temperature dependence”, *Nuclear Fusion and Plasma Physics*, 2002, 22 (4), 209-214 (in Chinese).
- 18 **CHEN Jiming**, T. Muroga, XU Zengyu, QIU Shaoyu, XU Ying, “Alloying design for fusion application vanadium alloys based on hydrogen embrittlement resistance”, *Acta Metallurgica Sinica*, 2002, 38(8) 109-112 (in Chinese).